Molecular Mechanism of the Ribosome Recycling Factor ABCE1

Dissertation

zur Erlangung des Doktorgrades

der Naturwissenschaften

(DE30)

vorgelegt beim Fachbereich 14

Biochemie, Chemie und Pharmazie

der Johann Wolfgang Goethe-Universität

in Frankfurt am Main

von Elina Nürenberg-Goloub

aus Riga

Frankfurt am Main, 2018

Vom Fachbereich 14
Biochemie, Chemie und Pharmazie
der Johann Wolfgang Goethe-Universität
als Dissertation angenommen

Dekan: Prof. Dr. Clemens Glaubitz

1. Gutachter: Prof. Dr. Robert Tampé
2. Gutachter: Prof. Dr. Michaela Müller-McNicoll

Datum der Disputation:

Publications:

Nürenberg-Goloub E, Heinemann H, Gerovac M, and Tampé R (2018). Ribosome recycling is coordinated by processive events in two asymmetric ATP sites of ABCE1. *Life Science Alliance* 1: e201800095.

Gouridis G, Hetzert B, Kiosze-Becker K, de Boer M, Heinemann H**, Nürenberg-Goloub E**, Cordes T, and Tampé R. Dynamics of the ribosome recycling factor ABCE1 controlled by an asymmetric conformational equilibrium.
Manuscript in preparation.

Kiosze-Becker K, Ori A, Gerovac M, Heuer A, **Nürenberg-Goloub E**, Rashid UJ, Becker T, Beckmann R, Beck M, and Tampé R (2016). Structure of the ribosome post-recycling complex probed by chemical cross-linking and mass spectrometry. *Nature Communications* 7: 13248.

Nürenberg E, and Tampé R (2013). Tying up loose ends: ribosome recycling in eukaryotes and archaea. *Trends in Biochemical Sciences* 38: 64-74.

"Nothing is more evident than that Nature hates Mind."

Oscar Wilde

Table of Contents

Declaration 13

Zusammenfassung 15

Abstract 19

1. Introduction 21

1.1. Translation 21

1.1.1. Features of the ribosome 22

1.1.2. Initiation 24

1.1.3. Elongation 27

1.1.4. Termination 29

1.1.5. Ribosome recycling 30

1.1.6. mRNA surveillance and ribosome-based quality control 32

1.2. Structure and mechanics of ABC proteins 35

1.3. The ribosome recycling factor ABCE1 37

Aims of this Work 39

2. Results and Discussion 41

2.1. Molecular mechanism of ribosome recycling by ABCE1 41

2.1.1. Asymmetry and allostery in ABCE1 42

2.1.2. Pre-splitting complex formation 45

2.1.3. Ribosome splitting 49

2.1.4. ABCE1 occludes two nucleotides to split the ribosome 52

2.1.5. Formation of the post-splitting complex 54

2.1.6. Molecular model of ribosome recycling – A novel ABC-type mechanism 57

2.2. The archaeal post-splitting complex 61

2.3. Tying up loose ends: ABCE1 in translation initiation 65

2.3.1. Reconstitution of archaeal translation initiation 65

2.3.2. Structural studies of archaeal translation initiation complexes 67

Loose Ends – The Outlook 71

3. Material and Methods 73

3.1. General microbiological and biochemical methods 73

3.1.1. Bacterial strains and media 73

3.1.2. Growth of *S. solfataricus* 74

3.1.3. Transformation of *E. coli* 74

3.1.4. Agarose gel electrophoresis 75

3.1.5. Urea-PAGE 75

3.1.6. SDS-PAGE 75

3.1.7. Immunoblotting 76

3.1.8. Size exclusion chromatography (SEC) 77

3.1.9. Sucrose density gradient (SDG) centrifugation 77

3.2. Molecular genetics 79

3.2.1. Cloning 79

3.2.2. Site directed mutagenesis 79

3.2.3. Plasmid preparation and sequencing 80

3.3. Expression and purification of proteins and tRNA 81

3.3.1. ABCE1 82

3.3.2. aRF1 and aPelota 83

3.3.3. aIF6 83

3.3.4. Initiation factors 84

3.3.4.1 aIF1 84

3.3.4.2 aIF1A 84

3.3.4.3 aIF2α 85

3.3.4.4 aIF2β 85

3.3.4.5 aIF2γ 86

3.3.4.6 aIF5B 86

3.3.5. MetRS 87

3.3.6. tRNA 87
3.4. Purification of ribosomal particles 89
3.4.1. *Thermococcus celer* ribosomes 89
3.4.2. *Sulfolobus solfataricus* ribosomes 89
3.5. Biochemical activity assays 91
3.5.1. Radioactive ATPase assay 91
3.5.2. Nucleotide occlusion assay 91
3.5.3. 70S binding assay 92
3.5.4. Ribosome splitting assay 92
3.5.5. 30S binding assay 92
3.6. Assembly of the archaeal initiation complex 93
3.6.1. tRNA methionylation 93
3.6.2. Pelleting assay 93
3.6.3. SDG centrifugation binding assay 93
3.6.4. Co-immunoprecipitation 94
3.7. Cryo- and negative stain electron microscopy 95
3.7.1. Sampe preparation 95
3.7.2. Negative stain-EM 95
3.7.3. Cryo-EM of the archaeal post-splitting complex 96
3.7.4. Model building of the archaeal post-splitting complex 96
3.7.5. Cryo-EM of the archaeal initiation complexes with ABCE1 96
3.8. Graphics 98
References 99
Supplementary Information 109
Abbreviations 117
Danksagung ..... **Fehler! Textmarke nicht definiert.**
Curriculum vitae ..... **Fehler! Textmarke nicht definiert.**

Declaration

Except where stated otherwise by reference or acknowledgment, the work presented was generated by myself under the supervision of my advisors during my doctoral studies or by students that were supervised by me. The material listed below was obtained in the context of collaborative research.

Figure 13: Interactions within the post-splitting complex of Archaea and Eukarya.
Collaboration partner: Prof. Roland Beckmann, LMU, Munich. All sample optimization and preparation was done by Elina Nürenberg-Goloub and Holger Heinemann; Cryo electron microscopy, image processing and calculation of the final electron density map were done by Dr. André Heuer, Dr. Thomas Becker, Lukas Kater, Ivan Penchev, Hanna Kratzat, Dr. Otto Berninghausen, and Susanne Rieder. Model building and refinement were done by Elina Nürenberg-Goloub with the help of Dr. Christoph Thomas. The Figure was entirely designed and prepared by Elina Nürenberg-Goloub.

Figure 15: Intermediate resolution cryo-EM of archaeal translation initiation complexes.
Collaboration partner: Prof. Roland Beckmann, LMU, Munich. All sample optimization and preparation was done by Elina Nürenberg-Goloub and Holger Heinemann; Cryo electron microscopy, image processing and calculation of the final electron density map were done by Dr. André Heuer, Dr. Thomas Becker, Lukas Kater, Ivan Penchev, Hanna Kratzat, Dr. Otto Berninghausen, and Susanne Rieder. The Figure was entirely designed and prepared by Elina Nürenberg-Goloub.

Whenever a figure, table or text is identical to a previous publication, it is stated explicitly in the thesis and copyright permission and/or co-author agreement has been obtained.

The following parts of the thesis have been previously published:

Chapter 2.1 "Molecular mechanism of ribosome recycling by ABCE1"
in *Life Science Alliance* 1 (2018) as "Ribosome recycling is coordinated by processive events in two asymmetric ATP sites of ABCE1" by Elina Nürenberg-Goloub, Holger Heineman, Milan Gerovac, and Robert Tampé:
Figures "7 (modified), 8, 9, 10, 11, 12" and
Supplemental Figures "S1, S2, S3, S4, S5, S6"

Zusammenfassung

Proteinbiosynthese ist ein essentieller zellulärer Prozess, der in allen Königreichen des Lebens konserviert ist. Die Aminosäuresequenz für jedes Protein ist als Abfolge von jeweils drei Desoxyribonukleinbasen, den sogenannten Codons, in den entsprechenden Genen kodiert. Diese werden auf *messenger* Ribonukleinsäuren (mRNS) kopiert und anschließend Codon für Codon in Proteine übersetzt. Der Weg von einer Genomsequenz, über die mRNS zur Aminosäuresequenz wurde als „zentrales Dogma der Molekularbiologie“ 1958 von Francis Crick beschrieben. Die vorliegende Arbeit befasst sich mit der Übersetzung (Translation) der mRNS in eine Aminosäuresequenz. Translation findet in der Zelle am Ribosom statt, einem makromolekularen Komplex, welcher in zwei dynamischen Untereinheiten organisiert ist. Jede Untereinheit besteht aus großen ribosomalen RNS (rRNS) Molekülen und dutzenden peripheren Proteinen (Ramakrishnan, 2014). Die Translation wurde in Lehrbüchern als linearer Prozess betrachtet und in drei Phasen unterteilt; die Initiation, Elongation und Termination. Während der Initiation werden die ribosomalen Untereinheiten auf einer aktivierten mRNS zu einem funktionalen Ribosom zusammengebaut. Im aktiven Zentrum des initiierten Ribosoms befindet sich die erste *transfer* RNS (tRNS), ein Adapter zwischen dem Startcodon auf der mRNS und dem N-terminalen Methionin des Proteins (Hinnebusch and Lorsch, 2012). Während der Elongation bewegt sich das Ribosom entlang der mRNS und gibt die Codons eins nach dem anderen für die entsprechenden tRNS frei. Die Bildung neuer Peptidbindungen wird von konservierten Basen der rRNS katalysiert (Voorhees and Ramakrishnan, 2013). Sobald das Ribosom ein Stoppcodon erreicht, wird das Polypeptid durch eine Hydrolysereaktion freigesetzt und das Ribosom bleibt als Post-Terminationskomplex (Post-TK) mit den gebundenen mRNS und tRNS erhalten (Hellen, 2018). Es war seit langem bekannt, dass bakterielle Post-TK durch spezifische Recyclingfaktoren aktiv in die ribosomalen Untereinheiten gespalten wurden. Die kleine Untereinheit wird zeitgleich an Initiationsfaktoren weitergegeben, was die bakterielle Translation über die vierte Recycling-Phase als zyklischen Prozess definiert. In Archaeen und Eukaryoten war wenig über Ribosom-Recycling bekannt, bis das *ATP-binding cassette* (ABC) Protein der Unterfamilie E, ABCE1, als wichtigster Ribosom-Recycling-Faktor parallel in den

archaealen, Hefe- und Säugetiersystemen identifiziert wurde (Nürenberg and Tampé, 2013). Es ist bemerkenswert, dass ABCE1 ursprünglich eine katalytische Rolle bei der eukaryotischen Initiation zugeschrieben wurde. Das Ziel dieser Arbeit bestand darin, den archaealen und eukaryotischen Translationszyklus zu schließen, indem der molekulare Mechanismus des Ribosom-Recycling durch ABCE1 aufgedeckt und dessen Verbindung zur Initiation definiert werden.

Neben zahlreichen, gut erforschten translationalen GTPasen ist ABCE1 der einzige ATP-abhängige essentielle Faktor. Die in ATP gespeicherte Energie wird durch zwei Nukleotid-Bindedomänen (NBD) und eine konservierte Eisen-Schwefel-Cluster Domäne für die Spaltung des Ribosoms in seine Untereinheiten verbraucht. In dieser Arbeit definiere ich, wie die allosterisch gekoppelten Bindung und Hydrolyse von ATP in zwei asymmetrischen aktiven Zentren (*sites*) von ABCE1 die Spaltung des Ribosoms antreiben und regulieren. Dafür wurden Mutanten des lebenswichtigen ABCE1 Proteins generiert, erfolgreich exprimiert und gereinigt. Der Austausch funktional bedeutender Aminosäuren konnte entweder den Einschluss oder die Hydrolyse von ATP in einem oder beiden *sites* verhindern. Übereinstimmend mit der Funktionsweise von ABC-Proteinen, können die *sites* von ABCE1 beim ATP-Einschluss schließen und nach der ATP Hydrolyse wieder öffnen. Messungen der ATPase-Aktivität von freiem Wildtyp ABCE1 und den Mutanten zeigten, dass *site I* ein hohes ATP-Umsatzpotential hat und *site II* hingegen ATP nur langsam hydrolysiert. Die demnach „*power site*“ genannte *site I* wird jedoch nur durch den Einschluss von ATP in *site II* aktiviert, welche hierfür entsprechend den Namen „*control site*“ erhält. Bindungsstudien mit isolierten archaealen Ribosomen zeigten, dass der ATP-Einschluss in der *control site* für die Bindung des Post-TK notwendig ist. Dem folgt die allosterische Aktivierung der *power site*. Solange die langsame *site II* ein ATP-Molekül hydrolysiert, setzt die schnelle *site I* mehrere ATP-Moleküle um, ohne die geschlossene Konformation einzunehmen. Dieser Hydrolysemodus erlaubt ABCE1, recycling-kompetente Ribosomen von allen anderen Spezies zu unterscheiden. Erst der Einschluss eines weiteren ATP-Moleküls und somit das Schließen der *site I* führt zu einer Rotationsbewegung der Eisen-Schwefel-Cluster-Domäne und hat die Spaltung des Ribosoms in seine Untereinheiten zur Folge. ABCE1 bleibt anschließend an der kleinen ribosomalen Untereinheit gebunden, welche dann als Post-Spaltungskomplex (Post-SK) bezeichnet wird. Auch die

Bindung an die kleine ribosomale Untereinheit wird von der *control site* gesteuert. Die ATPase-Aktivität in beiden *sites* von ABCE1 im Post-SK ist deutlich herabgesenkt. Die Freisetzung von ABCE1 erfordert die Hydrolyse beider gebundenen ATP-Moleküle und Öffnung beider *sites*. Somit durchläuft ABCE1 während des Ribosom-Recyclings einen allosterisch gekoppelten Zyklus von sequentiellem Schließen und Öffnen beider *sites* in Übereinstimmung mit dem *processive clamp* Modell für die Funktion von ABC-Proteinen. Die Beschreibung des molekularen Mechanismus von ABCE1 erklärt auch die Auswirkungen früher beschriebener ABCE1-Mutanten auf die Lebensfähigkeit, das Wachstum und die Differenzierung der Zelle (Nürenberg-Goloub et al., 2018).

Da ABCE1 zusätzlich zur Ribosom-Recycling-Aktivität auch die Assoziation der Untereinheiten verhindert, hält der Post-SK kleine ribosomale Untereinheiten für die Bindung aktivierter mRNS und Initiationsfaktoren bereit und trägt somit als zentraler makromolekularer Komplex zwischen Ribosom-Recycling und Translationsinitiation zur Ribosomhomöostase und der Translationsregulation in der Zelle bei (Gerovac and Tampé, 2018). In dieser Arbeit wird die Struktur des archaealen Post-Spaltungskomplexes mittels Kryo-Elektronenmikroskopie (Kryo-EM) aufgeklärt. Er ähnelt dem zuvor beschriebenen eukaryotischen Post-SK. Die Konformation von ABCE1 ist vollständig geschlossen und bestätigt somit den oben beschriebenen molekularen Mechanismus des Ribosom-Recycling (Heuer et al., 2017; Kiosze-Becker et al., 2016). Die Eisen-Schwefel-Cluster-Domäne nimmt eine neue Position am 30S Ribosom ein und interagiert mit der konservierten 16S rRNS Helix 44 sowie dem universell konservierten ribosomalen Protein uS12. Konservierte Arginin-Reste von ABCE1 wechselwirken mit der 16S rRNA und dem ribosomalen Protein eS6. Bemerkenswert ist der in Archaeen ebenfalls konservierte Mechanismus der Rotation der Eisen-Schwefel-Cluster-Domäne. Wie auch in der Hefe, entfaltet eine Helix am Übergang zur NBD1, um einen flexiblen *loop* zu bilden. Dieser wird durch ionische Interaktionen dreier Aminosäurereste miteinander sowie mit dem Peptidrückgrat des *loops* stabilisiert.

Um den Translationszyklus strukturell zu schließen, wurde die archaeale Initiation vollständig rekonstituiert. Dazu wurden die Initiationsfaktoren aIF1, aIF1A und aIF2 sowie die initiale tRNS rekombinant exprimiert und gereinigt. Die tRNS wurde *in vitro* mit Methionin beladen. Zusätzlich wurde synthetisch hergestellte mRNS für den

Zusammenfassung

Aufbau von Initiationskomplexen auf Basis des Post-Spaltungskomplexes in Anwesenheit von ABCE1 verwendet. Die Bildung der Komplexe wurde biochemisch untersucht und deren Struktur mittels Kryo-EM in intermediärer Auflösung aufgeklärt. Co-Immunpräzipitation aller Initiationsfaktoren sowie der 30S ribosomalen Untereinheit zusammen mit ABCE1 zeigte, dass archaeale Initiation am post-SK stattfinden kann. In der Kryo-EM konnte zusätzlich zu ABCE1 den Faktoren aIF1, aIF1A sowie der tRNS Elektronendichte über die 30S Untereinheit hinaus eindeutig zugeordnet werden. Hochauflösende Kryo-EM Aufnahmen der hergestellten und bereits eingefrorenen Komplexe werden Aufschluss über direkte oder indirekte Interaktionen von ABCE1 mit den Initiationsfaktoren sowie den Einfluss von ABCE1 auf die Dynamik bedeutender Strukturen des 30S Ribosoms geben. Somit schließt diese Arbeit funktional und strukturell den archaealen Translationszyklus nach dem bakteriellen Vorbild und ebnet den Weg für ein ganzheitliches Verstehen der Proteinbiosynthese.

Abstract

Protein biosynthesis is a conserved process, essential for life. Proteins are assembled from single amino acids according to their genetic blueprint in the form of a messenger ribonucleic acid (mRNA). Peptide bond formation is catalyzed by ancient ribonucleic acid (RNA) residues within the supramolecular ribosomal complex, which is organized in two dynamic subunits (Ramakrishnan, 2014). Each subunit comprises large ribosomal RNA (rRNA) molecules and several dozens of peripheral proteins. mRNA translation has been divided into three phases, namely translation initiation, elongation and termination in biochemistry textbooks. During initiation, the ribosomal subunits assemble into a functional ribosome on an activated mRNA and acquire the first transfer RNA (tRNA), an adapter between the start codon on the mRNA and the N-terminal methionine of the protein (Hinnebusch and Lorsch, 2012). During elongation, the ribosome translocates along the mRNA exposing one codon after the other, and amino acids are delivered to the ribosome by the respective tRNAs, and attached to the nascent polypeptide chain. During termination, the polypeptide is released and the ribosome remains loaded with mRNA and tRNA at the end of the open reading frame for the translated gene (Hellen, 2018). Bacterial ribosomes are subsequently recycled by a specific ribosome recycling factor and the small ribosomal subunit is simultaneously consigned to initiation factors for a next round of translation – rendering bacterial translation as a cyclic process with an additional ribosome recycling phase. However, the process of ribosome recycling remained enigmatic in Eukarya and Archaea until the simultaneous discovery of the twin-ATPase ABCE1 as the major ribosome recycling factor. Strikingly, ABCE1 has initially been shown to participate in translation initiation (Nürenberg and Tampé, 2013). Thus, closing the translation cycle by revealing the detailed molecular mechanism of ABCE1 and its role for translation initiation are the two goals of this research.

Beyond the plenitude of well-studied translational GTPases, ABCE1 is the only essential factor energized by ATP, delivering the energy for ribosome splitting *via* two nucleotide-binding sites. Here, I define how allosterically coupled ATP binding and hydrolysis events in ABCE1 empower ribosome recycling. ATP occlusion in the low-

turnover control site II promotes formation of the pre-splitting complex and facilitates ATP engagement in the high-turnover site I, which in turn drives the structural re-organization required for ribosome splitting. ATP hydrolysis and ensuing release of ABCE1 from the small subunit terminate the post-splitting complex. Thus, ABCE1 runs through an allosterically coupled cycle of closure and opening at both sites consistent with a processive clamp model. This study delineates the inner mechanics of ABCE1 and reveals why various ABCE1 mutants lead to defects in cell homeostasis, growth, and differentiation (Nürenberg-Goloub et al., 2018).

Additionally, a high-resolution cryo-electron microscopy (EM) structure of the archaeal post-splitting complex was obtained, revealing a central macromolecular assembly at the crossover of ribosome recycling and translation initiation. Conserved interactions between ABCE1 and the small ribosomal subunit resemble the eukaryotic complex (Heuer et al., 2017). The conformational state of ABCE1 at the post-splitting complex confirms the molecular mechanism of ribosome recycling uncovered in this study. Moving further along the reaction coordinate of cellular translation, I reconstitute the complete archaeal translation initiation pathway and show that essential archaeal initiation factors are recruited to the post-splitting complex by biochemical methods and cryo-EM structures at intermediate resolution. Thus, the archaeal translation cycle is closed, following its bacterial model and paving the way for a deeper understanding of protein biosynthesis.

1. Introduction

1.1. Translation

Translation of the genetic information into functional polypeptides marks a revolution in the development of life and constitutes an ancient and essential process in every living cell. The origin of translation is inextricably related to the universal genetic code as described by Carl Woese (Woese, 2001). Since the initial direct recognition of nucleobases by amino acids (Woese, 1968), evolution has assembled large ribonucleoprotein (RNP) complexes to catalyze translation and developed a sophisticated network to regulate and survey it. In contemporary life, genetic information is more or less securely stored in large deoxyribonucleic acid (DNA) molecules termed chromosomes and organized in genes, regulatory elements, and junk DNA with yet unknown function (Bickmore and van Steensel, 2013). Upon requirement, highly regulated cellular mechanisms allow the transcription of a requested gene into messenger ribonucleic acid (mRNA). Decoding of the mRNA triplet code into a polypeptide chain is coordinated and catalyzed within the ribosome, a macromolecular factory comprising ribosomal RNA (rRNA) and proteins (rps) which build a functional translating element (70S/80S ribosomes in Prokarya/Eukarya) out of a small (30S/40S) and large (50S/60S) subunit. Transfer RNAs (tRNAs) function as adapter molecules, carrying an antisense triplet to decode the mRNA and deliver the correct amino acid to elongate the polypeptide chain accordingly. The tightly coupled assembly, translocation and disassembly of the ribosome as well as the delivery of tRNA is managed by translation factors and divided into four phases: initiation, elongation, termination and ribosome recycling. The complexity of each phase increases with the complexity of the living cell. Bacteria utilize few translation factors and begin decoding of their polycistronic mRNAs simultaneously with transcription, while Eukarya process their monocistronic messages post-transcriptionally in the nucleus, export them into the cytoplasm and translate them with the help of numerous additional proteins. Archaea adopted bacterial and eukaryotic features, in accordance with their position in the phylogenetic tree, and adapted them to often harsh survival conditions they were confronted with. Therefore, Archaea exhibit a yet neglected third mechanism of translation.

1.1.1. Features of the ribosome

The ribosomal subunits consist of universally conserved core rRNA and rps but also of shell elements specific for each phyla, organism and even organelle (Greber and Ban, 2016; Jenner et al., 2012; Klinge et al., 2012; Ramakrishnan, 2014; Steitz, 2008). Distinguishing features of specialized ribosomes within one cell contribute to the selectivity of gene translation, introducing an additional regulatory level to protein biosynthesis (Xue and Barna, 2012). Prokaryotic 70S ribosomes (Figure 1) have a molecular mass of 2.5 MDa; the large 50S (1.6 MDa) subunit harbors two rRNAs (23S and 5S) and around 30 rps, while the small 30S (0.9 MDa) subunit comprises one 16S rRNA molecule and approximately 20 rps. The larger 4.5 MDa eukaryotic 80S consists of the 60S (2.8 MDa) subunit with 18S, 5.8S, and 5S rRNA supported by almost 50 rps, as well as the small 40S (1.4 MDa) subunit harboring 18S rRNA and more than 30 rps. A first structural impression of bacterial ribosomes was gained by negative stain-electron microscopy (EM) in 1976, revealing a model of the large ribosomal subunit embracing the small one (Lake, 1976). An assembled ribosome is highly dynamic and undergoes large conformational rearrangements of the two subunits against each other as well as within each subunit (Aitken et al., 2010; Puglisi et al., 2000; Steitz, 2008). The conserved interface composes three ribosomal tRNA binding sites for aminoacylated tRNA (A-site), peptidyl-tRNA (P-site), and deacylated tRNA (E-site, exit site) (Agrawal et al., 1996; Rheinberger et al., 1981; Stark et al., 1997). The conserved and elastic helix 44 (h44) of the 16S/18S rRNA maintains subunit association during translocation and contributes to translation fidelity (Jenner et al., 2010; Liu and Fredrick, 2016; Qin et al., 2012). The mRNA can be recruited by conserved motifs (anti-Shine-Dalgarno/anti-Kozak in Prokarya/Eukarya) at the 3'-end of the 16S/18S rRNA, in close proximity of h44. During translation, the mRNA moves codon by codon along the mRNA entry site past the tRNA binding sites, between the body and head of the small subunit. Catalysis takes place deep within the large ribosomal subunit, in the conserved peptidyl transferase center (PTC) constituted by the 23S/28S (Prokarya/Eukarya) rRNA component. The emerging polypeptide is pushed through the peptide exit tunnel, which is approximately 100 Å long and allows folding of the nascent chain into helical secondary structures in a shielded environment (Aitken et al., 2010; Klinge et al., 2012; Ramakrishnan, 2014; Steitz, 2008). At the solvent exposed side of the large subunit, the N-terminus of the partially folded polypeptide encounters chaperones,

signal recognition particles for trafficking, or other regulatory factors (Kramer et al., 2009). The sarcin-ricin loop (SRL) in the 23S/28S rRNA and the P-stalk control translational factors, which orchestrate each phase of protein synthesis (Voorhees and Ramakrishnan, 2013). Consequently, cleavage of the SRL by the toxins sarcin and ricin results in total arrest of translation and cell death (Garcia-Ortega et al., 2010). De novo synthesis of ribosomal subunits requires over 200 additional proteins and is therefore a highly energy-intensive process for the cell (Kressler et al., 2017). Disorders in ribosome biogenesis are connected to various human diseases referred to as ribosomopathies (Mills and Green, 2017; Narla and Ebert, 2010). On the other hand, deactivation of ribosomes immediately arrests the synthesis of all proteins and can protect cells from viral assault or starvation. Thus, ribosome homeostasis is critical during cell stress, development and proliferation.

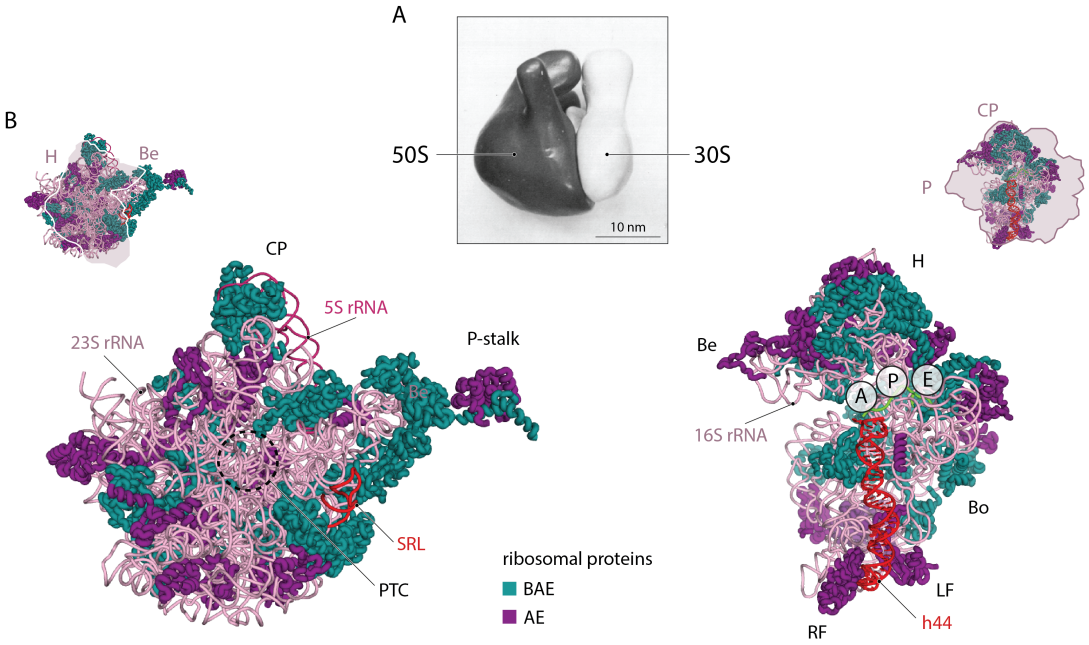

Figure 1: Structural features of the archaeal ribosome. A) The historical model of a bacterial 70S ribosome gained in 1976 illustrates its basic assembly from two subunits embracing each other at their interface (Lake, 1976). **B)** Structures of archaeal ribosomal subunits, with their interfaces oriented toward the viewer. The thumbnails illustrate the position of the opposing subunit within the assembled 70S complex. Universally conserved proteins found in Bacteria, Archaea and Eukarya (BAE) are distinguished from proteins only found in Archaea and Eukarya (AE). The conserved PTC is inwardly buried within the 23S rRNA component of *Haloarcula marismortui* 50S (PDB 4V9F). The 5S rRNA only found in Archaea and Eukarya is located at the central protuberance (CP). The P-stalk and SRL are in control of translational GTPases. The archaeal 30S subunit from *Pyrococcus abysii* (PDB 5JBH, 5JB3) has a universally conserved, characteristic duck-like shape. A head (H) with a beak (Be) and a body (Bo) with a right (RF) and left foot (LF) can adopt different conformational states to permit or prevent initiation. The mRNA is guided along the ribosomal A-, P-, and E-sites. The conserved helix 44 (h44) spans the 30S body from head to feet.

1.1.2. Initiation

The term "initiation" describes the assembly of a translation-competent ribosome (70S/80S) on a particular mRNA molecule to begin decoding of its genetic information. Bacterial initiation is kinetically controlled and requires only three initiation factors (IFs). IF3 removes the previously translated mRNA and deacylated tRNA from the 30S subunit, maintains initiation fidelity, and regulates ribosome homeostasis in the cell. IF2 recruits the acylated initiator-$tRNA_i$ and promotes joining

of the 50S ribosomal subunit. IF1 controls the molecular dynamics of the small ribosomal subunit, modulates the selection of mRNA and tRNA, and stabilizes IF2 and IF3 within the pre-initiation complex (PIC). The start codon, universally an AUG at the beginning of each open reading frame (ORF), is distinguished by the purine-rich Shine-Dalgarno (SD) motif in the 5'-untranslated region (5'-UTR) of the mRNA. The SD pairs with a complementary sequence (anti-SD) of the 16S rRNA component of the bacterial small ribosomal subunit (Kozak, 1999; Milon and Rodnina, 2012; Rodnina and Wintermeyer, 2009).

Canonical initiation in Eukarya is extensively, but still not exhaustively described. It begins in the cytoplasm with the activation of mRNA previously modified by a 7-methyl-guanosine (m^7G) 5'-Cap and a poly-adenosine (poly-A) 3'-tail in a closed loop structure by the multisubunit initiation factor 4 (eIF4) and poly-A-binding proteins (PABPs). The activated mRNA is recognized by the 43S PIC, which comprises the small ribosomal subunit (40S), eIF1 (functional homolog of IF3), eIF1A (ortholog of IF1), the eIF2 ternary complex with the methionylated initiator-$tRNA_i$ and GTP, the enormous eIF3 complex, and eIF5. The 43S PIC then begins 5'-3'-scanning along the activated mRNA until the antisense loop of $tRNA_i$ matches the start codon and arrests the complex in a 48S pre-initiation state. The GTPase eIF5B (ortholog of IF2) provokes displacement of other initiation factors and catalyzes subunit joining, which results in an 80S initiation complex ready for the elongation phase (Jackson et al., 2010; Kozak, 1999; Rodnina and Wintermeyer, 2009). As in Bacteria, archaeal transcription and translation are coupled, allowing the two central processes to regulate each other (French et al., 2007). Structural and functional studies with *in vitro*-reconstituted initiation systems from *Sulfolobus solfataricus* show that Archaea utilize IFs similar to their eukaryotic orthologs, but the sequence of events follows the bacterial route (La Teana et al., 2013). Polycistronic archaeal mRNAs initiate *via* the classical SD/anti-SD interaction with the 30S subunit (Benelli et al., 2003). However, leaderless monocistronic mRNA devoid of a 5'-UTR are prevalent in *Sulfolobus sp.* (She et al., 2001) and require the interaction of Met-$tRNA_i$ with the AUG start codon to initiate at 30S or 70S (Benelli et al., 2003; Moll et al., 2004). As in Eukarya, the fidelity of this interaction on 30S subunits is monitored by aIF1 (ortholog of eIF1, both functional homologs of IF3), while aIF1A (ortholog of eIF1A and IF1) has synergistic stimulatory effects on aIF2 (homolog of eIF2) binding (Hasenohrl et al., 2009; Passmore et al., 2007; Pestova et al., 1998). In contrast to its eukaryotic counterpart,

aIF2 does not function as a Met-tRNA$_i$ shuttle in the cytoplasm, but is bound to 30S ribosomal subunits together with aIF1 and aIF1A, where it recruits Met-tRNA$_i$ similar to bacterial IF2 (Hasenohrl et al., 2009; Milon et al., 2010; Richter and Lipmann, 1970). On the 30S, aIF2 acts like a spring (Figure 2) and directly assists Met-tRNA$_i$ in probing for a cognate start codon (Coureux et al., 2016), a mechanism putatively essential for translation of leaderless mRNAs. Interestingly, aIF2 globally regulates translation and mRNA homeostasis during cell stress by shielding the 5'-triphosphates of the messages. This specific interaction requires an additional factor termed translation recovery factor (Trf) to be resolved after stress relief (Martens et al., 2014). A regulatory function in translation initiation has also been assigned to eIF2 (Clemens et al., 1982; Leroux and London, 1982), emphasizing the central role of these factors for translational control in both kingdoms of life. In absence of functional e/aIF2, Met-tRNA$_i$ can be efficiently recruited to the small ribosomal subunit by e/aIF5B (homologs of IF2) to rescue translation (Dmitriev et al., 2011; Maone et al., 2007; Terenin et al., 2008). GTP-dependent subunit joining by aIF5B constitutes the last step of archaeal translation initiation and yields an elongation competent 70S ribosomal unit with acylated tRNA$_i$ tightly bound to the AUG start codon in the ribosomal P-site.

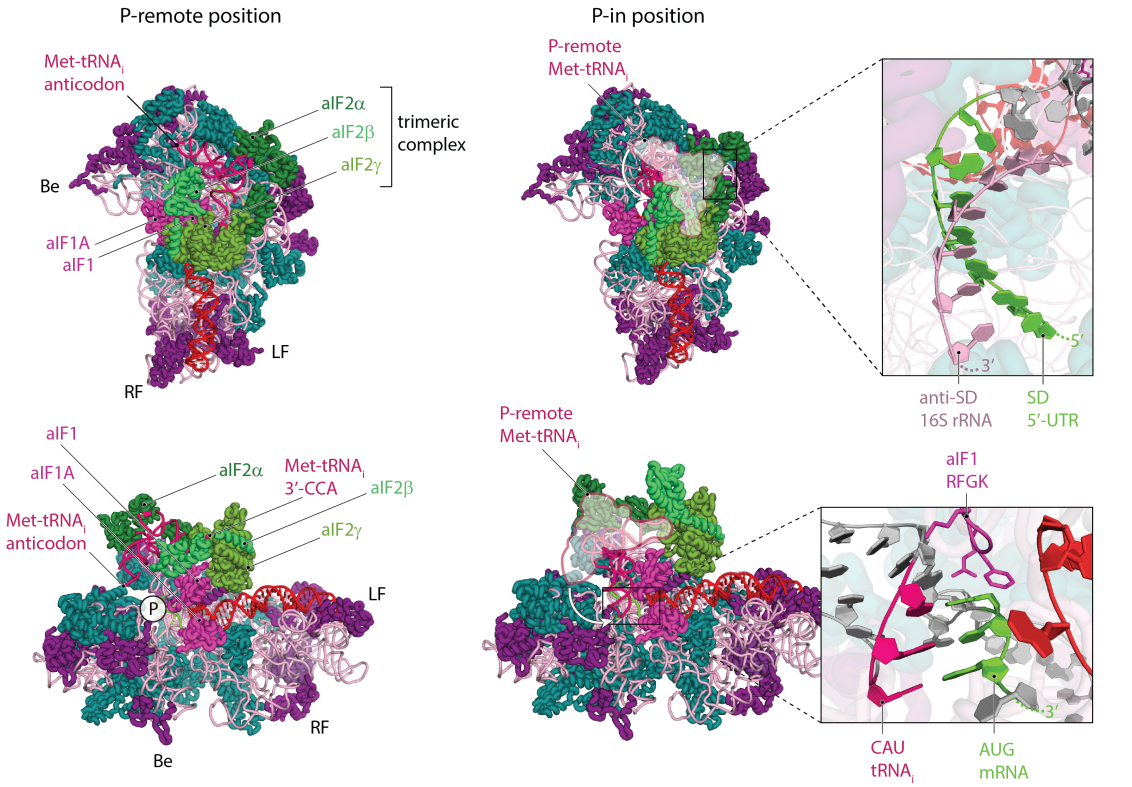

Figure 2: General mechanism of canonical initiation in Archaea. rRNA and rps are colored as in Figure 1. The initiation factors 1 and 1A bind in close proximity of the P-site, at the base of helix 44, to control the fidelity of initiation and accelerate aIF2 recruitment, respectively. In the absence of a P-site start codon (AUG), the trimeric aIF2 complex stabilizes Met-tRNA$_i$ in a P-remote state, with the anticodon loop swung out above the 30S head. mRNA (with or without start codon) within these *P. abysii* complexes (PDB 5JBH, 5JB3) initiates at the 5'-UTR *via* classical SD-anti-SD interaction at the 3'-end of 16S rRNA. If AUG is located at the P-site, aIF2 locks Met-tRNA$_i$ in a P-in position, where the anticodon can pair with the start codon. Conserved residues of aIF1 survey this interaction.

1.1.3. Elongation

During elongation, the nascent polypeptide chain is extended by individual amino acids within the ribosomal PTC in accord with the mRNA blueprint. Elongation factors (EFs) ensure efficiency and fidelity of this most conserved translation phase (Dever and Green, 2012; Rodnina and Wintermeyer, 2009). It begins with formyl-methionine (fMet, Bacteria) or methionine (Met, Eukarya and Archaea) delivered by tRNA$_i$ during initiation at the start codon in the ribosomal P-site. Canonical decoding of each subsequent codon requires correct pairing between the mRNA base triplet in the A-site and the cognate anti-codon of the respective aminoacylated tRNA (aa-tRNA).

The hydrolysis-sensitive aa-tRNAs are scavenged in the cytosol with nanomolar affinity (Gromadski et al., 2007) and delivered to the ribosomal A-site in a random, diffusion-controlled order by the homologous translational GTPases EF-Tu (Bacteria), eEF1 (Eukarya), or aEF1α (Archaea). GTP hydrolysis is stimulated by the sarcin-ricin loop (SRL) of the 23S/28S rRNA (Prokarya/Eukarya) component of the large ribosomal subunit, and the GDP-bound delivery factor dissociates (Voorhees et al., 2010). This allows either non-cognate tRNA to leave and liberate the A-site for another candidate, or enables ribosome translocation after successful decoding and elongation. The ribosome acts like an entropy trap (Sievers et al., 2004) and catalyzes the nucleophilic reaction by perfect positioning of the two amino acids within the PTC (Weinger et al., 2004). Interestingly, recent functional and structural data revealed the crucial role of the highly abundant and essential eukaryotic eIF5A in assisting the PTC independently of the translated codon by its conserved post-translationally attached hypusine moiety (Schmidt et al., 2016; Schuller et al., 2017). In contrast, the bacterial eIF5A homolog EF-P lacks hypusine, is not essential, and accelerates elongation only during formation of the first peptide bond and at sterically unfavorable sequences such as poly-proline (Doerfel et al., 2013; Glick and Ganoza, 1975; Schuller et al., 2017). The archaeal aIF5A is poorly characterized, but has strikingly common features with the eukaryotic eIF5A: it is hypusinylated at the same modification site and is essential for cell viability, at least in *Haloferax volcanii* (Gabel et al., 2013; Prunetti et al., 2016). Once a new peptide bond is formed, the ribosome and tRNA translocate along the mRNA in a ratchet-like movement including multiple transient intermediate states. The GTPases EF-G (Bacteria) or e/aEF2 (Eukarya/Archaea) are also controlled by the SRL and ensure directionality of translocation. At the end of each elongation cycle, the ribosomal A-site is free, while the P- and E-sites accommodate the peptidyl-tRNA and deacylated tRNA, respectively (Belardinelli et al., 2016; Dever and Green, 2012; Puglisi et al., 2000). Once an mRNA stop codon reaches the A-site, translation is terminated. In case of aberrant or truncated messages, as well as impassable secondary structures, multiple mRNA surveillance and ribosome quality control mechanisms ensure the detection and degradation of mRNA and nascent chain (Brandman and Hegde, 2016; Buskirk and Green, 2017; Dever and Green, 2012; Graille and Seraphin, 2012).

1.1.4. Termination

Canonical termination involves recognition of the stop codon in the ribosomal A-site and peptide release by the cooperative action of class I and class II release factors (RFs). Termination in Bacteria (Korostelev, 2011) differs significantly from the eukaryotic mechanism, while Archaea follow the eukaryotic route, albeit with a reduced set of factors (Dever and Green, 2012; Nürenberg and Tampé, 2013). Class I e/aRF1 comprise three flexible domains and structurally mimic a tRNA molecule (Song et al., 2000). They are delivered to the ribosomal A-site in a stable ternary complex with the translational GTPases eRF3 (Alkalaeva et al., 2006; Zhouravleva et al., 1995) or aEF1α (Kobayashi et al., 2012), both functional homologs of EF-G. In Eukarya, GTP hydrolysis and dissociation of eRF3 allows the full accommodation of eRF1 in the A-site, leading to peptide release. The decisive fidelity and efficiency of decoding factor accommodation during elongation (aa-tRNA), termination (eRF1) and mRNA surveillance (ePelota) depends on a complex interplay between decoding and (de-)stabilization of mRNA in the A-site, conformational changes of the small ribosomal subunit, in bacteria also referred to as domain closure (Ogle et al., 2002), activation of the respective delivery GTPase, and structural rearrangements within the decoding factor (Shao et al., 2016). The conserved NIKS motif in the N-terminal (N) domain of eRF1 recognizes the stop codon in a precise geometric arrangement, which includes mRNA compaction and aromatic stacking interaction with the A^{1825} base in the ribosomal helix 44 (Figure 3). The additional conserved GTS and YxCxxxF motifs in eRF1 discriminate against sense codons (Brown et al., 2015). Upon successful decoding, GTP hydrolysis within eRF3 is activated *via* the SRL, and eRF3•GDP dissociates. Thereby, the middle (M) domain of eRF1 is liberated and swings into the PTC, where the universally conserved GGQ motif assists the nucleophilic attack of a water molecule to release the nascent chain (Frolova et al., 1999). Notably, these structural rearrangements in class I RFs, rather than peptide release, mark the formation of a post-termination complex (post-TC) ready for ribosome recycling.

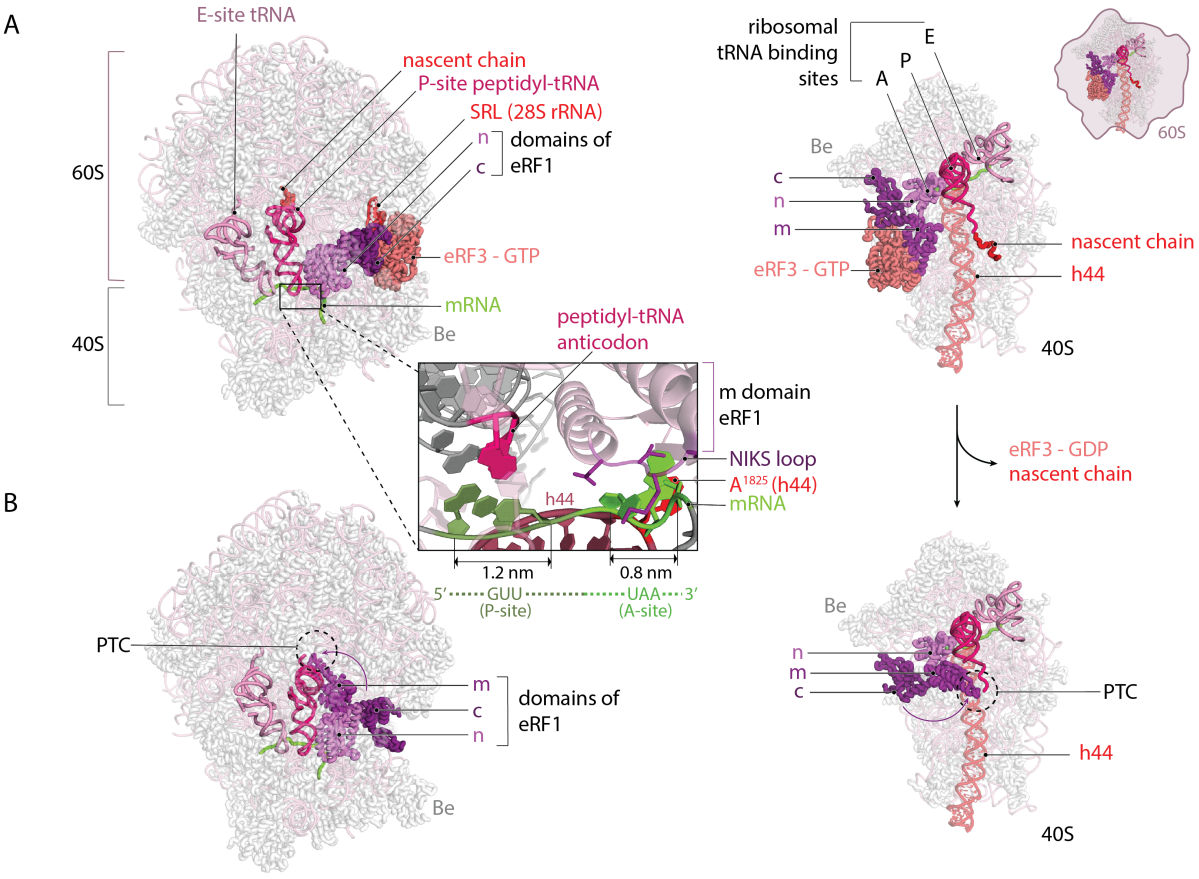

Figure 3: Decoding and peptide release during canonical termination. Cryo-EM reconstructions of the 80S **A)** pre-termination complex with eRF3•GTP (GMP-PNP) at the ribosomal GTPase control center and **B)** post-termination complex with fully accommodated eRF1. A hydrogen bonding network of the conserved NIKS-loop in the n-domain of eRF1 with 18S rRNA and compacted mRNA in the A-site restricts the identity of the bases, disqualifying sense codons during termination. 18S rRNA helix 44 (h44) participates in decoding, as base A^{1825} additionally stacks with the wobble position of the stop codon. Successful stop codon recognition activates GTP hydrolysis *via* the SRL of 28S rRNA and allows subsequent dissociation of eRF3. Thereby, the m-domain of eRF1 is unlocked and can swing into the PTC, allowing peptide bond hydrolysis by the conserved GGQ motif at the tip of the m-domain and release of the nascent chain.

1.1.5. Ribosome recycling

Within the canonical translation cycle, terminated ribosomes are recycled into free subunits. Ribosome recycling is tightly regulated and represents a key process in translational control. In Bacteria, a specific ribosome recycling factor (RRF) is delivered to the vacant A-site by EF-G to disassemble the bacterial post-TC. mRNA

and tRNA are removed from 30S by IF3, which can directly bridge over to the initiation phase (Karimi et al., 1999; Nürenberg and Tampé, 2013; Peske et al., 2005). In Eukarya and Archaea, ribosome recycling is executed by the essential and conserved ABC-type twin-ATPase ABCE1 (see section 1.2 and 1.3) in collaboration with the class I release factors in the A-site of the post-TC (Barthelme et al., 2011; Nürenberg and Tampé, 2013; Pisarev et al., 2010; Shoemaker and Green, 2011). ABCE1 attaches near the GTPase control center (Shao et al., 2016) and contacts the C-terminal (C) domain of the respective class I RF (Figure 4). ATP-dependent conformational changes of the nucleotide binding domains (NBDs) and the iron-sulfur cluster (FeS) domain in ABCE1 induce a translocation-like ribosome destabilization and disassembly (Pisarev et al., 2010). After splitting, ABCE1 remains at the small ribosomal subunit, establishing the post-splitting complex (post-SC) (Barthelme et al., 2011; Heuer et al., 2017; Kiosze-Becker et al., 2016; Nürenberg and Tampé, 2013). Within the post-SC, ABCE1 is in pole position to link ribosome recycling to translation initiation in a similar mode as bacterial IF3. Evidence on the role of ABCE1 in initiation was gained from human, fruit fly, and yeast systems before its definite assignment to ribosome recycling (Andersen and Leevers, 2007; Chen et al., 2006; Dong et al., 2004). Today, ribosome recycling is regarded as a regulatory gateway in canonical and aberrant translation and has been shown to be strongly connected to ribosome homeostasis (Young et al., 2015).

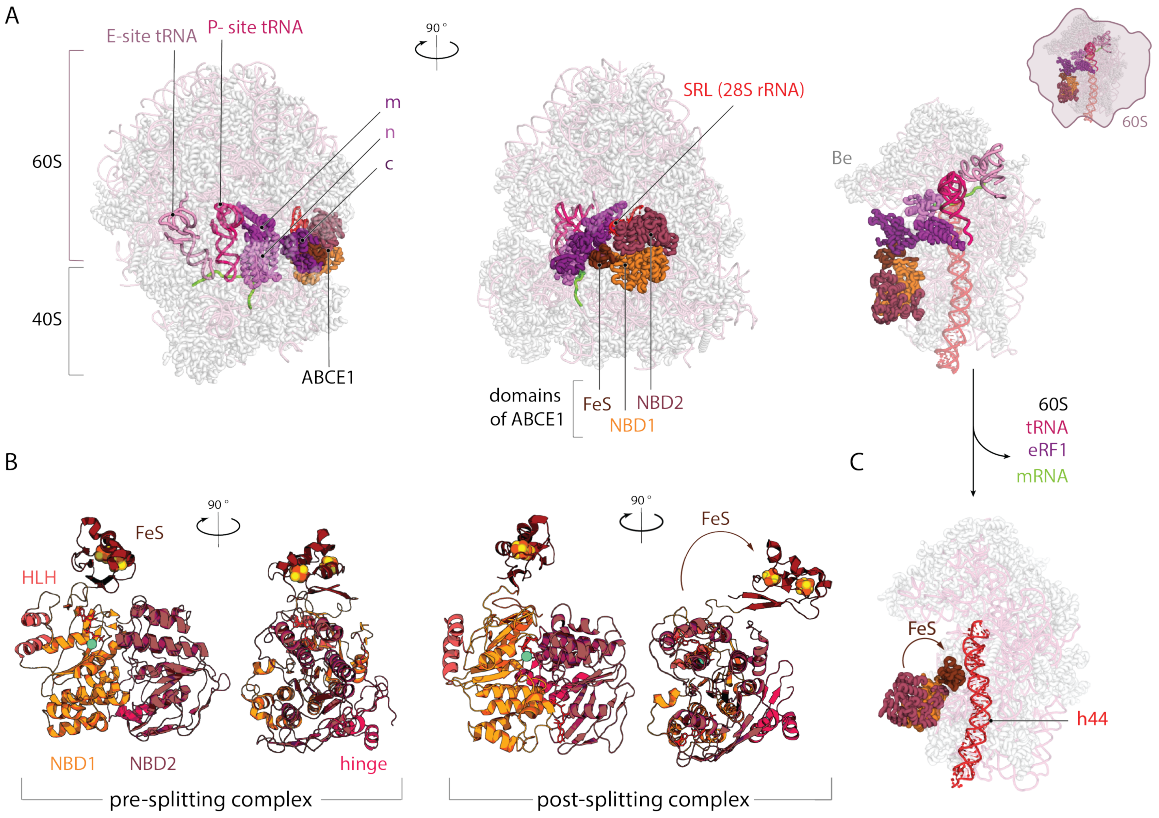

Figure 4: Recycling of eukaryotic and archaeal ribosomes by ABCE1. A) In the pre-SC (PDB 5LZV), ABCE1 occupies the ribosomal binding site for translational GTPases. NBD2 contacts the SRL and the FeS-cluster domain interacts with the C-terminal domain of eRF1 accommodated in the A-site. **B)** Upon binding of two ATP, the NBDs close and push the FeS-cluster domain into the ribosomal intersubunit space, leading to their destabilization and disassembly. **C)** At the post-SC (PDB 5LL6), the FeS-cluster domain contacts the conserved ribosomal decoding helix 44.

1.1.6. mRNA surveillance and ribosome-based quality control

Elongation can fail for numerous reasons, resulting in stalled ribosomes occupied by faulty mRNA and non-functional, potentially harmful polypeptides. Translational proofreading aims to eliminate mRNA, polypeptides and/or damaged ribosomes at the earliest time point, while they are still unambiguously connected to each other. Proofreading takes place directly at the ribosome, which allows the cell to simultaneously target aberrant polypeptides to the proteasome, degrade the respective mRNA, and activate stress response signaling (Brandman and Hegde, 2016; Graille and Seraphin, 2012). Bacteria utilize the trapped mRNA (tmRNA) molecule, a hybrid between tRNA and mRNA, and alternative rescue factors (Arfs),

like the small protein B (smpB), to append a specific sequence to the aberrant peptide, which serves as degradation signal (Graille and Seraphin, 2012; Huter et al., 2017; Keiler et al., 1996). Canonical termination and ribosome recycling are induced by a stop codon in the tmRNA, liberating the ribosome. mRNA is quickly degraded from its unprotected 3'-end. Thus, the bacterial pathway is highly efficient, as it requires only few additional components. On the other hand, it is strongly limited to stalls at truncated mRNA, since tmRNA only binds to A-sites of 70S lacking mRNA and tRNA. Notably, bacteria globally employ this quality control pathway to control co-translational protein folding (Hayes and Keiler, 2010), as well as during starvation to quickly adapt to environmental conditions (Keiler, 2008). The eukaryotic mRNA surveillance and ribosome-based quality control (RQC) system comprises multistep response pathways for a variety of translational errors induced by truncated or highly structured mRNAs (no-go decay, NGD), ORFs lacking (no-stop decay, NSD) or containing a premature in-frame stop codon (nonsense-mediated decay, NMD), aa-tRNA shortage, polypeptides blocking the ribosomal exit tunnel, or defective ribosomes (18S-NRD) (Brandman and Hegde, 2016; Buskirk and Green, 2017; Graille and Seraphin, 2012). After recognition by pathway-specific factors, the stalled 80S recruits the stop codon-independent release factor ePelota (Dom34 in yeast) and their delivery GTPase Hbs1 (Becker et al., 2011; Chen et al., 2010). Hbs1 senses the lengths of 3'-mRNA overhangs at the 80S (Shoemaker and Green, 2011) and recruits the superkiller (SKI) complex involved in fast degradation of the aberrant mRNA, in concert with the exosome and other nucleases (Graille and Seraphin, 2012; Saito et al., 2013). Subsequently, Hbs1 dissociates, leaving a post-termination complex with intact peptidyl-tRNA in the P-site and ePelota in the A-site. This complex is a substrate for the ribosome recycling factor ABCE1 (Becker et al., 2012; Nürenberg and Tampé, 2013; Pisarev et al., 2010; Shoemaker and Green, 2011). Erroneous peptide targeting and stress signaling take place downstream of recycling at 60S subunits harboring the intact peptidyl-tRNA and involve numerous factors with yet incompletely defined roles and operation modes (Brandman and Hegde, 2016). Remarkably, especially the NMD pathway is tightly coupled to post-transcriptional mRNA processing events, mRNA homeostasis and deterministic regulation of gene expression (He et al., 2003; Yap and Makeyev, 2013). It is not surprising that failure of NMD leads to various human diseases (Kurosaki and Maquat, 2016; Linder et al., 2015). Information about archaeal mRNA surveillance and RQC pathways is scarce,

but appears to include eukaryotic features: The stop-codon independent release factor aPelota is delivered to stalled ribosomes by aEF1α (Kobayashi et al., 2010) and recycling of stalled post-TCs likewise depends on ABCE1 (Becker et al., 2012). However, no data exist on up- and downstream events including recognition of ribosomal substrate, mRNA degradation and RQC at the 50S. Thus, it remains largely elusive how Archaea deal with translation and transcription errors, but a simplified eukaryotic system appears to be most probable. Furthermore, there are no indications that archaeal translational proofreading pathways are involved in any global cellular regulation.

1.2. Structure and mechanics of ABC proteins

ATP binding cassette (ABC) proteins are ubiquitous and characterized by several conserved sequence motifs, which couple the energy stored in ATP to mechanochemical work in various cellular processes (Linton, 2007; Locher, 2016; Schmitt and Tampé, 2002). They are subdivided into nine subfamilies, most of which (ABCA-D, ABCG-I) represent medically relevant ABC transporters (Theodoulou and Kerr, 2015). Soluble ABC proteins (ABCE and ABCF subfamilies) are involved in ribosome recycling and modulation of translation, chromatin organization, DNA repair, telomere maintenance, and mRNA trafficking (Boel et al., 2014; Hirano, 2002; Hopfner, 2009; Kozak et al., 2002; Murina et al., 2018; Nürenberg and Tampé, 2013). ABC-type molecular machines harbor two composite, allosterically coupled nucleotide-binding sites (NBSs) within two head-to-tail oriented nucleotide-binding domains (NBDs). Two ATP molecules can be sandwiched at the interface between the two NBDs leading to their tight dimerization (Smith et al., 2002). ATP hydrolysis and dissociation of ADP and inorganic phosphate relieve the NBDs. Thus, the NBDs perform a tweezer-like motion, which energizes associated domains to either transport substrates across the membrane or remodel nucleoprotein complexes (Locher, 2016; Thomas and Tampé, 2018). Each NBD consists of a core and α-helical subdomain (Hung et al., 1998). Conserved, but not invariant motifs within the core domain coordinate the nucleotide base (A-loop), the ribose moiety, α- and β-phosphates (Walker A), and the γ-phosphate *via* a water molecule (H-loop). The catalytic base (either aspartate or glutamate) is part of the Walker B motif. The D-loops are involved in allosteric crosstalk between the two sites, and the Q-loop extends to the NBD surface and the α-helical subdomain, thus it is likely involved in intradomain signaling and energy transfer. The α-helical subdomain contributes the ABC signature motif, which binds the γ-phosphate of ATP in the opposing NBD, leading to dimerization (Locher, 2016; Thomas and Tampé, 2018). Notably, numerous ABC proteins, including most human ABC transporters, are asymmetric with degenerate motifs in one of the two sites. Two mechanistic models are proposed for ABC proteins: the constant-contact model assumes permanent contact of the two NBDs *via* ATP occlusion in alternating sites. In contrast, the processive clamp model allows full closure and, most importantly, full opening of the NBD dimer upon simultaneous binding and hydrolysis of two ATP molecules at both sites (Janas et al., 2003; Senior et al., 1995; van der Does and Tampé, 2004). Given their enormous

structural and functional variety, many different mechanistic and energetic models are likely to operate the ABC proteins in living cells.

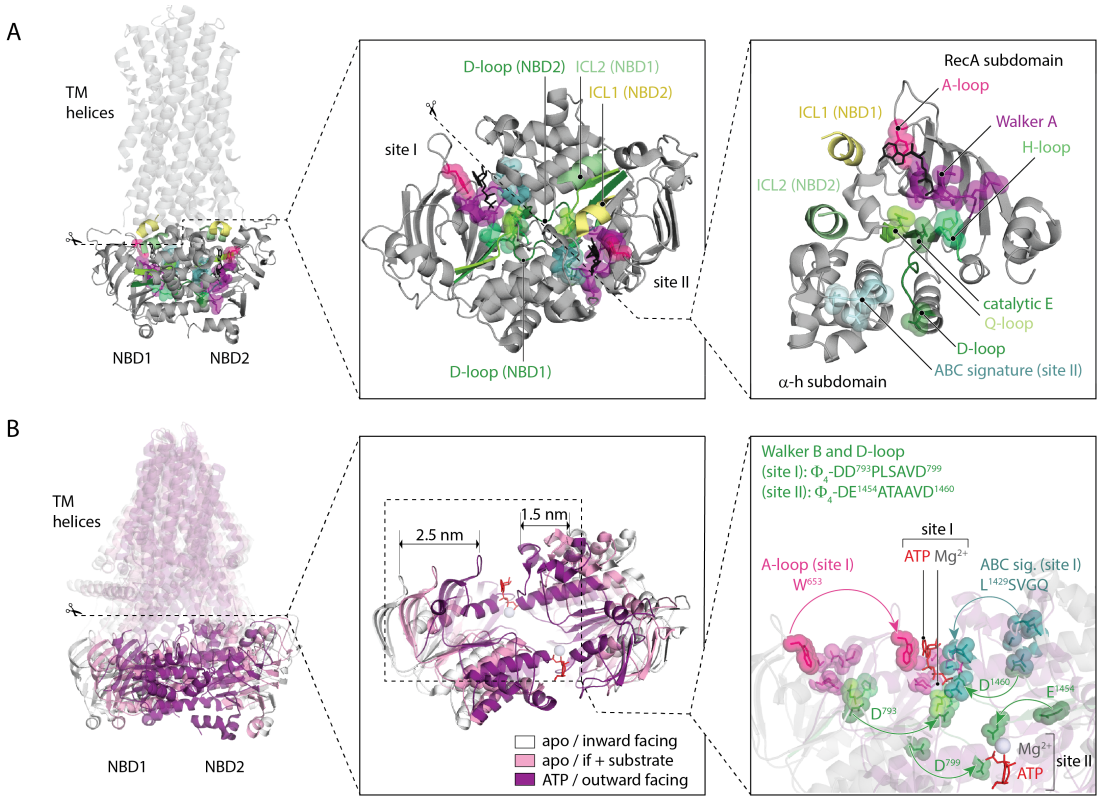

Figure 5: Structure and dynamics of ATP-binding cassette proteins. A typical, symmetric ABC system like the Sav1866 transporter (PDB 2HYD) in **A)** sandwiches two nucleotides at the interface between two NBDs, which are linked to the transmembrane (TM) helices and to each other by two internal coupling helices (ICL) from each NBD. Two composite sites embed the nucleotide within conserved motifs in RecA and α-helical subdomains oriented in a yin-yang fashion. In each site, the aromatic A-loop stacks against the base, the Walker A motif coordinates the α- and β-phosphates, the Q-loop and H-loop coordinate the γ-phosphate. The Walker B motif stretches out to the NBD surface and harbors the catalytic glutamate, which positions a water molecule for nucleophilic attack on the γ-phosphate. The D-loop communicates to the second site. Upon ATP binding, the ABC-signature motif from the opposing NBD approaches the nucleotide, starting a cascade of conformational changes within the ABC-protein. These dynamics are best illustrated by high-resolution cryo-EM reconstructions of the bovine multidrug resistance protein 1 (PDB 6BHU, 5UJ9, 5UJA) in **B)**. In the apo state, the NBDs are separated, and the TM helices await substrate binding in the inward-facing conformation. When substrate binds to the TM region of the transporter, the NBDs approach each other in a semi-closed state. Full closure of the NBDs occurs upon binding of two ATP molecules. This movement is transferred to the TM helices, which switch to the outward facing conformation and release the drug into the extracellular space.

1.3. The ribosome recycling factor ABCE1

ABCE1 is a non-membrane associated, mid-sized (~ 70 kDa) single-chain ATPase and represents the only member of ABC subfamily E. It is found only in Eukarya and Archaea, where it is evolutionarily conserved and essential. Like in a typical ABC protein, the two NBDs of ABCE1 are arranged head-to-tail and harbor two composite nucleotide binding sites at their interface. Additionally, ABCE1 possesses a unique N-terminal iron-sulfur cluster domain, which contains two diamagnetic 4Fe-4S^{2+} clusters, a helix-loop-helix insertion in NBD1, and a small and flexible hinge domain, which connects the two NBDs and supports their orientation. The A-loop in site II is degenerated in most Eukarya, while other conserved motifs are symmetric but atypical (D-loop: SYLD instead of SALD, ABC-signature: LSGGE instead of LSGGQ). Mutations in conserved functional motifs of ABCE1 are lethal at early embryonic stage and have asymmetric effects on the overall ATPase activity of the protein (Barthelme et al., 2011; Barthelme et al., 2007; Karcher et al., 2005; Karcher et al., 2008).

ABCE1 is primarily essential as ribosome recycling factor. It splits post-termination complexes into ribosomal subunits after canonical translation termination, in mRNA surveillance pathways, after hibernation during cell starvation, and as a licensing step during ribosome biogenesis (Barthelme et al., 2011; Pisarev et al., 2010; Shoemaker and Green, 2011; Strunk et al., 2012; van den Elzen et al., 2014). Ribosome recycling by ABCE1 is strictly dependent on a decoding factor (e/aRF1 or e/aPelota) accommodated in the A-site, as well as ATP or AMP-PNP (Barthelme et al., 2011; Pisarev et al., 2010; Shoemaker and Green, 2011), and can be broken divided into four steps: ABCE1 binding to the post-TC, resulting in a pre-splitting complex (pre-SC); ribosome splitting; formation of the post-splitting complex (post-SC) comprising 30S/40S and ABCE1; and dissociation of ABCE1 from the small ribosomal subunit. Strikingly, ABCE1 was earlier defined as an initiation factor dedicated to initiation complex formation in yeast, human, and fruit fly. It interacts with other *bona fide* initiation factors and promotes their association to small ribosomal subunits (Andersen and Leevers, 2007; Chen et al., 2006; Dong et al., 2004). Thus, as the only essential ribosome recycling factor, ABCE1 putatively links translation termination and initiation in a tightly regulated and essential process. Consistent with other ABC proteins, ABCE1 performs a tweezer-like movement controlled by ATP

binding and hydrolysis. Structural snapshots reveal an open conformation of ABCE1 with ADP bound in both sites (Barthelme et al., 2011; Karcher et al., 2005; Karcher et al., 2008), a semi-closed conformation with undefined nucleotides occluded within the pre-SC (Becker et al., 2012; Brown et al., 2015; Shao et al., 2016), and a closed conformation with two AMP-PNP molecules occluded within the post-SC (Heuer et al., 2017) (Figure 6). Despite comprehensive structural information, it remains unclear how ATP binding and hydrolysis in each of the two sites regulate the progression of ribosome recycling, provide the energy for splitting of the macromolecular cellular protein factory, and how ABCE1 discriminates against assembled ribosomes not destined for splitting.

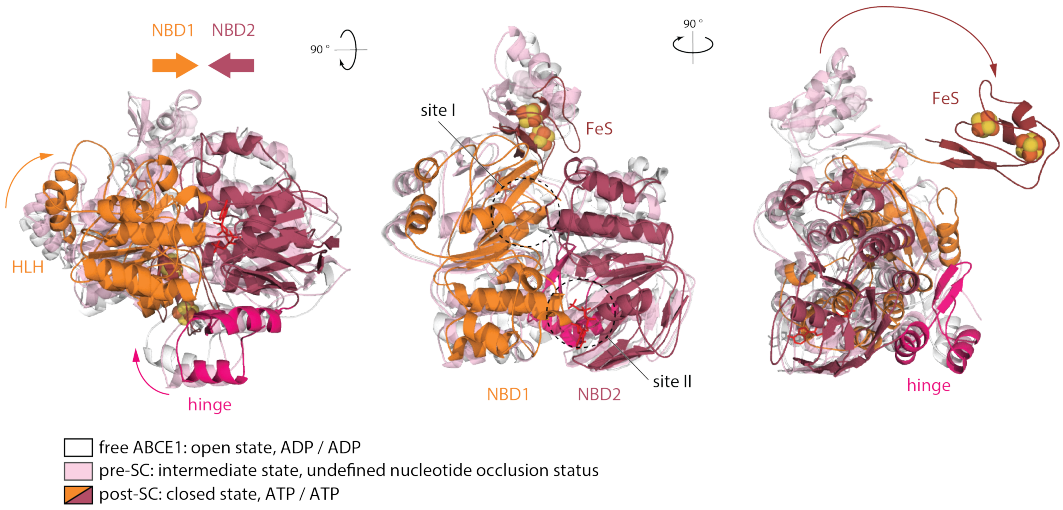

Figure 6: **Conformational dynamics of ABCE1.** Free ABCE1 crystallizes in the open conformation with two ADP molecules (PDB 3BK7, white) and the en domain at the interface between the two NBDs. Upon 80S binding and pre-SC formation, the largest changes are observed in site II, and the overall conformation of ABCE1 is described as intermediate (PDB 5LZV, lightpink). The nucleotide status of this intermediate structure is undefined. After ribosome splitting, ABCE1 remains recruited to the post-SC in a tightly closed conformation with two sandwiched ATP (AMP-PNP) molecules (PDB 5LL6, multicolor). The FeS-cluster domain is swung out and rotated, representing the largest conformational rearrangement of ABCE1.

Aims of this work

The fundamental mechanisms of translation have been studied for almost half a century. Structural and functional aspects of the ribosome and auxiliary factors were described (Hashem and Frank, 2018; Klinge et al., 2012; Ramakrishnan, 2014). Kinetic and thermodynamic parameters were determined (Aitken et al., 2010; Milon and Rodnina, 2012; Puglisi et al., 2000; Sievers et al., 2004). Constitutive pathways were identified explaining regulation and surveillance of translation, in particular during the synthesis of alternative products and for quality control and homeostasis of proteins, ribosomes, and mRNAs. Finally, numerous human diseases were traced back to disorders within translation-associated pathways (Brandman and Hegde, 2016; Kramer et al., 2009; Mills and Green, 2017; Rodnina, 2016; Xue and Barna, 2012; Yap and Makeyev, 2013). Additionally, many antibiotics target the translation system of pathogens at individual steps (Wilson, 2014). The advancement of structural biology during recent years has empowered our understanding of the ribosomal machinery and revealed even transient complexes during its assembly and recycling (Hashem and Frank, 2018; Hellen, 2018). However, structural and functional aspects of the cycle of translation are still incomplete in Eukarya and Archaea as a significant link is missing between ribosome recycling and translation initiation. In 2013, we hypothesized, that the essential and conserved ribosome recycling factor ABCE1 provides a platform for recruitment of initiation factors while being engaged in the post-splitting complex at the small ribosomal subunit (Nürenberg and Tampé, 2013). Control of ribosome recycling and formation of post-splitting complexes must be enciphered within the two asymmetric ATP binding sites of ABCE1. Therefore, my work aims at describing the molecular mechanism of ribosome recycling in respect to each of the two binding sites and link them to the known structural snapshots of eukaryotic pre- and post-splitting complexes. Additionally, I aim to resolve the archaeal post-splitting complex and structurally connect it to translation initiation.

To gain mechanistic insights into the twin-type ATPase ABCE1, a classic biochemical approach in an archaeal model system should be utilized. A few important questions

should be answered and discussed in the context of previously published biochemical work in Eukarya:

- Is there an allosteric connection between the two sites of ABCE1?
- How is ABCE1 recruited to the ribosome?
- What is the nucleotide occlusion status of ABCE1 at the pre-splitting complex?
- How does ABCE1 distinguish a correct substrate from a splitting-incompetent ribosome?
- What delivers the energy for ribosome splitting?
- Why is the post-splitting complex stably formed?

It remains to be elaborated how the post-splitting complex is resolved, and what role it plays within the cycle of translation *in vitro* and *in vivo* to enhance our understanding of protein biosynthesis.

To structurally connect ribosome recycling with translation initiation, the archaeal post-splitting complex should be resolved in collaboration with Dr. André Heuer and Dr. Thomas Becker from the Beckmann Laboratory at the Ludwig-Maximilians-University, Munich. This structure should set the stage for further studies of archaeal translation initiation in the presence of ABCE1. Therefore, the archaeal canonical translation initiation pathway should be assembled *in vitro*, the functionality of its components should be verified and translation initiation intermediates in context of the post-splitting complex should be visualized by cryo-electron microscopy.

2. Results and Discussion

2.1. Molecular mechanism of ribosome recycling by ABCE1

ABCE1 is an unusual, non-membrane associated twin-ATPase but likely resembles the working mechanism of other ABC-type proteins. Its function is linked to a tweezer-like closure and opening of its NBDs, caused by ATP binding, hydrolysis and release. Eukaryotic and archaeal post-termination complexes are recycled by ABCE1 in four phases:

1. ABCE1 binds to the 80S/70S ribosome, contacting the C-domain of the accommodated class 1 release factor and forming the pre-splitting complex.
2. ABCE1 closes upon ATP occlusion and the FeS-cluster domain protrudes into the intersubunit space, splitting the subunits apart.
3. The post-splitting complex is formed and the FeS-cluster domain anchors to its new position next to helix 44 on the small subunit.
4. ABCE1 opens and dissociates from the post-splitting complex after ATP hydrolysis and eventually release of ADP and inorganic phosphate.

Each phase must be tightly regulated to ensure that

- ribosomes not designated to be split remain intact (e.g. for further elongation or re-initiation down- or upstream on the same mRNA),
- the energy status of the cell allows restocking of free subunits for new rounds of translation,
- if so, the ribosomal subunits do not re-associate after splitting but remain accessible for canonical initiation factors.

Since ABCE1 is the major factor, which catalyzes ribosome recycling in Eukarya and Archaea, it must account for each regulative step at the respective recycling phase. The asymmetry within its two ATP binding sites adds another level of complexity to its molecular mechanism and implies that the nucleotide occlusion status and structural conformation of each site has a unique regulatory role during the four phases of recycling. Three structural snapshots of ABCE1 have already been captured. An open conformation was crystallized in the presence of ADP, which was

bound in both sites (Barthelme et al., 2011; Karcher et al., 2005; Karcher et al., 2008). A semi-closed form is engaged within the pre-splitting complex, where site II is partially closed and site I is still open (Becker et al., 2012; Brown et al., 2015). The nucleotide occlusion status remains only vaguely defined, owing to the high flexibility of site II, which does not display enough resolution for model interpretation in cryo-EM maps. The closed form of ABCE1 is found associated to the small ribosomal subunit within the post-splitting complex and shows two occluded AMP-PNP molecules and a rotated FeS-cluster domain in comparison to the open (free) and semi-closed (70S/80S-bound) forms. (Heuer et al., 2017; Kiosze-Becker et al., 2016) (Figure 6). Beyond doubt, these structural snapshots have shaped our current understanding of ribosome recycling but many aspects remain to be elucidated.

I used ABCE1 from the Crenarchaeon *Sulfolobus solfataricus*, which is accessible in functional form by heterologous expression, without toxic effects of lethal mutations. Mutations previously described to have severe effects on ABC-type proteins in either of the two ATP binding sites were studied individually whereas synergistic effects were derived from double mutants. Nucleotide binding capacity and turnover were determined and ribosome binding and splitting assays established with purified components to describe the physiological role of each site during ribosome recycling.

2.1.1. Asymmetry and allostery in ABCE1

To investigate the role of each nucleotide-binding site of ABCE1 in ribosome recycling, I substituted conserved residues required for ATP occlusion or hydrolysis (Figure 7), based on previous studies with similar mutants (Barthelme et al., 2011). The conserved glutamates E238 and E485 in each Walker B motif of site I and site II, respectively, act as the catalytic bases for ATP hydrolysis. Therefore, single and double alanine substitutions (EA-mutations: E238A, E485A, and E238A/E485A) were generated. Equivalent substitutions are known to deactivate ATP hydrolysis in other ABC proteins and arrest the fully closed conformation of their nucleotide-binding domains (Hopfner and Tainer, 2003; Smith et al., 2002; Urbatsch et al., 2000). Likewise, substitutions in ABCE1 lead to stable ATP occlusion in the corresponding sites by preventing ATP hydrolysis (section 2.1.4). In a complementary approach, I introduced a bulky, positively charged residue into the ABC-signature motif to prevent nucleotide occlusion (SR-mutations: S461R in site I and/or S214R in site II, later

referred to as disengagement mutations). The structural and functional role of the ABC-signature motif during nucleotide occlusion has been elaborated previously, indicating direct binding to the γ-phosphate moieties of ATP (Smith et al., 2002; Szentpetery et al., 2004). Additionally, I created two "mixed" mutants with one EA- and one SR-mutation in the opposite sites (E238A/S214R and S461R/E493A). All ABCE1 variants were purified to monodispersity with a characteristic absorption at 410 nm (Barthelme et al., 2007), demonstrating fully assembled iron-sulfur clusters of each construct (Figure S1).

The ABCE1 variants reveal a functional asymmetry with two distinct intrinsic ATP hydrolysis rates (Figure 7 and S2), consistent with previous studies of related mutants (Barthelme et al., 2011). In the absence of ribosomes, wild-type ABCE1 has a basal ATPase activity showing an ATP hydrolysis rate of 21 ATP per minute. Substitution of the catalytic bases or introduction of disengagement mutations in both sites strongly decrease ATP hydrolysis rates to five ATP or four ATP per minute, respectively. Inactivation of site I by the disengagement mutation S461R leads to reduced ATP turnover carried out solely by a low-turnover site II (17 ATP/min). Furthermore, ATP occlusion in site I of ABCE1^{E238A} has a weak inhibitory effect on ATP hydrolysis in site II (9 ATP/min). In contrast, ABCE1^{E485A} is hyperactive (172 ATP/min), indicating that ATP occlusion in site II allosterically activates a high-turnover site I. Moreover, the disengagement mutation in site II of ABCE1^{S214R} (5 ATP/min) impairs the ATPase activity to the same extent as the double-mutations. Hence, ATP occlusion in site II is a prerequisite for efficient ATP hydrolysis in site I. Owing to its allosteric impact on site I, the low-turnover site II is named *control site* while site I is termed *power site* due to its potentially high ATP turnover ability. Apparently, the *power site* exists in two states depending on the nucleotide occlusion status of *control site*: the inactivated state with negligible ATP turnover (reflected by S214R mutant) switches to an activated state as soon as the *control site* occludes ATP (reflected by E485A mutant). Notably, ABCE1^{E485A} displays an 8-fold increased activity compared to wild-type ABCE1, resembling the stimulated ATP hydrolysis of ABCE1 in the presence of splitting competent ribosomes and release factors (Figure 7, S2 and S3) (Pisarev et al., 2010; Shoemaker and Green, 2011). Thus, while site II occludes and hydrolyses one ATP molecule, site I in its activated state can perform several rounds of sequential ATP binding, occlusion, hydrolysis and release events (Nürenberg-Goloub et al., 2018) (Figure 7 and S2).

The allostery in ABCE1 was further investigated utilizing the mixed mutants ABCE1$^{E238A/S214R}$ with hydrolysis-deficient site I and occlusion-deficient site II, and ABCE1$^{S461R/E485A}$ with the respective mutations at the reciprocal sites (Figure S2). As expected, ABCE1$^{E238A/S214R}$ has a weak ATPase activity (8 ATP/min) as compared to wild-type (21 ATP/min). Surprisingly, the reciprocal mutant ABCE1$^{S461R/E485A}$ still retains an enhanced ATP turnover (36 ATP/min). In this mutant, site II stably occludes ATP due to the E485A mutation and allosterically activates site I. On the other hand, the S461R mutation disturbs the ATP hydrolysis cycle in site I by preventing full ATP occlusion. Thus, in contrast to the established working model for ABC proteins, activated site I can efficiently bypass the occlusion event and hydrolyze ATP directly after binding. Structural studies of other ABC proteins describe an induced fit mechanism for ATP, which involves the reorientation of individual residues and various rotational movements of the lobes within each NBD (Karpowich et al., 2001; Oswald et al., 2006). It is intriguing to speculate, that the allosteric activation of site I is initiated by the induced fit of ATP in site II and can therefore be observed even in the presence of a disengagement mutation in the *power site*. However, full activation is only achieved if the classical ATP hydrolysis cycle can be completed (Figure 7 and S2). It is certainly interesting to re-investigate other asymmetric ABC-type machines for allosteric activation mechanisms and incomplete ATP hydrolysis cycles and add them to the current working model.

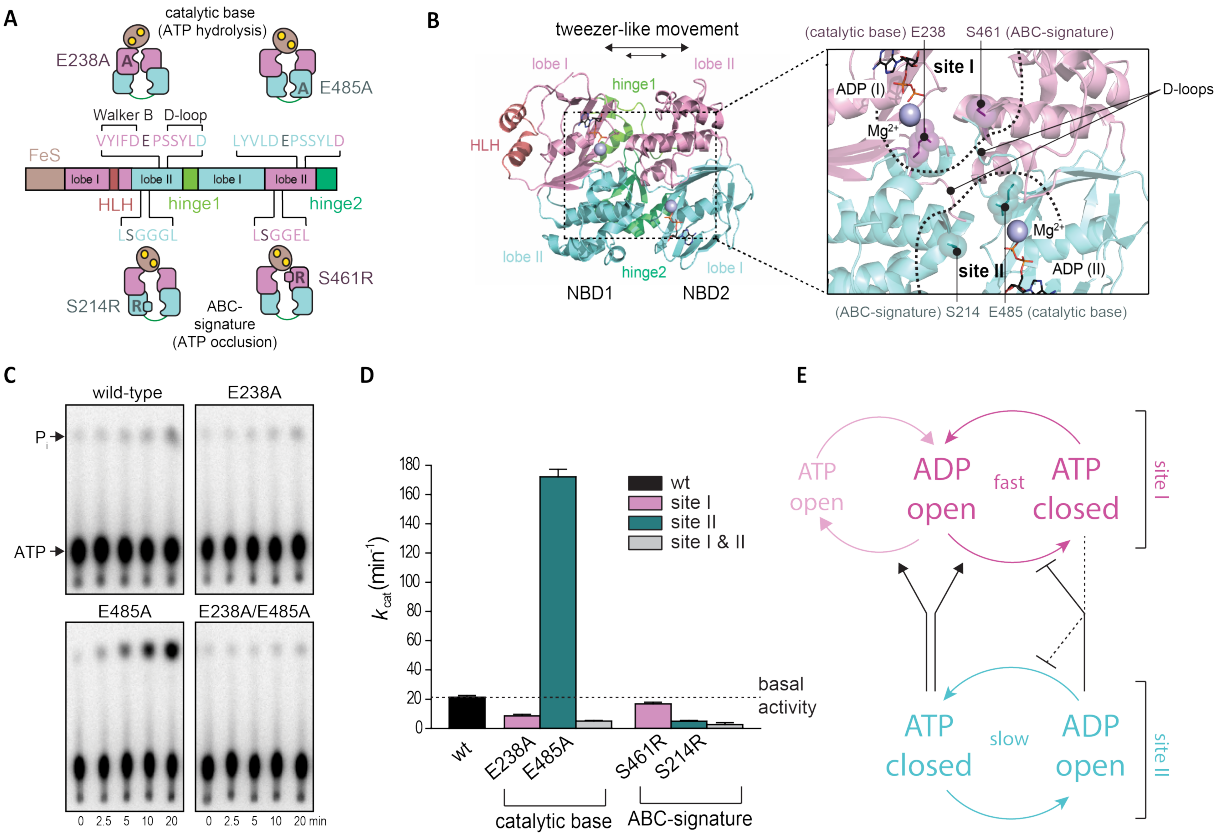

Figure 7: ATPase activity clockwork of free ABCE1. **A)** Domain organization of the ABCE1 polypeptide and strategic mutations used in this study to prevent ATP occlusion or ATP hydrolysis in the respective site. **B)** Crystal structure of *S. solfataricus* ABCE1 with truncated FeS-cluster domain in the open, ADP bound form (PDB 3OZX) illustrates the position of the exchanged residues in the sites. **C)** ^{32}P-γ-ATP hydrolysis activity of wild-type ABCE1 and the catalytic base mutants resolved by thin layer chromatography. **D)** ATP turnover numbers for the single and double catalytic base and disengagement mutants reveal the allosteric interdependencies between the two sites of ABCE1, which is displayed in panel **E)**. Modified from (Nürenberg-Goloub et al., 2018).

2.1.2. Pre-splitting complex formation

With up to several million copies per cell (Duncan and Hershey, 1983; Warner, 1999), ribosomes are the most abundant macromolecules and account for up to 20% of the cytosolic volume. Cryo-electron tomography studies suggested that ribosomes act as molecular crowders and tune phase-separation in the cytosol (Delarue *et al.*, in revision). In contrast, ABCE1 is less abundant with 300-500 copies per cell (Khan et al., 2013; Newman et al., 2006). Thus, the recruitment of ABCE1 must be highly

efficient to ensure a functional translation cycle. Recently, the ribosomal P-stalk protein rpP1 was shown to bind ABCE1 and several translational GTPases (Imai et al., 2018; Murakami et al., 2018; Tanzawa et al., 2018). The ribosomal P-stalk in Archaea comprises the large ribosomal protein P0 (approximately 40 kDa), which binds multiple copies of the small rpP1 (Naganuma et al., 2010). Flexible C-terminal tails of rpP1 at the ribosome are thereby exposed to the solvent and angle for translational factors including ABCE1 to accumulate them in spatial proximity of the GTPase center (Diaconu et al., 2005). In a crystal structure, the C-terminal peptide of rpP1 binds ABCE1 in the open, ADP bound conformation at the groove between the core lobe I and α-helical lobe II of NBD1 (Imai et al., 2018). Re-investigation of the archaeal and eukaryotic pre-splitting complexes (Becker et al., 2012) did not reveal additional density in this region of ABCE1. Notably, structural alignment showed several clashes of the rpP1 peptide with ABCE1 in the half-closed (70S/80S bound) conformation, suggesting that rpP1 is rejected as soon as ABCE1 docks to the GTPase center. The nucleotide dependency of rpP1 binding to ABCE1 was not investigated so far.

Contradicting biochemical data exist on the nucleotide status of ABCE1 at the eukaryotic pre-splitting complex. Rabbit ABCE1 binds 80S (strictly eRF1 dependent), 60S and 40S ribosomes in the absence of nucleotides. On the other hand, programmed 80S pre-termination complexes with wild-type eRF1 or mutant eRF1^{AGQ} in the A-site were decorated with ABCE1 only in the presence of AMP-PNP but not ATP (Pisarev et al., 2010). In contrast, yeast ABCE1 stably bound programmed 80S complexes with Dom34 (eRF1 homolog participating in mRNA surveillance) in the presence of ATP and AMP-PNP (Shoemaker and Green, 2011). In both systems, the flexibility of decoding factors was sufficiently high to escape the A-site in the absence of bound ABCE1, eRF3 (eRF1 delivery GTPase) or Hbs1 (eRF3 homolog delivering Dom34 and ePelota). Because *S. solfataricus* 70S ribosomes are intrinsically instable and cannot be isolated by sucrose density gradient (SDG) centrifugation (Barthelme et al., 2011; Londei et al., 1986), I used 70S ribosomes from *Thermococcus celer*. The high evolutional conservation of the translational machinery allows *S. solfataricus* ABCE1, aRF1, aPelota, and aIF6 to be functional with *T. celer* ribosomes (Barthelme et al., 2011). To stabilize isolated archaeal 70S during pre-splitting complex formation, I applied conditions previously established for *in vitro* translation

and pre-splitting complex formation in Archaea, even though they include non-physiologically high Mg^{2+} concentrations (50 mM) and low temperature (25 °C) (Becker et al., 2012; Endoh et al., 2006). In contrast to both native eukaryotic systems, the release factor co-sediments with 70S even in the absence of bound ABCE1 suggesting a reduced flexibility of aRF1 within the ribosomal complex and/or higher affinity for 70S ribosomes. Notably, rabbit eRF1 was retained within the 80S fraction, if *in vitro* transcribed, unmodified tRNA was inserted in the P-site of reconstituted pre-termination complexes (Pisarev et al., 2010), implicating that post-transcriptional processing of archaeal tRNA does not influence aRF1 association with 70S in contrast to eukaryotic tRNA modifications. Consistent with the yeast system, I observed a strict dependency on aRF1 and AMP-PNP for pre-SC formation with isolated 70S ribosomes and wild-type ABCE1 (Figure 8). ABCE1^{E238A} (site I) moderately forms pre-SCs while ABCE1^{E485A} (site II) efficiently binds to 70S ribosomes in the presence of AMP-PNP and ADP and partially splits them even at non-permissive conditions. I conclude that nucleotide occlusion in the control site II triggers a conformation of ABCE1 primed to form a pre-SC. Notably, pre-SCs with the ATPase deficient double mutant ABCE1$^{E238A/E485A}$ could not be isolated as it splits most 70S. The essential role of site II in pre-SC formation is further accentuated by comparing the disengagement SR mutants. If nucleotide occlusion in control site II is impeded by the S214R substitution, pre-splitting complexes cannot form even with AMP-PNP. In contrast, ABCE1^{S461R} displays a similar behavior as the wild-type. Thus, blocking nucleotide occlusion in the high-turnover site I does not affect pre-SC formation. In accordance, ABCE1$^{S461R/E485A}$ binds to 70S ribosomes with AMP-PNP and ADP. Given that no additional occlusion event in site I can take place in the mixed mutant S461R/E485A, this corroborates my findings that ATP occlusion in site II induced by the catalytic E485A substitution is sufficient for pre-SC formation. Consistently, the reciprocal mutant S214R/E238A did neither bind nor split ribosomes (Figure 8). The semi-closed conformation of site II within the pre-SC (Figure 6) is either induced by the ribosome and/or a bound ATP/AMP-PNP molecule. This biochemical data strongly support that nucleotide occlusion in site II is essential for pre-SC formation (Nürenberg-Goloub et al., 2018). Thus, it remains to speculate on why ABCE1 is recruited to various ribosomal complexes from rabbit in the absence of nucleotides but not in the presence of ADP or ATP (Pisarev et al., 2010). Given the cellular ATP concentration of 1-10 mM and an ATP affinity below 1 mM for typical

ABC-type proteins, both sites of ABCE1 will be saturated with nucleotides *in vivo*. Thus, it is very unlikely, that ABCE1 binds assembled ribosomes or ribosomal subunits only when both ATP sites are unoccupied. However, a high conformational flexibility is characteristic to ABC proteins in the apo-state (Oswald et al., 2006). The thermostability of ABCE1 is significantly increased in the presence of nucleotides, indicating that it is not an exception (D. Barthelme, PhD thesis). Increased flexibility might lead to spontaneous semi-closure of site II followed by ribosome binding and a subsequent conformational switch, locking ABCE1 on 80S or 40S particles. Since eRF1 greatly enhanced pre-SC formation in the absence of nucleotides, it may be involved in apo-ABCE1 trapping. Additionally, in the case of 80S and 60S ribosomal (sub)units, recruitment of ABCE1 to the ribosomal P-stalk might play a pivotal role. Even though the P-stalk is assembled only on 80S ribosomes and polysomes in yeast (Bautista-Santos and Zinker, 2014), the purification method for rabbit ribosomal subunits includes artificial disassembly of crude 80S during sucrose density gradient (SDG) centrifugation at low Mg^{2+} concentrations. Thus, the P-stalk might recruit the apo-form of ABCE1 to 80S ribosomes and also 60S subunits. In a nutshell, the cellular environment, intrinsic properties of ABC proteins and cryo-EM reconstructions of the pre-SC support my biochemical data, showing that ATP occlusion in site II is an essential prerequisite for pre-splitting complex formation.

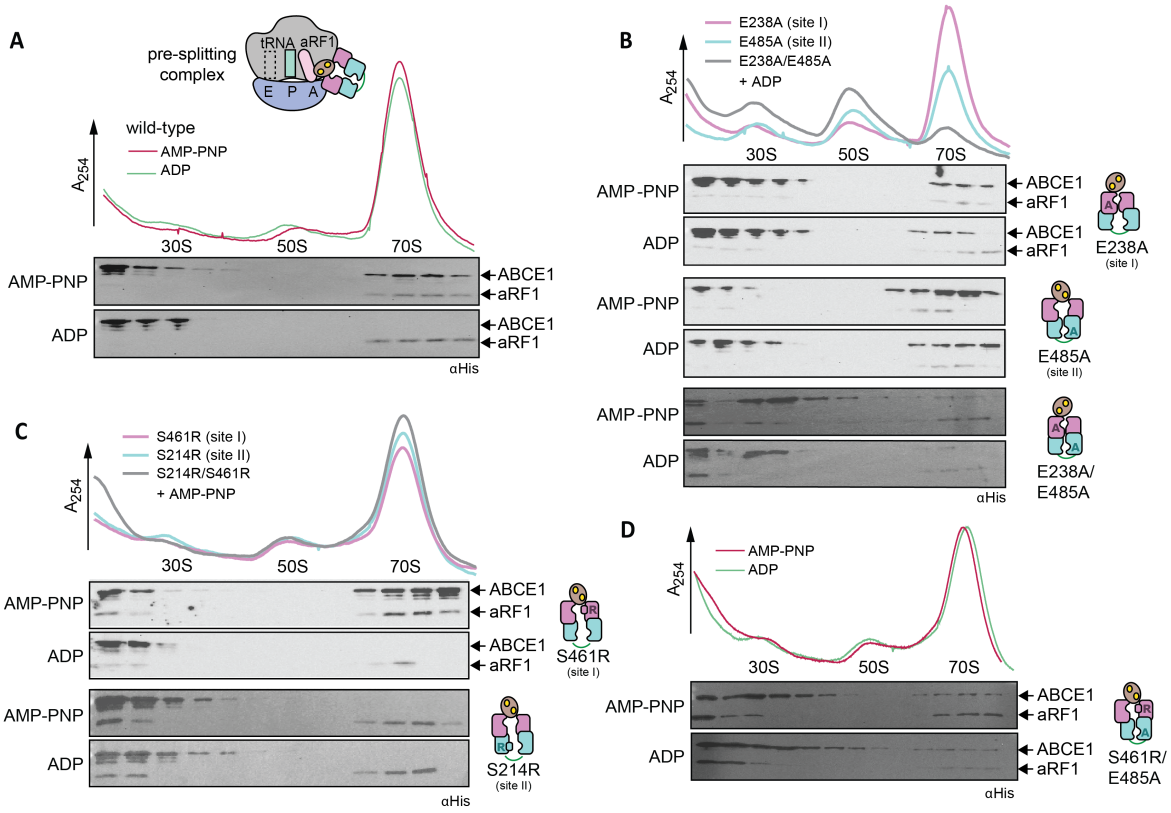

Figure 8: Site II controls pre-splitting complex formation. A) Pre-SC formation probed by SDG centrifugation. As expected, aRF1 is bound to the ribosome independently of the nucleotide supplemented, while wild-type ABCE1 is recruited only in the presence of AMP-PNP. **B)** Exchange of any catalytic glutamate enables nucleotide-independent ribosome binding. Pre-SC formation could not be assayed for the double-EA variant as it splits ribosomes even under high Mg^{2+} and low temperatures. Importantly, after splitting $ABCE1^{E238A/E485A}$ remains bound at 30S as seen in the respective fractions of the immunoblot. **C)** Steric hindrance by S214R mutation in site II prevents pre-splitting complex formation even in the presence of AMP-PNP. In contrast, blocking site I by S461R mutation does not affect pre-SC assembly. **D)** The mixed mutant S461R/E485A binds 70S in the presence of AMP-PNP and ADP (Nürenberg-Goloub et al., 2018).

2.1.3. Ribosome splitting

After formation of the pre-splitting complex, which requires nucleotide occlusion in site II of ABCE1, the ribosome can be split apart. In both eukaryotic systems investigated so far, ribosome splitting was strictly ATP dependent and did not occur

in the presence of AMP-PNP (Pisarev et al., 2010; Shoemaker and Green, 2011). In contrast, the high-resolution cryo-EM structure of the yeast post-splitting complex shows ABCE1 at the 40S subunit in an ATP occluded state and provides exhaustive evidence for an eRF1 dependent splitting mechanism based on ATP occlusion, not ATP hydrolysis (Heuer et al., 2017). In Archaea, isolated 70S ribosomes at 2.5 mM Mg^{2+} were efficiently split by wild-type ABCE1 in the presence of AMP-PNP and by the hydrolysis deficient ABCE1$^{E238Q/E485Q}$ in an aRF1 independent manner, while eRF1 promoted splitting in the presence of ATP (Barthelme et al., 2011). At 5 mM Mg^{2+}, no splitting was observed in the presence of ATP and aRF1. In contrast, archaeal ribosomes in whole-cell extracts programmed for translation (containing ATP and GTP) were split by wild-type ABCE1 and the double-EQ mutant without the addition of recombinant eRF1 even at 20 mM Mg^{2+}. An ABCE1 construct lacking the FeS-cluster domain, ABCE1ΔFeS, or the double-SR mutant were incapable of ribosome splitting (Barthelme et al., 2011). It remains enigmatic, why aRF1 dependent splitting of archaeal 70S was previously only observed at 2.5 mM Mg^{2+} in the presence of ATP. Notably, the eukaryotic mRNA surveillance factor Dom34 efficiently disassembles 80S ribosomes at 2.5 mM Mg^{2+} in the absence of ABCE1, implying a direct role of Dom34 in ribosome recycling at physiological conditions. Dom34-mediated recycling is abolished, if Hbs1 remains bound to 80S in the presence of GMP-PNP (Shoemaker et al., 2010). Consequently, isolated archaeal 70S could be split in a similar mechanism directly by aRF1 if ABCE1 is not locked on the 70S ribosome by the presence of AMP-PNP, which would add up to the higher splitting efficiency. On the other hand, ABCE1 acts as an anti-association factor when arrested on 40S by AMP-PNP (Heuer et al., 2017) and thus stabilizes spontaneously disassembled ribosomes independently of aRF1. Thus, to investigate active ribosome splitting by ABCE1, the experimental conditions had to be thoroughly fine-tuned.

To avoid unspecific 70S dissociation and to retain the aRF1-dependent function of ABCE1, I chose single-turnover conditions with isolated components using purified *T. celer* 70S ribosomes at 25 mM Mg^{2+} and at 45 °C (Becker et al., 2012; Endoh et al., 2006). Ribosome splitting by ABCE1 was assisted by aRF1 and the addition of surplus aIF6 prevented reassociation of ribosomal subunits after a single round of splitting (Benelli et al., 2009). Wild-type ABCE1 splits ribosomes most efficiently with

AMP-PNP in an aRF1 dependent manner (Figure 9). Notably, the overall splitting efficiency of wild-type ABCE1 in my assay was comparable to the reconstituted rabbit system (Pisarev et al., 2010). No splitting was observed with ADP or in the absence of ABCE1 or aRF1. Strikingly, the ATPase of wild-type ABCE1 was accelerated 7-fold at splitting conditions in the presence of 70S and aRF1 (Figure S3), consistent with the specific activation of ABCE1 by assembled ribosomes (Pisarev et al., 2010; Shoemaker and Green, 2011). Ribosomes are also split by ABCE1 in concert with the Dom34 homolog aPelota (Figure S4). While substitution of any catalytic glutamate in ABCE1 promoted ribosome splitting (Figure S5), it is remarkable that even the substitution of both catalytic glutamates resulted in high splitting potential despite the significantly decreased ATPase activity of ABCE1$^{E238A/E485A}$. Thus, ribosome splitting per se does not directly depend on ATP hydrolysis (Figure 9). Importantly, splitting is diminished with ADP in the case of ABCE1^{E238A} (Figure 9), highlighting the crucial role of ATP occlusion and subsequent structural changes in control site II. Hence, control site II triggers an intramolecular switch and activates the high-turnover site I in the free (Figure 7) and ribosome-bound state (Figure 9). In turn, ATP occlusion and closure of site I drive the structural re-organization for ribosome splitting. Thus, the power site acts as molecular motor of ribosome splitting (Nürenberg-Goloub et al., 2018).

Along the ribosome recycling reaction, ABCE1 switches from a semi-closure of site II on the pre-SC to full closure of both sites on the post-SC (Becker et al., 2012; Brown et al., 2015; Heuer et al., 2017). Consequently, ABCE1^{E485A} or ABCE1$^{E238A/E485A}$ are primed to adopt the fully closed post-SC conformation and induce ribosome splitting with ATP, AMP-PNP, and ADP while ABCE1^{E238A} still requires ATP or AMP-PNP in the control site II to accomplish this task. Notably, a similar preference for the closed state has been reported for the catalytic base mutant of the homodimeric ABC transporter MsbA (Schultz et al., 2011). In order to disable the allosteric control of site I by site II, I analyzed the ribosome splitting ability of the disengagement mutants. None of them was able to split 70S, confirming that both sites must adopt a closed conformation to induce ribosome splitting (Nürenberg-Goloub et al., 2018).

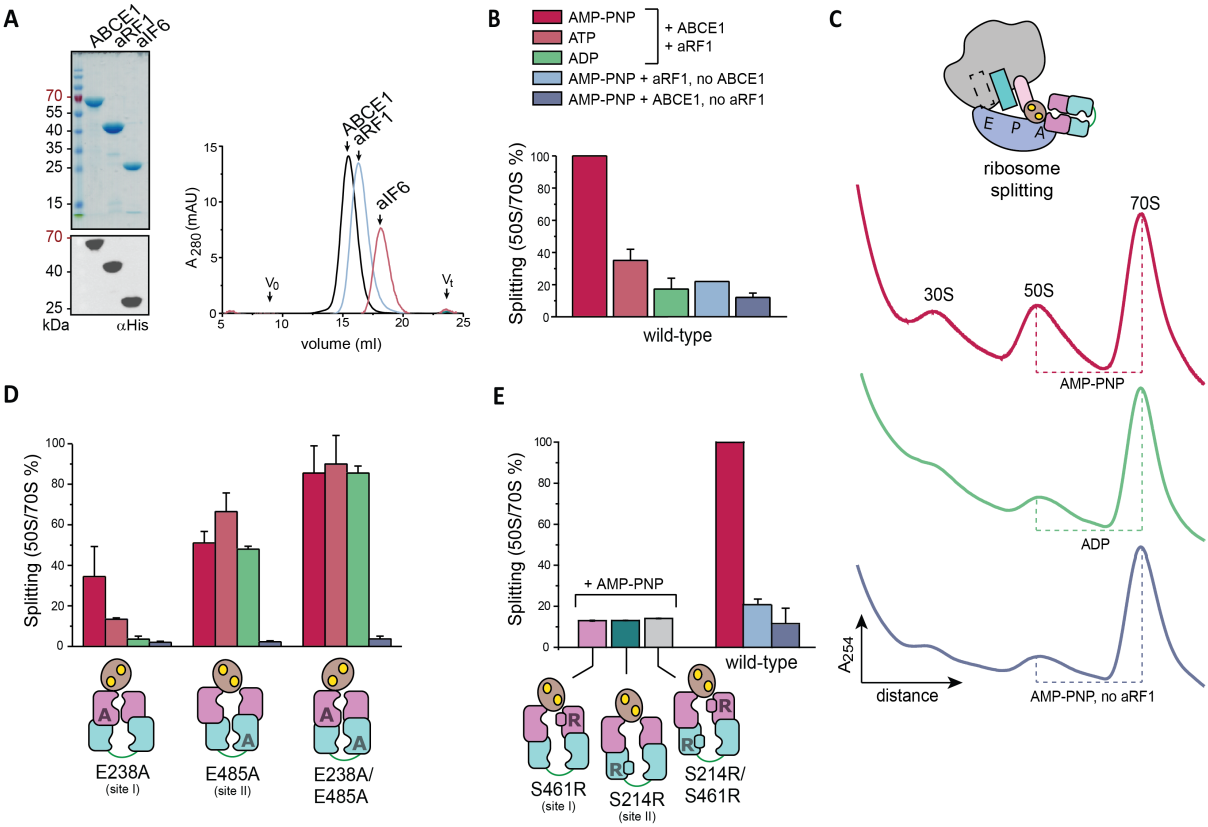

Figure 9: Both nucleotide-binding sites must close for efficient 70S splitting. A) A minimal set of splitting factors required for active splitting comprises ABCE1, aRF1, and aIF6 from *S. solfataricus.* All factors were pure and monodisperse as shown by SDS-PAGE (Coomassie), immunoblotting, and SEC. **B)** Specific 70S splitting requires aRF1, ABCE1, and AMP-PNP. Results were normalized to the highest splitting ratio for ABCE1 wild-type with AMP-PNP and aRF1. **C)** Traces corresponding to **B)** clearly demonstrate an increase of 50S in the presence of wild-type ABCE1, aRF1, and AMP-PNP. **D)** Ribosome splitting is most efficient, when both sites are in a closed, occluded state. Colors as in **B)**. **E)** Ribosomes are not actively split by any of the SR `disengagement´ mutants, showing that closure of both sites is a prerequisite for ribosome splitting. Colors as in **B)** (Nürenberg-Goloub et al., 2018).

2.1.4. ABCE1 occludes two nucleotides to split the ribosome

I independently studied the nucleotide occlusion in ABCE1 at splitting conditions. Mutations of one or both catalytic glutamates promote the stable binding of two nucleotides per ABCE1. Disengagement mutants with single substitutions in the ABC signature motif, S214R or S461R, occlude only one nucleotide in the opposite, unmodified site. Background levels of nucleotide occlusion were observed in the double-SR mutant (Figure 10). Wild-type ABCE1 was only partially occupied by ATP

and ADP, consistent with the intermediate amount of split 70S compared to almost complete splitting by the EA-variants (Figure 10). Thus, the exchange of one or both catalytic glutamates in ABCE1 facilitates the transition to a fully closed state with two occluded nucleotides, and therefore results in highly efficient ribosome splitting. The ATP-to-ADP ratios occluded by the single site mutants reflect the ATP turnover rate in the canonical site and illustrate the allosteric crosstalk between both asymmetric sites on single-turnover levels. ABCE1 with one catalytically active site harbors always one ATP molecule in the opposite ATPase-inactivated nucleotide-binding site, while the active site executes slow (E238A) or fast (E485A) ATP hydrolysis. As expected, the catalytically inhibited double E238A/E485A mutant occludes two unconverted ATP molecules. These single-turnover studies are consistent with the multiple (steady-state) ATPase activity assays and underline the significance of the low-turnover site II controlling the high-turnover site I. Altogether, these data demonstrate that the full closure of both sites, initiated by ATP occlusion in control site II, drives ribosome splitting (Nürenberg-Goloub et al., 2018).

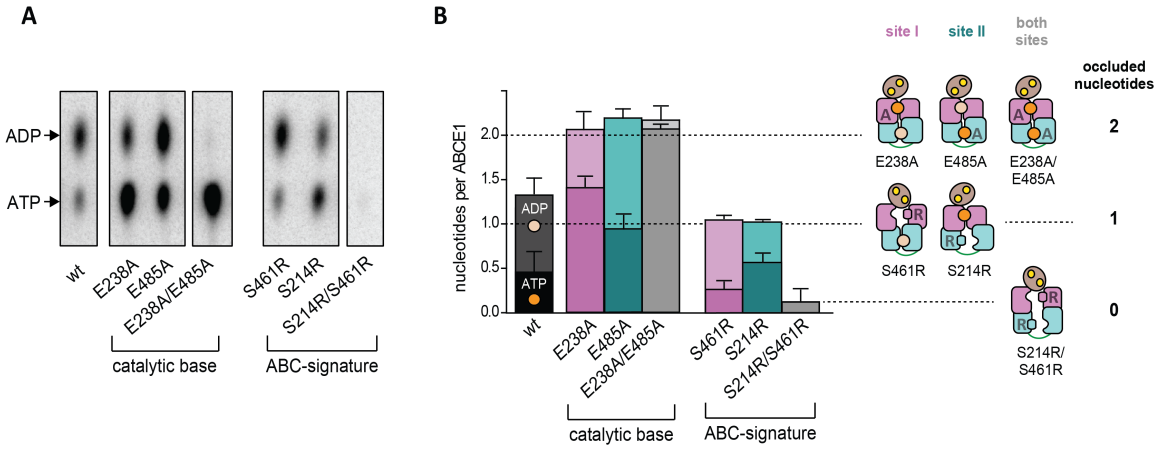

Figure 10: ABCE1 occludes two nucleotides during 70S splitting. A) Nucleotide occlusion is assayed at 70S splitting conditions by rapid gel filtration. Autoradiogram of the elution fractions from the nucleotide occlusion assay containing ABCE1 with the respective nucleotides securely trapped within the closed sites. Representative set of two independent experiments. **B)** Exchange of the catalytic glutamates facilitates closure of the nucleotide-binding sites and ATP occlusion, hence, all EA variants occlude two nucleotides. As intended, introduction of arginine into the ABC-signature motif prevents nucleotide occlusion in the respective site, leading to one or a background of 0.2 nucleotides per protein for single-SR and double-SR substitutions, respectively. The ATP-to-ADP ratio occluded by the SR variants reflects the ATP turnover rate in the intact site.

2.1.5. Formation of the post-splitting complex

The structurally described, reconstituted post-splitting complexes from Eukarya and Archaea comprise ABCE1 bound to the small ribosomal subunit in the presence of AMP-PNP (Heuer et al., 2017; Kiosze-Becker et al., 2016). However, the fate of mRNA and tRNA after ribosome splitting is still vaguely defined when translation is terminated by e/aRF1. Some eukaryotic post-splitting complexes can re-initiate translation at down- or upstream start codons of the bound mRNA, depending on the presence of canonical or non-canonical (re-) initiation factors (Lomakin et al., 2017; Skabkin et al., 2013). Thus, native post-SC intermediates likely retain mRNA and deacylated tRNA in the P-site similar to bacterial 30S after splitting (Peske et al., 2005). During Dom34/Pelota mediated mRNA surveillance, peptidyl-tRNA remains associated with 60S subunits and mRNA is promptly degraded (Brandman and Hegde, 2016). *In vitro*, rabbit ABCE1 binds isolated 40S subunits in the absence of nucleotides and is recruited efficiently in the presence of AMP-PNP but not ATP or ADP (Pisarev et al., 2010). The anti-association activity of ABCE1 in yeast strongly depends on AMP-PNP. Furthermore, ABCE1 is bound to yeast 40S in a fully closed state (Heuer et al., 2017), implicating the presence of a γ-phosphate at the nucleotide in both sites in consistency with other asymmetric ABC proteins (Lammens et al., 2011; Smith et al., 2002). Archaeal ABCE1 binds 30S ribosomes from whole cell extracts in the presence of ATP, but most efficient in the presence of AMP-PNP (Barthelme et al., 2011). This minor difference may point to a slightly altered mechanism of post-SC decomposition in Eukarya and Archaea or additional factors stabilizing the post-SC with ATP in whole cell extracts. Interestingly, yeast 40S can have both, an inhibitory and simulative effect on the ATP hydrolysis of ABCE1, depending on the purification procedure and final purity (unpublished results by Milan Gerovac, Tampé Lab), suggesting yet unknown factors to modulate the post-SC.

To reveal the intrinsic regulation of post-SC formation within ABCE1, I assayed 30S binding in whole cell lysates and isolated ribosomes with purified ABCE1 variants. Efficient post-SC formation with wild-type ABCE1 requires AMP-PNP and elevated temperatures (Barthelme et al., 2011; Kiosze-Becker et al., 2016). The post-SC can neither be formed in the presence of ADP nor at 4 °C (Figure 11). Substitution of the catalytic glutamate in either site abolishes the requirement for AMP-PNP or elevated temperatures for post-SC formation. However, at low temperature, ABCE1^{E485A}

(site II) or of the double E238A/E485A variant occupy the 30S ribosomal subunit significantly more efficient than ABCE1^{E238A} (Figure S6). Furthermore, the S214R mutation (preventing closure of control site II) eliminates post-SC formation even in the presence of AMP-PNP and high temperature. In contrast, the disengagement mutation S461R in power-stroke site I does not impact post-SC formation (Figure 11). To strengthen this conclusion, I analyzed post-SC formation by the mixed mutant ABCE1$^{S461R/E485A}$, which excludes a nucleotide occlusion event in site I. The additional disengagement mutation in site I (S461R) did not alter post-SC formation in comparison to E485A alone, since binding was observed at 4 °C with AMP-PNP and ADP. Hence, primarily, closure of control site II stabilizes the post-SC until ABCE1 release by a yet undefined trigger (Nürenberg-Goloub et al., 2018).

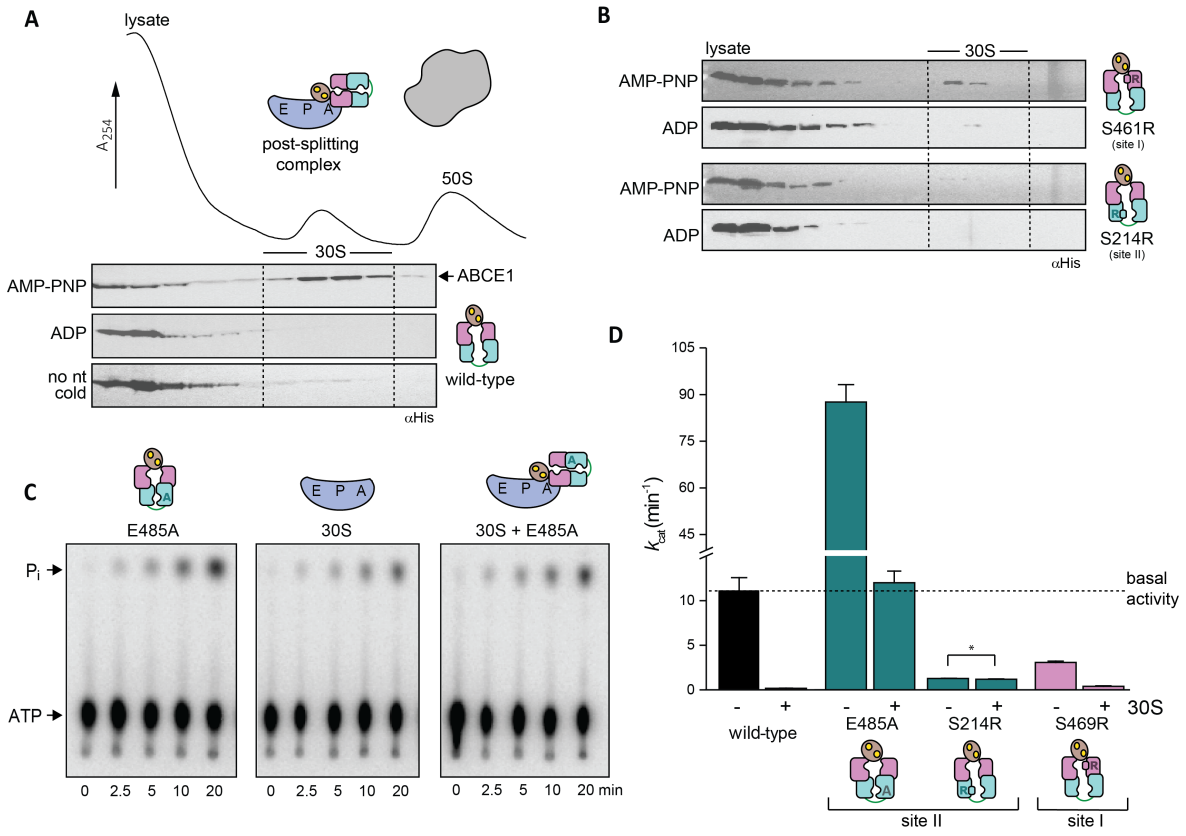

Figure 11: ABCE1 sets the lifetime of the post-splitting complex. A) The post-SC is assembled from *S. solfataricus* cell lysate (contains only 30S and 50S subunits) and recombinant ABCE1. Wild-type protein essentially requires high temperature and AMP-PNP for 30S binding. **B)** Blockage of site II by the S214R mutation severely inhibits post-SC formation. **C)** 30S binding inhibits the ATPase activity of ABCE1^{E485A} (1 µM), as demonstrated by TLC of ^{32}P-γ-ATP (2 mM). ATP hydrolysis drops to the level of background 30S activity if the small subunit (4 µM) is added to the hyperactive E485A variant. **D)** ATPase activity of ABCE1 is inhibited if a post-SC is efficiently formed. Strikingly, ATP hydrolysis rate of ABCE1^{S214R} does not change upon addition of 30S (*), since the S214R mutation prevents 30S binding. The overall drop of k_{cat} for ABCE1 in this experiment results from the higher Mg^{2+} (20 mM) concentration used for 30S binding compared to 2.5 mM Mg^{2+} in the ATPase measurements with ABCE1 only (Nürenberg-Goloub et al., 2018).

2.1.6. Molecular model of ribosome recycling – A novel ABC-type mechanism

Based on the findings above, I derive an elaborated working model of ribosome recycling catalyzed by ABCE1, which represents a novel ABC-type mechanism (Figure 12). Pre-splitting complexes are formed when ABCE1 is recruited to ribosomes during classical termination or mRNA surveillance. In *phase 1*, the low-turnover site II adopts a semi-closed conformation upon ATP binding, acting as a checkpoint site in a modality similar to GTPases. In *phase 2*, an allosteric switch activates the high-turnover site I. The ATPase activity of ABCE1 is stimulated by splitting competent ribosomes and aRF1 but inhibited by the small ribosomal subunit. Thus, the power-stroke site I can hydrolyze several nucleotides in attempt to occlude one ATP and switch to the closed conformation. Consequently, ABCE1 adopts a fully closed state with two occluded ATP and splits the ribosome. Full closure of both sites displaces the FeS-cluster domain, which is allosterically coupled to site I (Heuer et al., 2017). The FeS-cluster domain protrudes into the intersubunit space and causes a rearrangement in the pre-SC, thus leading to its destabilization and disassembly (Heuer et al., 2017; Kiosze-Becker et al., 2016). In *phase 3*, both sites remain locked in the closed form at the small ribosomal subunit. Consistently, ATP hydrolysis by ABCE1 is strongly inhibited within the post-SC. In *phase 4 and 5*, ATP hydrolysis schedules dissociation of ABCE1 from the post-SC potentially triggered by initiation factors (Nürenberg-Goloub et al., 2018).

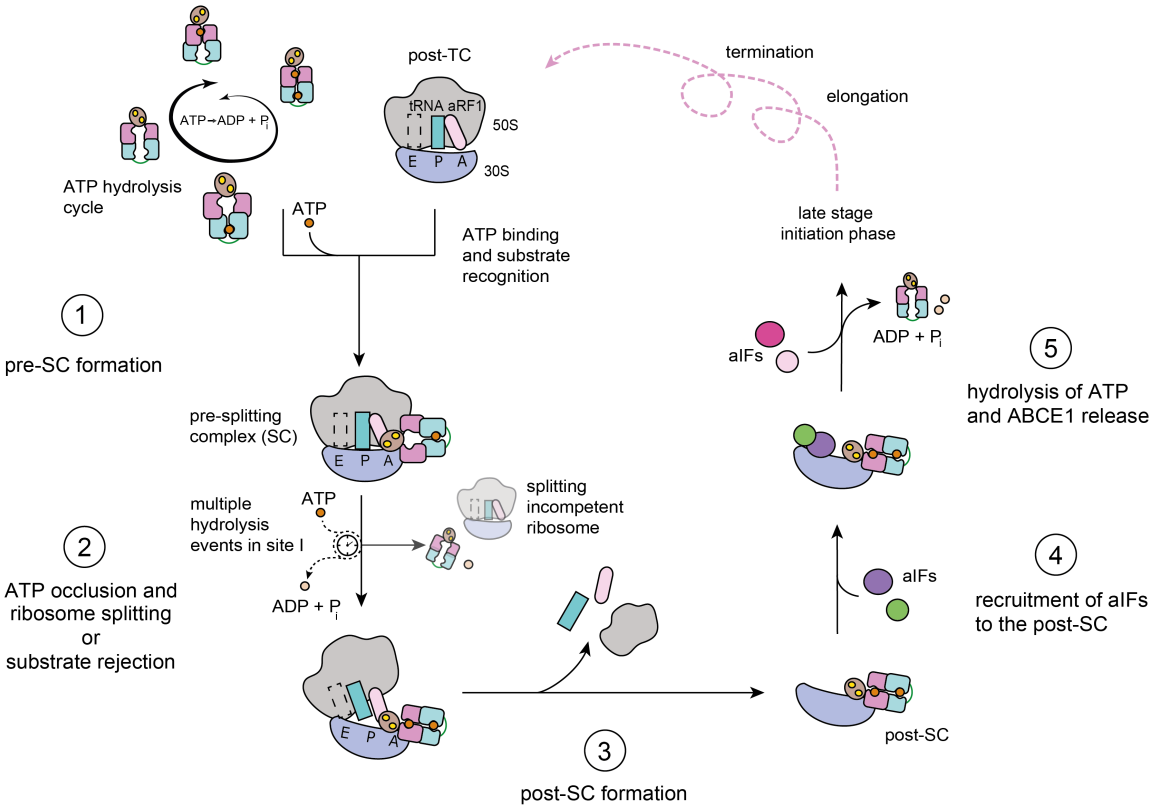

Figure 12: Molecular mechanism of ribosome recycling by ABCE1. Ribosome recycling is initialized by formation of the pre-SC *via* ABCE1 binding to assembled ribosomes. Substrate (post-TC) recognition is most efficient after binding of ATP in site II (see Fig 8). Pre-SC harbors ABCE1 with half-closed site II and open site I (step **1**). In this conformation, site I is allosterically activated and can pass multiple hydrolysis rounds before one ATP is securely occluded and site I can close, which, in turn, leads to ribosome splitting as a second step in the recycling process (see Fig 9 and 10). Alternatively, a splitting incompetent post-TC is rejected after ATP hydrolysis in the control site II (step **2**). A stable post-SC is formed with two closed nucleotide binding sites, significant for the third step of ribosome recycling. Post-SC formation is only possible if site II is occupied but, unlike the previous 70S splitting step, does not depend on closure of site I (see Fig 11; step **3**). The fourth step connects ribosome recycling with translation initiation on the 30S subunit and includes recruitment of initiation factors in the presence of bound ABCE1 (step **4**) as shown in recent cryo-EM reconstructions as well as early biochemical studies. The last step requires a trigger for ATP hydrolysis, which might be an external signal from the 30S subunit or a component of the initiation complex. Once both sites are open, ABCE1 dissociates from free or decorated 30S (step **5**).

Each phase includes important checkpoints that regulate the progression of ribosome recycling. The occlusion of one ATP is essential for recognition of the post-TC with

e/aRF1 or homologous factors. This evidence accounts for the regulation of translation in accord with the energy status of the cell. In addition, this model includes several ATP-hydrolysis rounds in site I of 70S-bound ABCE1 at *phase 2*, which explains the previously observed ATP dependency of ribosome splitting (Pisarev et al., 2010; Shoemaker and Green, 2011) and represents an important checkpoint for ABCE1. Once engaged in a pre-SC with ATP occluded in control site II, ABCE1 can either occlude an additional ATP in power-stroke site I, close both sites and split a terminated ribosome in an authorized recycling process or hydrolyze ATP in site II, open and dissociate from a splitting incompetent ribosome. Strikingly, *phase 2* (splitting) and *phase 3* (post-SC) explain the unequal impact of various site I and site II mutants in ABCE1 on cell viability (Dong et al., 2004; Karcher et al., 2005) and embryonic development (Coelho et al., 2005). Mutations interfering with closure of the nucleotide-binding sites (S223R, S469R) and thus preventing ribosome splitting in *phase 2*, are lethal but not dominant negative (Nürenberg-Goloub et al., 2018). These results are in accordance with a different set of ABC-signature mutants in yeast (G224D, G225D in site II and G470D, G471D in site I) (Dong et al., 2004). In fruit fly, a mutation in the ABC signature motif of site II (Q231L in LSGGELQ) resulted in embryonic lethality (Coelho et al., 2005). In line with the proposed mechanism (Figure 12), ABC signature mutants of ABCE1 fail to split ribosomes (Figure 9) but are not permanently engaged in ribosomal complexes (Figure 11) and thus do not interfere with translation initiation on newly synthesized ribosomal subunits. In contrast, mutations preventing ATP hydrolysis and stabilizing the ATP occluded state in site II (E493A/Q) are dominant negative and lethal, while equal distractions in site I (E247A/Q) are tolerated (Nürenberg-Goloub et al., 2018), emphasizing the crucial control task of site II. Corresponding mutations are lethal in yeast (E247Q, E493Q) and fruit-fly (E501Q) (Andersen and Leevers, 2007; Dong et al., 2004; Karcher et al., 2005). The dominant negative effect of ABCE1^{E493Q} (Dong et al., 2004) can now be explained by prolonged engagement of small ribosomal subunits in the post-SC (Figure 11) at phase three of ribosome recycling (Figure 12). This is consistent with decreased polysome levels and an inhibition of luciferase expression in whole cell extracts (Dong et al., 2004). The analogous *Drosophila melanogaster* PIXIE mutant E501Q shows a redistribution to 40S subunits (Andersen and Leevers, 2007).

My proposed model for sequential ATP binding and hydrolysis in the active sites of ABCE1 during ribosome recycling is endorsed by similar results for ABC transporters

(Abele and Tampé, 2004). It supports the processive clamp or switch model for ABC proteins as simultaneous closure of both sites is required to split the ribosome, and their concurrent opening allows dissociation of ABCE1 from the small subunit. Allosteric regulation as in ABCE1 has been reported for other ABC-type proteins and involves crosstalk of the conserved D-loops (Grossmann et al., 2014; Hohl et al., 2014; Timachi et al., 2017; Vedovato et al., 2015). Strikingly, a division of work between two asymmetric nucleotide-binding sites has recently been reported for the gating cycle of the medically relevant ABC-transporter CFTR (Sorum et al., 2017).

How are ATP hydrolysis and subsequent ABCE1 release triggered on the post-SC at phase four? Initiation factors may well serve this purpose regarding the previously demonstrated role of ABCE1 in translation initiation complex formation in yeast (Dong et al., 2004; Heuer et al., 2017) and human (Chen et al., 2006). Further, ABCE1 associates with reconstituted 43S pre-initiation complexes. Structural data indicate a function of ABCE1 in translation initiation (Heuer et al., 2017), thus supporting our early hypothesis of this versatile protein being the missing link between ribosome recycling and translation initiation (Nürenberg and Tampé, 2013). I suggest that the ribosome recycling factor ABCE1 acts as a regulator of mRNA translation and surveillance. In *Caenorhabditis elegans*, ABCE1 depletion results in embryonic lethality and slow growth (Zhao et al., 2004). ABCE1 depletion in *Xenopus laevis* fertilized eggs inhibited embryonic development before the late gastrula phase (Chen et al., 2006), thus further emphasizing the importance of ABCE1 for cell viability and embryonic development.

2.2. The archaeal post-splitting complex

The archaeal post-splitting complex comprises the 30S ribosomal subunit, ABCE1 and ATP or AMP-PNP (Barthelme et al., 2007; Kiosze-Becker et al., 2016; Nürenberg-Goloub et al., 2018). ABCE1 from yeast occludes two AMP-PNP molecules when engaged with the 40S ribosomal subunit (Heuer et al., 2017). The post-SC may serve as an adaptor between ribosome recycling and translation initiation and is therefore of high interest when studying translation as a closed cycle. So far, the archaeal post-SC from *S. solfataricus* was analyzed by chemical crosslinking and mass spectrometry (XL-MS, in collaboration with Beck Laboratory, EMBL, Heidelberg) as well as low-resolution cryo-EM (in collaboration with Beckmann Laboratory, LMU, Munich), roughly defining the global position of ABCE1 on 30S ribosomes and the interaction of the FeS-cluster domain with the ribosomal protein uS12 on its new position (Kiosze-Becker et al., 2016). To resolve delicate movements of ribosomal elements, especially 16S rRNA helix 44, and possible direct or indirect interactions with initiation factors, a high-resolution structure is highly desirable. However, we encountered severe problems during our initial cryo-EM experiments with purified *S. solfataricus* 30S subunits:

- Electron density for helix 44 was absent in all recorded datasets, indicating that h44 is either missing or highly flexible.
- The occupancy of ABCE1 on the 30S particles was very low.
- The 30S particles and post-SCs displayed a severe orientation bias, impeding structural reconstruction.

We screened for h44 electron density in *S. solfataricus* 30S ribosomes without ABCE1 applying different purification strategies, thereby excluding a preparation artifact, but it was absent in all preparations. Helix 44 plays a crucial role in ribosomal subunit association (Liu and Fredrick, 2016). Notably, crenarchaeal 70S are intrinsically instable and can only be assembled from purified subunits during *in vitro* translation but not directly purified from cell lysates (Barthelme et al., 2011; Londei et al., 1986). It is intriguing to speculate, that pronounced flexibility of h44 leads to weak subunit association *in vivo* and was implemented during evolutional adaptation to extreme environmental conditions. On the other hand, poly-uridine translation by crenarchaeal ribosomal subunits purified from cells harvested at early exponential

growth phase was five to six times more efficient compared to subunits isolated from cells in late exponential phase (Londei et al., 1986). In *Escherichia coli*, h44 is endonucleolytically removed from 30S subunits at late exponential phase to arrest translation and prevent starvation (Failmezger et al., 2016; Piir et al., 2011). This mechanism may well be exploited by crenarchaea, which must be even more sensitive to nutrient shortage.

To circumvent this unique feature of crenarchaeal ribosomes, we analyzed purified 30S subunits from the Euryarchaeon *T. celer*, which exhibited the expected electron density for h44 and was extensively characterized in terms of pre-SC formation and splitting by ABCE1 (see section 2.1). To increase ABCE1 occupancy on the 30S particles for cryo-EM, we used ABCE1$^{E238/E485A}$, which remains stably bound to 30S subunits after ribosome splitting (Nürenberg-Goloub et al., 2018). In collaboration with Dr. André Heuer, Lukas Kater, Ivan Penchev, Hanna Kratzat and Dr. Thomas Becker from the Beckmann Laboratory at the LMU, Munich, we analyzed the archaeal post-splitting complex formed after ribosome splitting of isolated *T. celer* 70S ribosomes. A large dataset of the 30S-ABCE1 sample was recorded on the TITAN KRIOS^{TM} cryo-transmission electron microscope (cryo-TEM). From 13,000 micrographs about 1.3 million particles were selected using GAUTOMATCH and processed using RELION-2.0. 3D refinement followed by 3D classification revealed, that the majority of particles contained ABCE1. However, the 3D reconstructions appeared distorted due to orientational bias of the particles on the carbon-coated cryo-EM grids. Lukas Kater and Ivan Penchev developed a thorough 3D classification regiment to minimize the distortional effect of orientation bias. In brief, particles with the same angular orientation were grouped and partially eliminated from the dataset using statistical measures. Moreover, the flexible head region was excluded from refinements using a soft mask. The final reconstruction yielded an overall resolution of the 30S body-ABCE1 of 3.8 Å. This map was used for further model building.

I built a molecular model of the post-SC based on the published models for the yeast (PDB 5LL6) and archaeal (PDB 5LW7) post-splitting complexes, and the *Pyrococcus abyssii* initiation complex (PDB 5JBH) in closed conformation (Coureux et al., 2016; Heuer et al., 2017; Kiosze-Becker et al., 2016). Therefore, the available models were first docked into the cryo-EM map as rigid bodies. At the given resolution, density for

long, bulky amino acid side chains (such as Phe, Tyr, Trp, Arg and Lys) was present in the map which enabled me to perform flexible fitting approaches in COOT (Emsley et al., 2010) followed by refinement in PHENIX (Afonine et al., 2012). The final model allowed detailed analysis of the interactions between ABCE1 and the 30S ribosomal subunit.

The archaeal post-SC structurally resembles the yeast 40S-ABCE1 complex. ABCE1 is in the closed conformation, which is largely identical (RMSD 1.34 Å over all residues) to the one observed in yeast. One of the most striking conformational rearrangements within ABCE1 occurs at the conserved FeS-cluster domain, which rotates by 150 ° into a new binding pocket at the 40S ribosome. The main structural feature at this hinge point is the so called cantilever helix (Heuer et al., 2017). As in yeast, we also observe unwinding of a cantilever helix into a loop in archaeal ABCE1. Thus, the mechanism of FeS-cluster domain rotation seems to be conserved. In yeast and Archaea, it involves the formation of new interactions between NBD1 and the loop (former helix). In particular, Lys^{90} (Lys^{93} in yeast) from NBD1 establishes an electrostatic bond with Glu^{74} (Gln^{78} in yeast) from the unwound cantilever helix and NBD1 Tyr^{292} (Tyr^{301} in yeast) interacts with the backbone of the loop to additionally stabilize this interaction (Figure 13). The interaction network of ABCE1 with the ribosome is preserved at major positions including the FeS-cluster domain - helix 44 and hinge 2 - eS6 contacts (Figure 13). Two basic residues flanking Cys^{15} (Cys^{21} in yeast), which coordinates the ferredoxin-type iron-sulfur cluster, interact with the backbone of helix 44. The interaction with eS6 occurs by electrostatic contact of the basic Arg^{584} (Lys^{592} in yeast) with a glutamate in eS6. In contrast, the archaeal ribosomal protein eS24 lacks the C-terminal stretch present in yeast and human and therefore does not interact with ABCE1 at the post-SC. Thus, while the overall binding mode and conformational rearrangements of ABCE1 during post-SC formation are conserved from Archaea to Eukarya, individual interactions may vary, leading to slight changes in affinity of ABCE1 for the small ribosomal subunit and its regulatory function within the post-SC.

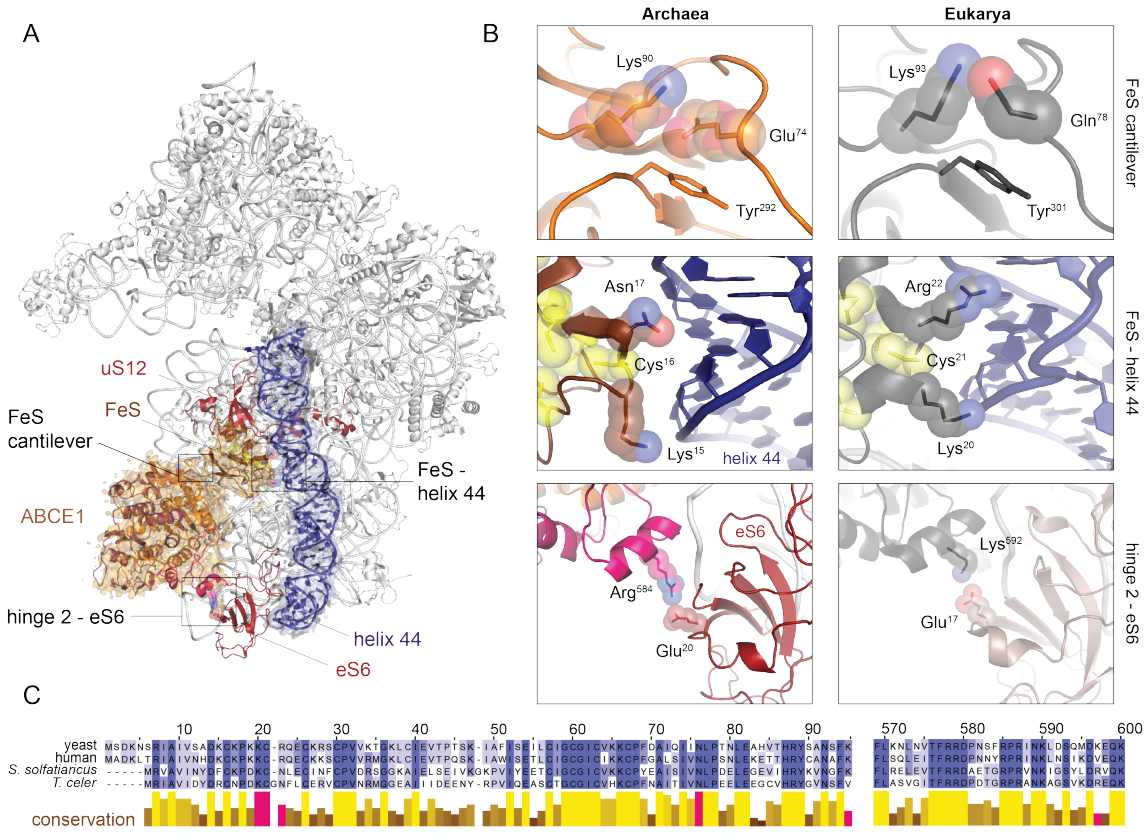

Figure 13: Interactions within the post-splitting complex of Archaea and Eukarya (PDB 5LL6)**. A)** Model of the archaeal post-SC with cryo-EM densities for ABCE1 and helix 44 represented as surface. ABCE1 binds 30S *via* its nucleotide binding domain 1 (NBD1), the FeS-cluster domain and hinge regions. Final electron density maps were provided by the Beckmann Laboratory, LMU, Munich. The post-SC was modelled based on *P. abyssii* 30S (PDB 5JBH) utilizing Coot (Emsley et al., 2010) and refined using phenix (Afonine et al., 2012). **B)** Zoom-in into crucial areas of the archaeal post-SC highlighted in A) in comparison with the yeast structure (PDB 5LL6). The rotation of the FeS-cluster domain is supported by interactions of the unwound cantilever helix with NBD1. The FeS-cluster domain and the hinge 2 region interact with helix 44 and ribosomal protein eS6, respectively. Residues of the intra- and intermolecular network of ABCE1 are highlighted as pink bars in **C)** the sequence alignment of eukaryotic and archaeal ABCE1 FeS-cluster domains and hinge 2 regions and vary from high to low conservation status.

2.3. Tying up loose ends: ABCE1 in translation initiation

In the context of translation, ABCE1 was initially described as an initiation factor, promoting the assembly of various initiation complexes in a catalytic fashion (Chen et al., 2006; Dong et al., 2004). The molecular mechanism of ribosome recycling by ABCE1 in Eukarya and Archaea includes the formation of a stable post-splitting complex on the small ribosomal subunit (Heuer et al., 2017; Kiosze-Becker et al., 2016; Nürenberg-Goloub et al., 2018). The release of ABCE1 must be attended by ATP hydrolysis in both sites, which is triggered by a yet unknown mechanism. Archaeal translation initiation begins with decoration of 30S ribosomes by aIF1 and aIF1A, which accelerate the recruitment of aIF2. Upon 30S binding, aIF2's affinity for Met-tRNA^{Met} rises 40-fold, thus facilitating trimeric complex formation (Hasenohrl et al., 2009). Mostly leaderless mRNA in *S. solfataricus* is acquired based on the interaction of the start codon with the initiator tRNA within the initiation complex (Benelli et al., 2003). Subunit joining is catalyzed by aIF5B (Maone et al., 2007) and presumes preceding dissociation of aIF1, which sterically interferes with 50S binding. In Eukarya, eIF1 and eIF1A bind 40S in a cooperative fashion (Maag and Lorsch, 2003). Upon AUG recognition by the trimeric complex, eIF1 is released and eIF5B is recruited by eIF1A (Maag et al., 2006; Mitchell and Lorsch, 2008). In Archaea, the involvement of aIF5B has only been studied independently of other initiation factors (Maone et al., 2007). However, aIF5B was of minor interest for this work as eIF5B shares a common binding site with ABCE1 on the small ribosomal subunit (Fernandez et al., 2013) and naturally can only be recruited after ABCE1 release.

2.3.1. Reconstitution of archaeal translation initiation

To study the order of events downstream of post-SC formation, I reconstituted the archaeal translation initiation pathway until the recognition of the AUG start codon in the P-site by the initiator tRNA. I established the heterologous expression and purification of archaeal initiation factors aIF1, aIF1A, the aIF2 subunits α, β and γ as well as aIF5B and the 50S anti-association factor aIF6 based on published protocols (Barthelme et al., 2011; Hasenohrl et al., 2009; Maone et al., 2007). *E. coli* initiator tRNA^{fMet} expression and purification (Stolboushkina et al., 2013) was optimized based on a protocol kindly provided in personal communication with Elena Stolboushkina at the Garber Lab, Institute of Protein Research, Moscow. The tRNA

was methionylated by a previously described truncated version of the *E. coli* methionine-tRNA-synthetase (MetRS), likewise homologously expressed and purified (Stolboushkina et al., 2013). All components in hands, I verified the integrity of aIF2 and its ability to specifically bind only methionylated Met-tRNA^{fMet} by size exclusion chromatography (Figure 14). As expected, aIF2 was recruited to 30S independently of ABCE1 and *vice versa* (Figure 14 and S7). Recruitment of aIF1, aIF1A, aIF2 as well as the trimeric complex aIF2-Met-tRNA^{fMet}-GMP-PNP to post-SCs was confirmed by co-immunoprecipitation with ABCE1$^{E238A/E485A}$-FLAG and sucrose density gradient centrifugation in the presence of 30S ribosomes and GMP-PNP (Figure 14 and S7). Thus, canonical translation initiation complexes in Archaea assemble likewise in the absence and presence of ABCE1. However, since my studies primarily aimed towards structure determination under steady state conditions, I used non-hydrolysable nucleotide analoga and the hydrolysis-deficient ABCE1$^{E238A/E485A}$ mutant. Thus, kinetic and thermodynamic parameters as well as allosteric nucleotide hydrolysis and factor release remain to be elucidated by further biochemical experiments.

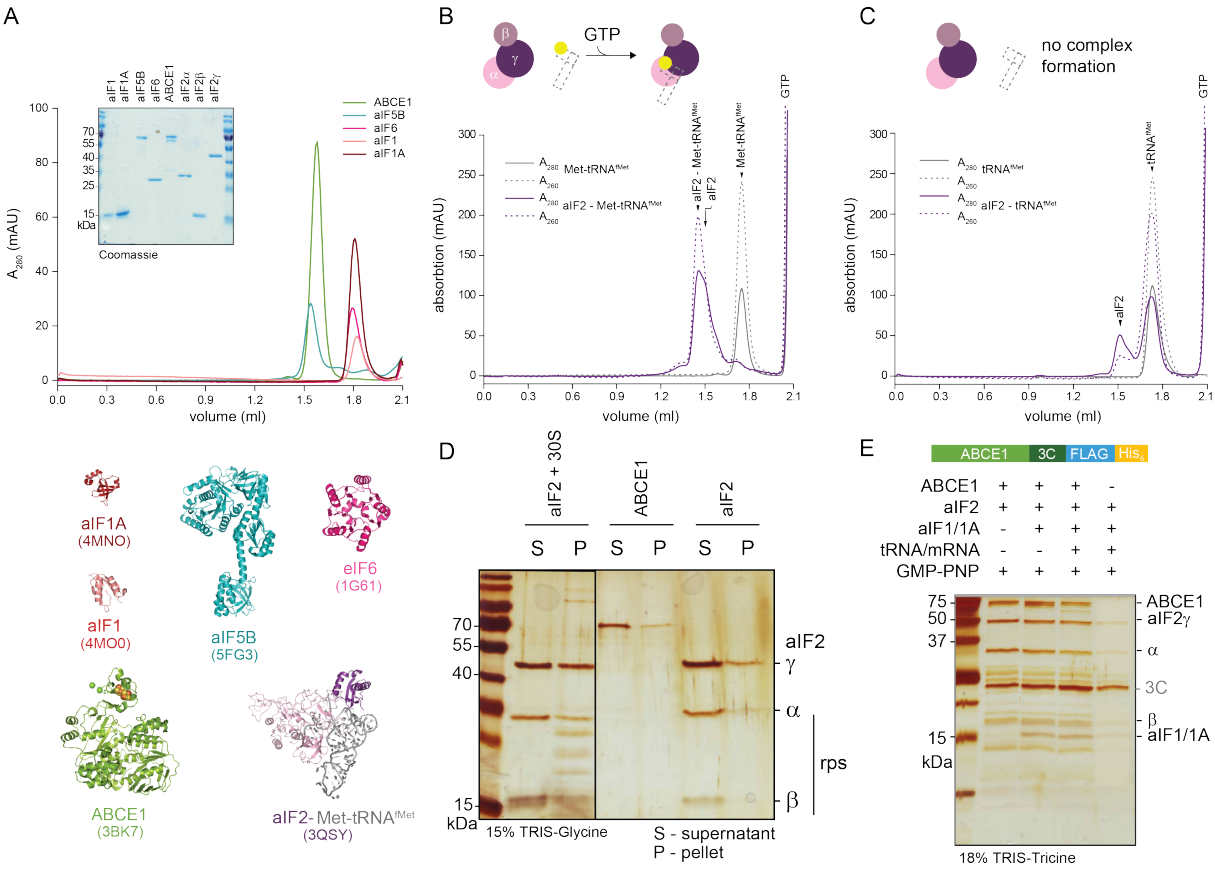

Figure 14: Reconstitution of the archaeal translation initiation. A) Initiation factors from *S. solfataricus* were purified to monodispersity as seen in SEC and SDS-PAGE. The structures of all archaeal initiation factors were determined by protein crystallography and X-ray diffraction. Note that the large IFs aIF2, aIF5B as well as ABCE1 are likely to adopt distinct conformations to fulfill their function during translation initiation at 30S ribosomes. **B)** aIF2-GTP quantitatively binds methionylated $tRNA^{fMet}$ but not **C)** the uncharged tRNA, confirming the functionality of aIF2 and successful *in vitro* methionylation of the tRNA by recombinant MetRS. **D)** aIF2 co-sediments with 30S ribosomes in the presence of GTP. **E)** anti-FLAG immunoprecipitation of post-splitting/pre-initiation complexes *via* $ABCE1^{E238A/E485A}$-FLAG (0.8 µM) demonstrates the presence of all initiation factors (1 µM aIF1/1A, 0.8 µM aIF2, 0.96 µM Met-$tRNA^{fMet}$, 4 µM mRNA) and ABCE1 on 30S ribosomes (0.4 µM) in the presence of GMP-PNP (0.2 mM).

2.3.2. Structural studies of archaeal translation initiation complexes

After completing ribosome recycling, ABCE1 remains engaged with the small ribosomal subunit in Eukarya and Archaea (Heuer et al., 2017; Kiosze-Becker et al., 2016; Nürenberg-Goloub et al., 2018). Additionally, it associates with initiation factors

and facilitates their recruitment to 40S ribosomes in yeast and human (Chen et al., 2006; Dong et al., 2004). Both observations indicate an involvement of ABCE1 in initiation, which would close the cycle of mRNA translation. However, the molecular mechanism of ABCE1 in initiation is still elusive. Previous low-resolution cryo-EM studies of native post-SCs from yeast reveal the simultaneous presence of ABCE1 and initiation factors at the 40S subunit but do not allow conclusions about their interplay (Heuer et al., 2017). Compared to the elaborate canonical initiation pathway in Eukaryotes, the archaeal system comprises only the conserved core-machinery and is therefore the ideal model to study defined, reconstituted post-splitting/pre-initiation complexes. However, peripheral regions of archaeal initiation complexes including all initiation factors remain only poorly resolved by cryo-EM in the absence of ABCE1 (Coureux et al., 2016). Thus, precise positioning of secondary structure elements, not to mention individual sidechains, is not possible. In order to study the allosteric crosstalk of initiation factors with the ribosome and ABCE1, a high-resolution structure is inevitable. Therefore, I reconstituted a section of archaeal translation starting with *T. celer* 70S ribosome splitting by ABCE1$^{E238A/E485A}$ and aRF1/aPelota, subsequent decoration of stably formed post-SCs with aIF1, aIF1A and Shine-Dalgarno-leader-mRNA and finally the recruitment of the trimeric complex aIF2-Met-tRNA^{fMet}-GMP-PNP (Figure S8). Notably, this *in vitro* assembly line does not perfectly reflect the putative *in vivo* situation, which was, however, also derived from *in vitro* experiments (Hasenohrl et al., 2009). The post-splitting/pre-initiation complexes were purified by sucrose density gradient centrifugation. Initiation complex reconstitution and sample preparation was systematically improved and finally analyzed by negative stain and cryo-EM at the Beckmann Laboratory, LMU, Munich.

A small dataset was recorded on the TECNAI^{TM} SPIRIT cryo-TEM and processed using RELION-2.0. This microscope allows for low/intermediate resolution (15-20 Å) characterization of the sample. After 2D classification, particles were refined and subjected to 3D classification to analyze particle composition and heterogeneity. Four classes were obtained. One class showed density for ABCE1 as observed in the high resolution structure presented above (see section 2.2). Three classes displayed additional density for initiation factors, yet showing heterogeneity.

The four particle classes (Figure 15) reflect putative intermediates of the biochemically described archaeal translation initiation pathway (Hasenohrl et al., 2009). ABCE1 was present in all particle classes and 30S ribosomes were in part decorated with aIF1, aIF1A, and tRNA. However, density for aIF2 was disappointing weak, though present in stoichiometric amounts (Figure S8). Nevertheless, initiation complexes containing ABCE1 represent novel translational intermediates. Taken together, my work sets the stage for further analysis of archaeal initiation using high resolution data with a TITAN KRIOS™ cryo-TEM. This data might clarify, if a – possibly transient – direct interaction between ABCE1 and initiation factors exists. Moreover, subtle changes in 16S rRNA helix 44 or the universally conserved ribosomal protein uS12 could transmit initiation factor binding to ABCE1 *via* the FeS-cluster domain.

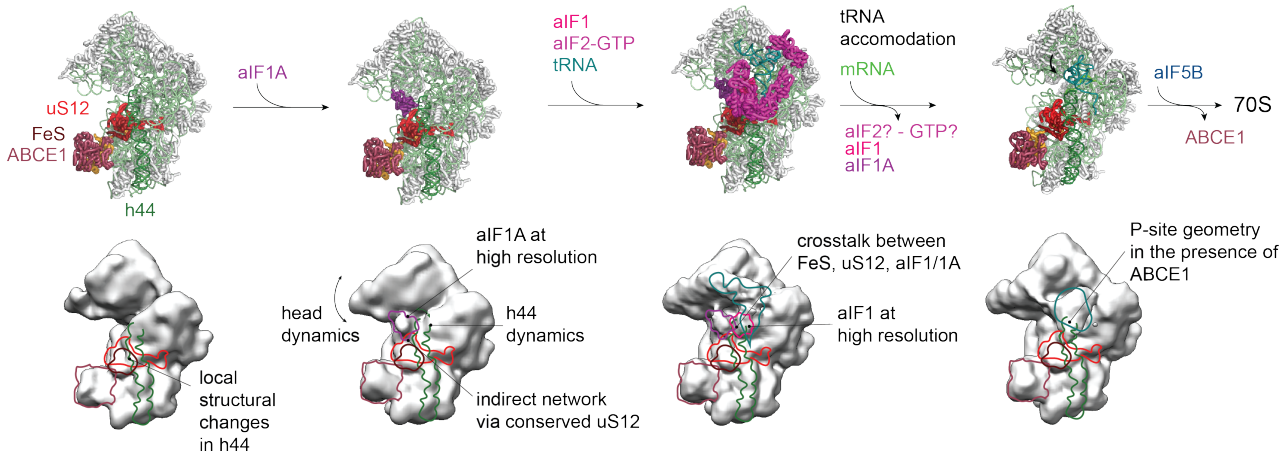

Figure 15: Intermediate resolution cryo-EM of archaeal translation initiation complexes. The four classes obtained after 3D classification were sorted according to the presence of extraribosomal density. Rigid body fits of molecular models putatively explaining the EM maps are shown on top (PDB 5LW7, 5JB3, 5JBH). Outlines were drawn for factors with clearly assignable densities. While ABCE1, aIF1, aIF1A, and tRNA are clearly present, only residual density was found for aIF2. Note, that the four classes might explain a potential assembly pathway of archaeal translation initiation.

Loose Ends – The Outlook

Protein biosynthesis *via* mRNA translation at the ribosome is one of the most conserved cellular pathways, essential for the viability, proliferation, and development of cells from all three kingdoms of life. From unicellular Archaea to mammals, ribosome recycling by the conserved twin-ATPase ABCE1 is a regulatory gateway between termination and initiation. It closes the cycle of archaeal and eukaryotic translation and represents a linchpin to coordinate mRNA translation, mRNA surveillance, ribosome-associated protein quality control, ribosome homeostasis and associated pathways. This study precisely describes the molecular mechanism of ABCE1 during ribosome recycling and structurally connects it to translation initiation. However, these novel insights rise open questions to be answered in future research. Obviously, high-resolution structures of the reconstituted initiation complexes with ABCE1 must be solved. Biochemical experiments should reveal the exact function of ABCE1 during initiation and the trigger for ABCE1 release from the post-splitting / pre-initiation complex. Additionally, the studies of ABCE1's role during initiation should be enhanced by *in vivo* approaches like viability studies with relevant mutants or structural investigation of native complexes. Besides these central questions, it remains to be elucidated what role the iron-sulfur clusters in ABCE1 play for the regulation of protein biosynthesis. It is intriguing to speculate, that the remarkable conservation of such a complex ligand is the result of a yet unknown evolutional advantage. The dependence of ribosome homeostasis on e.g. oxygenic stress or the cellular nutrition status would perfectly fit the regulatory role of the ribosome recycling process and holistically embed it into the complex network of cellular pathways.

3. Material and Methods

3.1. General microbiological and biochemical methods

3.1.1. Bacterial strains and media

Table 1: *E. coli* strains used in this study

strain	genotype	purpose	source
Mach1	W Δ*recA1398 endA1 fhuA* Φ80Δ(*lac*)M15 *Δ(*lac*)X74* hsdR*(*$r_K^-m_K^+$*)*	plasmid amplification	Invitrogen
BL21 (DE3) pLysS	B F^- *ompT gal dcm lon hsdS*$_B$($r_B^-m_B^-$) λ(DE3 [*lacI lacUV5-T7p07 ind1 sam7 nin5*]) [*malB*$^+$]$_{K-12}$(λ^S) pLysS[*T7p20 ori*$_{p15A}$](Cm^R)	heterologous protein expression	stock in Tampé lab
MRE600	not specified, RNase I deficient	tRNA expression	National Collection of Type Cultures (NCTC 8164)

Table 2: Media used for *E. coli* growth

medium	component	final concentrations
LB	NaCl	1.0% (w/v)
	Yeast extract	0.5% (w/v)
	Tryptone / Peptone	1.0% (w/v)
added for LB plates	Agar-agar	1.5% (w/v)
TB	Yeast extract	1.2 % (w/v)
	Tryptone / Peptone	2.4 % (w/v)
	Glycerol	0.5 % (v/v)
	KH_2PO_4	17.0 mM
	K_2HPO_4	72.0 mM
SOB	Yeast extract	5 g/l
	Tryptone	20 g/l
	NaCl	10.0 mM
	KCl	2.5 mM
	$MgSO_4$	10.0 mM
	$MgCl_2$	10.0 mM
SOC	SOB-medium	-
	Glucose	10.0 mM

Table 3: Medium used for growth of *S. solfataricus* (Brock et al., 1972)

medium	**component**	**final concentration**
modified Brock	$CaCl_2$	0.48 µM
pH set to 3.5 with H_2SO_4	$(NH_4)SO_4$	0.10 M
	$MgSO_4$	1.00 mM
	H_2SO_4	10 µl/L
	KH_2PO_4	2.00 mM
	$MnCl_2$	50.00 pM
	$Na_2B_4O_7$	0.60 nM
	$ZnSO_4$	3.20 nM
	$CuCl_2$	2.50 pM
	$NaMoO_4$	0.50 pM
	$CoSO_4$	1.50 pM
	$NiSO_4$	0.45 pM
	H_2SO_4	5 µl/L
	Bacto™ Tryptone	0,1% (w/v)
	$FeCl_3$	7.50 µM

3.1.2. Growth of *S. solfataricus*

S. solfataricus is cultured in Brock medium (Table *3*), which needs to be preheated before inoculation. During culture growth, pH is kept constant in a range of 3.5 – 4.8 by dropwise addition of H_2SO_4. First and second pre-cultures (50 ml and 400 ml, respectively) are grown at 80 °C until an OD_{600} of app. 0.6 before the main culture (10-12 L) is inoculated. The main culture harvested at an OD_{600} of app. 0.6 in late logarithmic growth phase. Therefore, the culture is cooled to 20-30 °C before centrifugation at 4500 *g* for 30 min at 4 °C. The pellet is washed in ribosome extraction buffer (20 mM TRIS pH 7.5, 40 mM NH_4Cl, 10 mM $Mg(OAc)_2$) and again centrifuged at 5000 *g* for 20 min at 4 °C. Cells are again resuspended in ribosome extraction buffer and the cell suspension is dropwise transferred into liquid nitrogen. The cell spherules are then stored at – 80 °C.

3.1.3. Transformation of *E. coli*

For transformation, 50-100 µl Mix & Go (Zymo Research) competent cells prepared according to manufacturer's guide were mixed with 50-100 ng plasmid DNA on ice. After 10 min incubation on ice, 400-600 µl SOC medium (Table *2*) were added. The

cells were incubated for 1 h at 37 °C with mild agitation before being plated on LB-agar plates with the respective antibiotics.

3.1.4. Agarose gel electrophoresis

Agarose gel electrophoresis was routinely used to control PCR results. Therefore 1-2% (w/v) agarose was melted in TEA-buffer (40 mM TRIS pH 8.5, 0.035% (v/v) AcOH, 1 mM EDTA) and gels were prepared. The samples were mixed with 6x DNA loading buffer (Thermo Scientific) before being loaded onto the gel and a total volume of 10-12 µl was loaded per lane. The electrophoresis was performed in TEA-buffer at 150 V for 45 min. As marker the GeneRuler 1 kb DNA Ladder (Thermo Scientific) was used. The gels were stained with ethidium bromide for 30 min before being analyzed under a UV-screen.

3.1.5. Urea-PAGE

Urea gels were prepared as described in Table *4*. The samples were mixed with 1:1 (v/v) RNA loading buffer (95% (v/v) formamide, 0.02% (w/v) SDS, 0.02% (w/v) Bromphenol blue, 0.01% (w/v) Xylene cyanol, 1 mM EDTA pH 8.0) and heated to 70 °C for 5 min before being loaded onto the gel. 10 µl were loaded per lane. The electrophoresis was performed at 180 V in TBE-buffer (0.1 M TRIS, 0.1 M boric acid, 2 mM EDTA pH 8.0). The bands were visualized under UV light after ethidium bromide staining for 30 min.

Table 4: Composition of Urea-PAGE gels

component	volume / weight
Rotiphorese Gel 40 (19 : 1) acrylamide / bisacrylamide	5.0 ml
Urea	12 g
10x TBE buffer	2.5 ml
H_2O	add up to 25.0 ml
10% (w/v) APS stock solution	125 µl
TEMED	25 µl

3.1.6. SDS-PAGE

Discontinuous SDS-PAGE gels (Laemmli, 1970) were prepared as described in Table *5* and Table *6*. Samples were mixed with 4 x SDS-loading buffer (200 mM

TRIS pH 6.8, 6% (w/v) SDS, 30% (v/v) glycerol, 0.06% (w/v) Bromphenole blue, 6 mM β-mercaptoethanol (BME)) and heated at 95 °C for 10 min before loading. Varying sample volume was loaded per lane. 1 kb PAGE Ruler Protein Ladder (Thermo Scientific) was used as protein weight marker. An electric field of 160-180 V was applied for 1 h in TRIS-glycine (25 mM TRIS, 190 mM glycine, 0.1% (w/v) SDS) or TRIS-tricine (anode: 200 mM TRIS pH 9.9; cathode: 100 mM TRIS, 100 mM tricine, 0.1% (w/v) SDS) running buffer system for the respective gels. Gels were either processed for Western Blotting or stained with InstantBlue™ Protein Stain (Expedeon) according to manufacturer's suggestion or silver according to a standard protocol.

Table 5: Composition of TRIS-glycine SDS-PAGE gels

component	resolving gel	stacking gel
Rotiphorese Gel 30 (37.5 : 1) acrylamide / bisacrylamide	9.4 ml	1.3 ml
1.5 M TRIS pH 8.8 0.4 % (w/v) SDS	8.0 ml	-
0.5 M TRIS pH 6.8 0.4 % (w/v) SDS	-	2.2 ml
H_2O	2.4 ml	5.4 ml
10% (w/v) APS stock solution	120 µl	90 µl
TEMED	60 µl	30 µl

Table 6: Composition of TRIS-tricine SDS-PAGE gels

component	resolving gel	stacking gel
Rotiphorese Gel 40 (19 : 1) acrylamide / bisacrylamide	15.0 ml	3.2 ml
Gel buffer	15.0 ml	7.5 ml
Glycerol	6.0 ml	-
H_2O	9.3 ml	20.0 ml
10% (w/v) APS stock solution	200 µl	240 µl
TEMED	20 µl	24 µl

3.1.7. Immunoblotting

Proteins were transferred from SDS-PAGE gels onto a nitrocellulose membrane (GE Healthcare) (Burnette, 1981; Renart et al., 1979) using the semi-dry immunoblot technique in transfer buffer (25 mM TRIS, 192 mM glycine, 20% (v/v) methanol. The membrane was blocked (20 mM TRIS pH 8.0, 150 mM NaCl, 5% (w/v) skim milk

powder, 0.1% (v/v) Tween20, 0.1% (w/v) NaN_3) for at least 30 min before incubation with the primary mouse monoclonal anti-poly-His antibody (Novagen) in blocking buffer at a dilution of 1:1000 (v/v) over night at 4 °C. The membrane was washed three times for at least 5 min with TBS-T (20 mM TRIS pH 8.0, 150 mM NaCl, 0.1% (v/v) Tween20), incubated with the secondary anti-mouse-IgG-HRP antibody (Sigma Aldrich) at a dilution of 1:20,000 (v/v) in TBS-T for at least 1 h at room temperature and washed three more times in TBS-T before read-out. For picture acquisition, the membrane was shortly incubated with ECL1 (100 mM TRIS pH 8.0, 2.5 mM luminole, 0.4 mM coumarine) and ECL2 (100 mM TRIS pH 8.0, 0.02% (v/v) H_2O_2) solutions and immediately transferred to a luminescent imaging system.

3.1.8. Size exclusion chromatography (SEC)

ABCE1, aRF1, aPelota and aIF6 were analyzed by analytical SEC (Superdex™ 200, 24 ml column, GE Healthcare) on the Äkta Prime Plus chromatography system (GE Healthcare) in SEC^{25} buffer (20 mM TRIS pH 7.5, 250 mM NaCl, 5 mM $MgCl_2$, 15% (v/v) glycerol, 2 mM DTT) at room temperature, because aRF1 and aPelota tend to precipitate during prolonged incubation at 4 °C. All variants of ABCE1 were additionally run on a 2.4 ml Superose™ 6 column (GE Healthcare) on Äkta Ettan chromatography system (GE Healthcare) in SEC^4 buffer (20 mM TRIS pH 7.5, 250 mM NaCl, 5 mM $MgCl_2$, 2 mM DTT) at 4 °C recording the absorption at 280 nm and 410 nm to analyze the integrity of the iron-sulfur clusters. Initiation factors and (Met-)tRNA were analyzed on a Superdex™ 200, 2.4 ml column (GE Healthcare) on the Äkta Ettan Chromatography System (GE Healthcare) or Superdex™ 200, 24 ml column (GE Healthcare) on the Äkta Purifier chromatography system (GE Healthcare) at 4 °C in acidic SEC buffer (50 mM Bis-TRIS pH 5.8, 150 mM KCl, 10 mM $MgCl_2$, 4 mM BME) to preserve the labile ester bond of the methionylated tRNA.

3.1.9. Sucrose density gradient (SDG) centrifugation

SDG was routinely used for ribosome purification and biochemical assays as described in detail in the respective sections. In general, continuous gradients were prepared from sucrose solutions of the required density (Biocomp Instruments) and centrifuged in a SW41 rotor (Beckmann Coulter) at either 40,000 rpm for 3 h or 20,000 rpm for 14 h. Gradients were fractionated by Piston Gradient Fractionator (Biocomp Instruments) into 0.5 ml fractions. For ribosome purification, those were

analyzed regarding their absorption at 254 nm to identify the ribosome-rich fractions. For SDS-PAGE and immunoblot analysis, the fractions were precipitated by addition of ice-cold acetone overnight and pelleted by centrifugation at 16,000 *g* for 1h, the pellets were then resuspended in TBS and prepared for SDS-PAGE.

3.2. Molecular genetics

3.2.1. Cloning

To construct the ABCE1-FLAG protein, a 3C-FLAG DNA sequence was introduced between ABCE1 and the His_6 tag in the pSA4 vector by overlapping DNA primers between ***Bam*HI** and ***Hind*III** precision sites and ligated by a standard protocol. The primers 5'-**gat cc**c tgg aag tgc tgt ttc agg gcc cgg att ata aag atg atg atg ata aac atc atc acc acc atc act aga-3' and 5'-**agc tt**c tag tga tgg tgg tga tga tgt tta tca tca tca tct tta taa tcc ggg ccc tga aac agc act tcc agg-3' were purchased from MWG Eurofins (Göttingen, Germany).

The archaeal IF1 with an N-terminal His_6-tag and enterokinase cleavage site was cloned from the pRSETB vector into the pSA4 vector due to expression problems in pRSETB. Therefore, the aIF1 construct was amplified using the 5'- gac ata **cca tgg** tgc atc atc atc atc atc atg gta tgg cta gca tg-3' and 5'-gca tgt c**aa gct tt**c atc aaa taa cta gaa tat tgg att ctg cat atc cc-3' primers (MWG Eurofins, Göttingen, Germany) and cloned into pSA4 using ***Nco*I** and ***Hind*III** restriction sites by a standard protocol.

Amplification specificity was checked using agarose gel electrophoresis. FastDigest restriction enzymes (Thermo Scientific) were used and digested vector and insert were purified by from bulk (insert) or agarose gel cut-outs (vector) using the QUIamp® DNA Mini Kit (Quiagen). Ligation was performed with T4 DNA Ligase (Invitrogen) with the provided buffers using a molar ratio of 1:7 (vector : insert). Concentration of the purified DNA components was estimated by A_{260}.

3.2.2. Site directed mutagenesis

Point mutations were introduced into ABCE1 by two-step megaprimer PCR as described (Barik, 1996). Megaprimers were generated using the 5'- gga gta tta ggg aag aat gga gta ggg aaa ac-3' non-mutagenic primer and the 5'- cat tct ttc cct aac atc tag ata aga aga agg t**g**c gtc aaa tat gta tac-3' primer for the E238A and the 5'-ctt cga cat cga gat aag agg aag gt**g** cat cca aaa c-3' primer (MWG Eurofins, Göttingen, Germany) for the E485A **mutations**. Amplification specificity for the megaprimer was checked using agarose gel electrophoresis before the whole-vector PCR step.

3.2.3. Plasmid preparation and sequencing

Plasmids were isolated using the NucleoSpin® Plasmid purification kit (Macherey-Nagel) according to manufacturer's instruction with slight modifications. In particular, the spin column was dried for 10 min at 73 °C before plasmid elution to evaporate residual ethanol. Sanger sequencing of all constructs created and used in this work was performed either at Seqlab (Microsynth, Göttingen, Germany) or MWG (Eurofins, Ebersberg, Germany) Laboratories with provided standard primers for T7 promoter and terminator regions.

3.3. Expression and purification of proteins and tRNA

All proteins were expressed in *E. coli* BL21 (DE3), cotransformed with *pRARE* plasmid (Novagen) in the presence of 25 µg/ml chloramphenicol (cm). Cells were grown overnight in LB medium with 100 µg/ml carbenicillin (amp) or 30 µg/ml kanamycin (kan) at 37 °C and used to inoculate the main culture in TB medium with the same resistance markers at a ratio of 1:20. Cells were grown at 37 °C until an OD_{600} of 0.6-0.8 and expression was carried out according to Table *7*.Table *7* $tRNA^{fMet}$ was constitutively expressed in *E. coli* MRE600, a strain lacking several cytoplasmic RNAses, under the native promoter. Transformed colonies were washed from the agar plate into LB medium containing 100 µg/ml carbenicillin and grown under extensive shaking (200 rpm) according to Table *7*. Cells were harvested *via* centrifugation at 5000 x *g* for 15 min at 4 °C and pellets were stored frozen at -20 °C. Plasmids carrying the respective gene and selection marker for the expression of ABCE1 were previously constructed at the Tampé Laboratory (Barthelme et al., 2011). Plasmids for aIF2α and aIF2γ were kindly donated by the Wöhnert Laboratory. Plasmids for aIF1, aIF1A and aIF2β were kindly donated by Prof. Udo Bläsi, Max F. Perutz Laboratories, Vienna, Austria. Plasmids for $tRNA^{fMet}$ and MetRS were kindly donated by Prof. Maria Garber, Institue of Protein Research, Moscow, Russia. The plasmid for the expression of aIF5B was donated by Prof. Paola Londei, Sapienza University of Rome, Rome, Italy.

Table 7: Expression conditions for proteins and tRNA

protein	T (°C)	[IPTG] (mM)	T (h)	resistance marker
ABCE1	20	1.0	20	amp, cm
aRF1	20	0.5	20	amp, cm
aPelota	20	0.5	20	amp, cm
aIF1	37	0.5	3	amp, cm
aIF1A	37	1.0	5	amp, cm
aIF2α	20	1.0	20	amp, cm
aIF2β	20	1.0	20	kan, cm
aIF2γ	20	1.0	20	amp, cm
aIF5B	37	0.4	5	amp, cm
aIF6	18	0.3	12	amp, cm
MetRS	20	0.5	20	kan, cm
$tRNA^{fMet}$	37	-	20	amp

For protein purification, frozen cell pellets were supplemented 1:1 (v/v) with the appropriate Lysis buffer, thawed at 4 °C and disrupted with 5-8 pulses of 2 min on ice, using a Branson Sonifier 250 at 70% output. The lysate was centrifuged at 130,000 x *g* for 20-40 min. For purification of thermostable archaeal proteins, the supernatant was incubated at 65 °C for 10 min to precipitate host proteins, followed by a second centrifugation step at 130,000 x *g* for 30-60 min. The supernatant of the second centrifugation step was used for chromatographic purification. For purification of MetRS (section 3.3.5), the differential heat precipitation step was omitted.

3.3.1. ABCE1

All ABCE1 variants were purified by immobilized metal chelate (IMAC, HiTrap™ Chelating HP, 5 ml, GE Healthcare) and anion exchange chromatography (AIEX, HiTrap™ Q column, 1 ml, GE Healthcare) at room temperature utilizing different chromatography systems. Cell pellets were resuspended in Lysis buffer G (20 mM TRIS-HCl pH 8.0, 300 mM NaCl, 5 mM $MgCl_2$, 40% glycerol (v/v), and 8 mM BME) and lysate was prepared for chromatography using differential heat precipitation as described in section 3.3. The IMAC column was washed with buffer IMAC-G^{100} A (20 mM TRIS-HCl pH 8.0, 100 mM NaCl, 20 mM imidazole, 15% glycerol, and 2 mM BME) until the baseline of absorbance at 280 nm was reached. ABCE1 was then eluted by 100% buffer IMAC-G^{100} B (20 mM TRIS-HCl pH 8.0, 100 mM NaCl, 200 mM imidazole, 15% glycerol, and 2 mM BME). The buffer was exchanged against AIEX-G^{ABCE1} A (20 mM TRIS-HCl pH 8.5, 5 mM NaCl, 15% glycerol, and 2 mM BME) by a Sephadex™ G-25 desalting column (GE Healthcare), and ABCE1 was further purified by AIEX. After loading, the AIEX column was washed with buffer AIEX-G^{ABCE1} A until the baseline was reached. ABCE1 was then eluted by a gradient of 0-30% AIEX-G^{ABCE1} B (20 mM TRIS-HCl pH 8.5, 1 M NaCl, 15% glycerol, and 2 mM BME). Fractions containing ABCE1 were identified by SDS-PAGE and the brown color of the iron-sulfur clusters. Buffer of the pooled fractions was exchanged against Storage-G^{150} buffer (20 mM TRIS-HCl pH 7.5, 150 mM NaCl, 15% glycerol, and 2 mM BME) by PD10 gravity flow desalting columns (BioRad). Protein was concentrated using Amicon™ Ultra centrifuge device (30 kDa cut-off, Merck Millipore), snap-frozen in liquid nitrogen, and stored in small aliquots at -80 °C. Protein concentration was determined at A_{280} (ε_{280} = 58,000 M^{-1} cm^{-1}).

3.3.2. aRF1 and aPelota

aRF1 and aPelota were purified by IMAC (HiTrap™ Chelating HP, 5 ml, GE Healthcare) and AIEX (HiTrap™ Q column, 1 ml, GE Healthcare) at room temperature using an Äkta Prime Plus System (GE Healthcare). The respective steps were carried out in Lysis buffer G and IMAC-G^{240} buffers A (20 mM TRIS-HCl pH 8.0, 240 mM NaCl, 20 mM imidazole, 15% (v/v) glycerol, and 4 mM BME) and B (20 mM TRIS-HCl pH 8.0, 240 mM NaCl, 200 mM imidazole, 15% glycerol, and 4 mM BME). After loading, the IMAC column was washed with IMAC-G^{240} A until the baseline of absorbance at 280 nm was reached and aRF1/aPelota was eluted by a short gradient (0-100% buffer B in 30 ml), which yielded one major peak that mostly contained a protein of the expected size as verified by SDS-PAGE. For subsequent AIEX, the buffer of all major peak fractions was exchanged to AIEX-G^{aRF} A (20 mM TRIS-HCl pH 8.5, 40 mM NaCl, 4 mM $MgCl_2$ 15% glycerol, and 4 mM BME) by PD10 gravity flow desalting columns (BioRad). aRF1/aPelota was eluted from the AIEX column by a flat gradient; 0-30% AIEX-G^{aRF} B (20 mM TRIS-HCl pH 8.5, 1 M NaCl, 4 mM $MgCl_2$ 15% glycerol, and 4 mM BME) in 60 ml. Fractions containing aRF1/aPelota were identified by SDS-PAGE. Buffer of the pooled fractions was exchanged against Storage-G^{250} buffer (20 mM TRIS-HCl pH 7.5, 250 mM NaCl, 5 mM $MgCl_2$, and 15% glycerol) by PD10 gravity flow desalting columns (BioRad). Protein was concentrated using Amicon™ Ultra centrifuge device (10 kDa cut-off, Merck Millipore), snap-frozen in liquid nitrogen, and stored in small aliquots at -80 °C. Protein concentration was determined A_{280} (ε_{280} = 35,000 M^{-1} cm^{-1}).

3.3.3. aIF6

aIF6 was purified by IMAC (HiTrap™ Chelating HP, 5 ml, GE Healthcare) and AIEX (HiTrap™ Q column, 1 ml, GE Healthcare) at room temperature using an Äkta Prime Plus System (GE Healthcare). The respective steps were carried out in Lysis buffer G and IMAC-G^{300} buffers A (20 mM TRIS-HCl pH 8.0, 300 mM NaCl, 20 mM imidazole, 15% (v/v) glycerol, and 2 mM BME) and B (20 mM TRIS-HCl pH 8.0, 300 mM NaCl, 200 mM imidazole, 15% glycerol, and 2 mM BME). After loading, the IMAC column was washed with IMAC-G^{300} until the baseline was reached, followed by an additional washing step with three column volumes 20% IMAC-G^{300} B before elution with 100% IMAC-G^{300} B. Pooled fractions were dialyzed against AIEX-G^{aIF6} A (20 mM TRIS-HCl pH 8.5, 5 mM NaCl, 1 mM $MgCl_2$, 15% glycerol, and 2 mM BME)

overnight at 4 °C in a dialysis cassette (7 kDa cut-off, Slide-A-Lyzer™, Thermo Scientific) and loaded onto the equilibrated AIEX column. aIF6 was eluted from the AIEX column by a flat gradient of 0-30% AIEX-G^{aIF6} B (20 mM TRIS-HCl pH 8.5, 1 M NaCl, 1 mM $MgCl_2$, 15% glycerol, and 2 mM BME) in 60 ml. Fractions containing aIF6 were identified by SDS-PAGE. Buffer of the pooled fractions was exchanged against Storage-G^{300} buffer (20 mM TRIS-HCl pH 7.5, 300 mM NaCl, 5 mM $MgCl_2$, and 15% glycerol) by PD10 gravity flow desalting columns (BioRad). Protein was concentrated using Amicon® Ultra centrifuge device (10 kDa cut-off, Merck Millipore), snap- frozen in liquid nitrogen and stored in small aliquots at -80 °C. Protein concentration was determined at A_{280} (ε_{280} 5,700 $M^{-1}cm^{-1}$).

3.3.4. Initiation factors

3.3.4.1 aIF1

aIF1 was purified by IMAC (HiTrap™ Chelating HP, 5 ml, GE Healthcare) and AIEX (HiTrap™ Q column, 5 ml, GE Healthcare) at room temperature using an Äkta Prime Plus System (GE Healthcare). The respective steps were carried out in Lysis buffer IF^{150} (20 mM TRIS-HCl pH 7.5, 150 mM NaCl, 5 mM $MgCl_2$, 15% (v/v) glycerol) and IMAC-G^{300} buffers A and B. After loading, the IMAC column was washed with IMAC-G^{300} A until the baseline of absorbance at 280 nm was reached and aIF1 was eluted with 100% buffer B, which yielded one major peak that mostly contained a protein of the expected size as verified by SDS-PAGE. For subsequent AIEX, the buffer of all major peak fractions was exchanged to AIEX-G^{ABCE1} A by PD10 gravity flow desalting columns (BioRad). aIF1 was eluted from the AIEX column by a flat gradient; 0-30% AIEX-G^{ABCE1} B in 50 ml. Fractions containing aIF1 were identified by SDS-PAGE. Buffer of the pooled fractions was exchanged against Storage-IF buffer (20 mM HEPES-KOH pH 7.5, 200 mM KCl, 10% glycerol, 8 mM BME) by PD10 gravity flow desalting columns (BioRad). Protein was concentrated using Amicon™ Ultra centrifuge device (3 kDa cut-off, Merck Millipore), snap-frozen in liquid nitrogen, and stored in small aliquots at -80 °C. Protein concentration was determined at A_{280} (ε_{280} = 4,470 M^{-1} cm^{-1}).

3.3.4.2 aIF1A

aIF1A was purified by IMAC (HiTrap™ Chelating HP, 5 ml, GE Healthcare) at room temperature using an Äkta Prime Plus System (GE Healthcare). The respective steps

were carried out in Lysis buffer IF^{250} (20 mM TRIS-HCl pH 7.5, 250 mM NaCl, 5 mM $MgCl_2$, 10% (v/v) glycerol) and IMAC-G^{240} buffers A and B. After loading, the IMAC column was washed with IMAC-G^{240} A until the baseline of absorbance at 280 nm was reached and aIF1A was eluted with 100% buffer B, which yielded one major peak that contained a pure protein of the expected size as verified by SDS-PAGE. Buffer of the pooled fractions was exchanged against Storage-IF buffer by PD10 gravity flow desalting columns (BioRad). Protein was concentrated using Amicon™ Ultra centrifuge device (3 kDa cut-off, Merck Millipore), snap-frozen in liquid nitrogen, and stored in small aliquots at -80 °C. Protein concentration was determined at A_{280} (ε_{280} = 15,000 M^{-1} cm^{-1}).

3.3.4.3 aIF2α

aIF2α was purified by IMAC (HiTrap™ Chelating HP, 5 ml, GE Healthcare) at room temperature using an Äkta Prime Plus System (GE Healthcare). The respective steps were carried out in Lysis buffer $IF2^{250}$ (50 mM TRIS-HCl pH 8.0, 250 mM NaCl, 10 mM $MgCl_2$, 4 mM BME) and IMAC-IF2 buffers A (30 mM TRIS-HCl pH 8.0, 250 mM NaCl, 10 mM imidazole, 10 mM $MgCl_2$, 2 mM BME) and B (30 mM TRIS-HCl pH 8.0, 250 mM NaCl, 200 mM imidazole, 10 mM $MgCl_2$, 2 mM BME). After loading, the IMAC column was washed with IMAC-IF2 A until the baseline of absorbance at 280 nm was reached and aIF2α was eluted with 100% buffer B, which yielded one major peak that contained a pure protein of the expected size as verified by SDS-PAGE. Buffer of the pooled fractions was exchanged against Storage-IF2 buffer (30 mM TRIS-HCl pH 8.0, 250 mM NaCl, 10 mM $MgCl_2$, 2 mM BME) by PD10 gravity flow desalting columns (BioRad). Protein was concentrated using Amicon™ Ultra centrifuge device (10 kDa cut-off, Merck Millipore), snap-frozen in liquid nitrogen, and stored in small aliquots at -80 °C. Protein concentration was determined at A_{280} (ε_{280} = 45,000 M^{-1} cm^{-1}).

3.3.4.4 aIF2β

aIF2β was purified by IMAC (HiTrap™ Chelating HP, 5 ml, GE Healthcare) at room temperature using an Äkta Prime Plus System (GE Healthcare). The respective steps were carried out in Lysis buffer G and IMAC-G^{300} buffers A and B (see 3.3.3 aIF6). After loading, the IMAC column was washed with IMAC-G^{300} until the baseline was reached and aIF2β was eluted with 100% IMAC-G^{300} B, which yielded one major

peak that contained a pure protein of the expected size as verified by SDS-PAGE. Buffer of the pooled fractions was exchanged against Storage-IF2 buffer by PD10 gravity flow desalting columns (BioRad). Protein was concentrated using Amicon™ Ultra centrifuge device (10 kDa cut-off, Merck Millipore), snap-frozen in liquid nitrogen, and stored in small aliquots at -80 °C. Protein concentration was determined at A_{280} (ε_{280} = 14,600 M^{-1} cm^{-1}).

3.3.4.5 aIF2γ

aIF2γ was purified by cation exchange chromatography (CIEX, HiTrap™ SP, 5 ml, GE Healthcare) at room temperature using an Äkta Prime Plus System (GE Healthcare). The respective steps were carried out in Lysis buffer IF2γ (50 mM Bis-TRIS pH 5.8, 250 mM NaCl, 10 mM $MgCl_2$, 4 mM BME) in the presence of 200 µM GTP. After differential heat precipitation of host proteins, the lysate was diluted 10-fold to a final NaCl concentration of 25 mM, loaded onto the CIEX column and washed with buffer CIEX A (30 mM Bis-TRIS pH 5.8, 25 mM NaCl, 10 mM $MgCl_2$, 2 mM BME). aIF2γ was eluted by a flat salt gradient (0-25% in 80 ml) to CIEX B (like A with 1 M NaCl), which yielded one major peak with a shoulder at higher NaCl concentration. Both contained a pure protein of the expected size as verified by SDS-PAGE, the major peak was pooled and the shoulder discarded. Buffer of the pooled fractions was exchanged to Storage buffer (30 mM TRIS pH 8.0, 250 mM NaCl, 10 mM $MgCl_2$, 2 mM BME) *via* PD10 column (Biorad), snap-frozen in liquid nitrogen, and stored in small aliquots at -80 °C. Protein concentration was determined at A_{280} (ε_{280} = 50,000 M^{-1} cm^{-1}).

3.3.4.6 aIF5B

aIF5B was purified by IMAC (HiTrap™ Chelating HP, 5 ml, GE Healthcare) at room temperature using an Äkta Prime Plus System (GE Healthcare). The respective steps were carried out in Lysis buffer $IF2^{250}$ and IMAC-IF2 buffers A and B (see 3.3.4.3 aIF2α) with additional 10% (v/v) glycerol. After loading, the IMAC column was washed with IMAC-IF2 A until the baseline of absorbance at 280 nm was reached and aIF5B was eluted with 100% buffer B, which yielded one major peak that mostly contained a protein of the expected size as verified by SDS-PAGE. Buffer of the pooled fractions was exchanged against Storage-IF2 buffer by PD10 gravity flow desalting columns (BioRad). The protein was snap-frozen in liquid nitrogen, and stored in small aliquots at -80 °C. Protein concentration was determined at A_{280}

(ε_{280} = 32,000 M^{-1} cm^{-1}). The purification of aIF5B must be polished by an ion exchange chromatography step once the protein is required for sensitive biochemical assays, which was not the case in this study.

3.3.5. MetRS

MetRS was purified from 2 L of *E. coli* expression culture by IMAC (HiTrap™ Chelating HP, 5 ml, GE Healthcare) at room temperature utilizing an Äkta Prime Plus System (GE Healthcare). Cell pellets were resuspended in Lysis buffer G with 10% (v/v) glycerol and IMAC was performed using IMAC-G^{100} buffers (see section 3.3.1 ABCE1). After loading, the IMAC column was washed with IMAC-G^{100} A until the baseline of absorbance at 280 nm was reached and MetRS was eluted with 100% buffer B, which yielded one major peak that mostly contained a protein of the expected size as verified by SDS-PAGE. Buffer of the pooled fractions was exchanged against 2x aminoacylation buffer (30 mM TRIS-HCl pH 8.0, 30 mM KCl, 8 mM $MgCl_2$) by PD10 gravity flow desalting columns (BioRad), supplemented with 50% (v/v) glycerol and stored in small aliquots at -20 °C. Aliquots could be thawn and frozen again several times without loss of methionylation activity. Protein concentration was determined at A_{280} (ε_{280} = 95,000 M^{-1} cm^{-1}).

3.3.6. tRNA

tRNA was extracted by phenol directly from MRE600 cell pellet and purified by precipitation and AIEX (HiTrap™ Q column, 5 ml, GE Healthcare) as described previously (Stolboushkina et al., 2013), with minor changes. All steps, if not stated different, were performed on ice or at 4 °C. Cells from 1l culture were resuspended in 12 ml buffer S (1 mM TRIS-HCl pH 7.4, 10 mM MgOAc). The suspension was then mixed with the same volume (12 ml) water-saturated phenol (stabilized with 0.1% 8-hydroxycholine, Applichem) and mixed thoroughly for 1 h. Phases were separated for 30 min at 12,500 x *g* and the hydrophilic phase (top) was transferred to fresh tubes. Nucleic acids were precipitated with 1/10 volume of 20% (w/v) KOAc pH 5.2 and two volumes of ethanol abs. at -20 °C for 3 h and pelleted for 30 min at 12,500 x *g*. The supernatant was discarded, the air-dried pellet resuspended in 6 ml 1 M NaCl and left on ice for 1 h. To remove aggregated high molecular weight nucleic acids the sample was again centrifuged for 30 min at 12,500 x *g*. The supernatant was then mixed with two volumes of ethanol abs. and the tRNA precipitated overnight at

-20 °C. tRNA was pelleted for 30 min at 12,500 x *g*, the pellet was resuspended in 600 µl buffer D (2 M TRIS-HCl pH 8.8) and incubated for 3 h at 37 °C for complete deaminoacylation. The sample was chilled on ice and tRNA was precipitated with 200 µl 5 M NaCl and two volumes of ethanol abs. at -20 °C overnight. The pellet again was collected by centrifugation for 30 min at 12,500 x *g*, extensively dried and resuspended in 3.9 ml 300 mM KOAc pH 7.0 and 2.1 ml isopropanol. The solution was agitated for 30 min at room temperature, centrifuged for 30 min at 12,500 x *g.* The supernatant was transferred into fresh tubes, supplemented with 0.45 volumes of isopropanol and centrifuged for 30 min at 12,500 x *g*. The pellet was then resuspended in 600 µl ddH_2O and the tRNA precipitated overnight with three volumes of ethanol abs. and 1/10 volume 3 M KOAc pH 5.2 at -20 °C. After centrifugation for 30 min at 12,500 x *g* the pellet was resuspended in 1 ml buffer A (20 mM TRIS-HCl pH 7.5, 200 mM NaCl, 8 mM $MgCl_2$, 0.1 mM EDTA) and loaded onto the extensively washed (with 0.5 M NaOH) and equilibrated AIEX column. The column with the bound tRNA was washed with 30 ml buffer A before tRNA was eluted in a 24 ml gradient of 0 – 75% buffer B (20 mM TRIS-HCl pH 7.5, 1 M NaCl, 8 mM $MgCl_2$, 0.1 mM EDTA) yielding one major peak at 260 nm. Fractions of 0.5 ml were collected, aliquots were prepared for analysis by Urea PAGE and the remaining fractions were immediately frozen at – 80 °C for long-term storage. Concentration was determined at A_{260} (ε_{260} = 606,060 M^{-1} cm^{-1}) for each fraction before use.

3.4. Purification of ribosomal particles

3.4.1. *Thermococcus celer* ribosomes

Frozen cell pellets from *T. celer* were purchased from the Centre of Microbiology & Archaea, University of Regensburg, Germany. Ribosomes were purified according to (Becker et al., 2012). Cells were resuspended in S30-buffer (10 mM TRIS-HCl pH 7.5, 60 mM KOAc, 14 mM $MgCl_2$, 1 mM DTT) and lysed by ultrasonication with 2-3 rounds of 1 min on ice using a Branson Sonifier 250 at 60% output. Supernatant was cleared twice by centrifugation for 30 min at 30,000 x *g* at 4 °C. Ribosomes were stripped from all translation factors by a high-salt cushion (1 M sucrose, 0.5 M NH_4OAc, S30-buffer) during centrifugation for 1 h at 100,000 x *g* at 4 °C. The high-salt cushion was removed and the pellet was resuspended in TrB25 (56 mM TRIS-HCl pH 8.0, 250 mM KOAc, 80 mM NH_4OAc, 25 mM $MgCl_2$, 1 mM DTT). The absorption was measured at 280 nm and 260 nm for control. Pure ribosomes were obtained by SDG centrifugation on a 10-30% (w/v) sucrose gradient in 10 mM TRIS-HCl pH 7.5, 60 mM KOAc, 20 mM $MgCl_2$ for 70S purification or 2 mM $MgCl_2$ for 30S and 50S purification at 20,000 rpm in an SW41 rotor (Beckmann Coulter) at 4 °C for 14 h. Gradients were harvested by Piston Gradient Fractionator (Biocomp Instruments) recording absorption at 254 nm (BioRad). Gradients run with 20 mM $MgCl_2$ contained mostly 70S while ribosomes were completely dissociated at 2 mM $MgCl_2$. Buffer of the respective peak fractions was exchanged against S30-buffer by PD10 gravity flow desalting columns (BioRad). were concentrated using Amicon® Ultra centrifuge device (100 kDa cut-off, Merck Millipore), snap-frozen in liquid nitrogen, and stored in small aliquots at -80 °C. Ribosome concentration was estimated at A_{260} (70S ε_{260} 4.2 x 10^7 $M^{-1}cm^{-1}$, 50S ε_{260} 2.8 x 10^7 $M^{-1}cm^{-1}$, 30S ε_{260} 1.4 x 10^7 $M^{-1}cm^{-1}$).

3.4.2. *Sulfolobus solfataricus* ribosomes

30S ribosomes were prepared by ion exchange chromatography and SDG centrifugation from self-grown *S. solfataricus* cells (see 3.1.1) using cysteine-charged Sulfolink® resin (Thermo Scientific). Sulfolink® resin was charged once and used for up to 15 purifications. For charging, 10 ml of a 50% Sulfolink® coupling gel slurry were transferred into two 5 ml tubes and washed (850 x *g*, 5 min) with coupling buffer

(50 mM TRIS-HCl pH 8.5, 5 mM EDTA) three times. Next, the resin was mildly agitated for 1 h at room temperature with 5 ml of L-cysteine (50 mM) per tube, washed again three more times with coupling buffer, three times in ribosome binding buffer (20 mM HEPES-KOH pH 7.5, 60 mM NH_4Cl, 5 mM $Mg(OAc)_2$, 2 mM DTT) and stored at 4 °C. Binding buffer was removed directly before use. A_{260} and A_{280} were measured after each purification step to control the purification progress.

For purification of ribosomes, cells were resuspended in buffer M (30 mM HEPES-KOH pH 7.5, 50 mM KCl, 10 mM $MgCl_2$, 0.5 mM EDTA, 2 mM DTT) and lysed by ultrasonication with 2-3 rounds of 1 min on ice using a Branson Sonifier 250 at 60% output. Supernatant was cleared by centrifugation for 30 min at 30,000 x *g* at 4 °C. Ribosomes from the supernatant were bound to charged Sulfolink® resin in batch for 15 min on ice and the flow-through was removed at 1000 x *g* for 1 min. Batch-binding was repeated with the flow-through. Afterwards, the resin was washed three times with 5 ml of binding buffer. Ribosomes were eluted twice with 1 ml of elution buffer (20 mM HEPES-KOH pH 7.5, 500 mM NH_4Cl, 10 mM $Mg(OAc)_2$, 2 mM DTT). Ribosomes were concentrated by glycerol density centrifugation at 100,000 x *g* for 15 h at 4 °C, placing 2-3 ml of the elution fractions on 1 ml of cushion buffer (20 mM HEPES-KOH pH 7.5, 500 mM NH_4Cl, 10 mM $Mg(OAc)_2$, 2 mM DTT, 25% (v/v) glycerol). The pellet was washed twice and resuspended in 100 µl elution buffer by gently disruption with a glass rod and mild agitation for 1 h at 4 °C. Higher molecular weight aggregates were removed for 20 min at 16,000 x *g* and 4 °C. Ribosomal subunits were separated by SDG centrifugation on a 10-30% (w/v) sucrose gradient in 20 mM TRIS-HCl pH 7.5, 10 mM KCl, 2 mM $MgCl_2$, 1 mM DTT. Gradients were harvested by Piston Gradient Fractionator (Biocomp Instruments) recording absorption at 254 nm (BioRad). Buffer of the respective peak fractions was exchanged against ribosome storage buffer (20 mM HEPES-KOH pH 7.5, 100 mM KCl, 5 mM $MgCl_2$, 2 mM DTT) by PD10 gravity flow desalting columns (BioRad). Ribosomes were concentrated using Amicon® Ultra centrifuge device (100 kDa cut-off, Merck Millipore), snap-frozen in liquid nitrogen, and stored in small aliquots at -80 °C. Ribosome concentration was estimated at A_{260} (50S ε_{260} 2.8 x 10^7 $M^{-1}cm^{-1}$, 30S ε_{260} 1.4 x 10^7 $M^{-1}cm^{-1}$).

3.5. Biochemical activity assays

3.5.1. Radioactive ATPase assay

ATPase activity of ABCE1 was measured by hydrolysis of ^{32}P-γ-ATP (Hartmann Analytics, 222 TBq/mmol, 370 MBq/ml) and subsequent thin-layer chromatography on polyethylene imine (PEI) plates (Merck-Millipore) using a 0.8 M LiCl solution in 0.8 M acetic acid (Pisarev et al., 2010). 10fold cold ATP were supplemented 1:1000 with radioactive tracer. A final concentration of 1 µM ABCE1 and 5 mM ATP in 20 mM HEPES pH 7.5, 150 mM NaCl, 2.5 mM $MgCl_2$ and 1 mM DTT was used in a total volume of 50 µl for measurements with free ABCE1 at 70 °C. For ATPase stimulation 1 µM *T. celer* 70S, 1 µM ABCE1 and 37.5 µM ATP in TrB25 at 45 °C were used. For post-SCs 4 µM *S. solfataricus* 30S, 1 µM ABCE1 and 2 mM ATP in RB-buffer (20 mM HEPES-KOH pH 7.5, 100 mM KCl, 20 mM $MgCl_2$, 2 mM DTT) at 65 °C were used. Spots were set by withdrawing 1 µl sample at each point in time. After separation of the compounds, the plates were dried and exposed to a radio screen (BioRad) overnight. Spots were quantified using ImageJ (NIH, USA), and data were analyzed using Origin (OriginLab). The values of ATP auto-hydrolysis in samples without ABCE1 were subtracted during analysis.

3.5.2. Nucleotide occlusion assay

The occlusion of ATP and ADP by ABCE1 was determined by using ^{32}P-α-ATP (Hartmann Analytics, 222 TBq/mmol, 370 MBq/ml) and the analysis as already described for the ATPase assay. Here, 9 µM cold ATP was supplemented 1:500 with radioactive tracer, and final concentrations of 0.6 µM ATP and 0.3 µM ABCE1 were incubated for 30 s at 45 °C in TrB25. Samples were then quickly chilled on ice and supplemented with 0.5 mM cold ATP to reduce unspecific binding. To determine the intensity of the load, 1 µl sample was directly spotted onto the TLC plate. ABCE1 and occluded ATP molecules were separated from residual ATP by SEC in Micro Bio-Spin™ P30 columns (Biorad). 1 µl of the eluted sample were used for TLC analysis. Spots were quantified using ImageJ (NIH, USA), and data were analyzed using Origin (OriginLab). The signals for ATP and ADP in the load samples summed up to a total corresponding to 0.6 µM of ATP. Retention of ABCE1 by the SpinColumn was calculated using SDS-PAGE analysis.

3.5.3. 70S binding assay

Formation of the pre-splitting complex was analyzed by SDG centrifugation, subsequent fractionation, protein precipitation, and immunoblotting as described in (Barthelme et al., 2011; Becker et al., 2012). Samples of 25 µl in TrB50 (as TrB25 but with 50 mM $MgCl_2$) contained 125 pmol 70S, 150 pmol ABCE1, 125 pmol aRF1, as well as 2 mM nucleotides and were incubated at 25 °C for 1 h. Samples were cooled down on ice, loaded onto a 10-30% (w/v) SDG in TrB50, and centrifuged at 40,000 rpm in SW41 rotor for 3 h. Gradients were fractionated by Piston Gradient Fractionator (Biocomp Instruments) into 0.5 ml fractions. Those were precipitated by addition of ice-cold acetone overnight and pelleted by centrifugation at 16,000 x *g* for 1h; the pellets were resuspended in ATPase buffer before analysis by SDS-PAGE and immunoblotting.

3.5.4. Ribosome splitting assay

70S splitting was analyzed by SDG centrifugation and subsequent absorption read-out at 254 nm. For the reaction, 25 pmol of 70S, 100 pmol of ABCE1 and aRF1, 180 pmol of aIF6, and 2 mM nucleotides were incubated for 25 min at 45 °C in a total volume of 50 µl in TrB25. Reaction was stopped by rapid cooling on ice and loaded onto a 10-30% (w/v) SDG in TrB50. Gradients were centrifuged in an SW41 rotor (Beckmann Coulter) at 20,000 rpm for 14 h or 40,000 rpm for 3 h at 4 °C, and data recorded at 254 nm by Piston Gradient Fractionator (Biocomp Instruments). Splitting experiments were performed three times, the bars represent a mean ± SD value of the 50S/70S peak height ratio normalized to the mean value of the respective mutant with the highest splitting efficiency in each figure.

3.5.5. 30S binding assay

S. solfataricus lysate was used as the source of 30S ribosomal subunits. Lysate was prepared as for 70S purification from frozen cells grown as described previously (Barthelme et al., 2011). Lysate was diluted 1:1 with RB-buffer, 0.5 µM of ABCE1 and 2 mM of nucleotides were added. The reaction proceeded at 65 °C for 10 min. Samples were cooled down on ice and loaded onto 5-15% (w/v) SDG in 20 mM TRIS-HCl pH 7.5, 10 mM KCl, 20 mM $MgCl_2$, 1 mM DTT. Gradients were centrifuged, fractionated, and further analyzed as for 70S binding (see section 3.6.3).

3.6. Assembly of the archaeal initiation complex

3.6.1. tRNA methionylation

For selective methionylation, 40 µg of $tRNA^{fMet}$ were incubated with 40 µg of purified MetRS, 100 µM L-methionine and 10 mM ATP in 30 mM TRIS-HCl pH 8.0, 30 mM KCl, 16 mM $MgCl_2$ for 15 min at 37 °C. MetRS was removed by IMAC (equilibrated Ni-NTA agarose, Quiagen) in a small batch (1/10 of the reaction volume) and the buffer of the Met-$tRNA^{fMet}$ in the flow-through was immediately exchanged to the respective biochemical reaction or SEC buffer by ZebaSpin™ Desalting Column with a 7 kDa molecular weight cut-off (Thermo Scientific). Final concentration of Met-$tRNA^{fMet}$ was determined at A_{260} (ε_{260} = 606,060 M^{-1} cm^{-1}).

3.6.2. Pelleting assay

Sucrose density centrifugation (pelleting) assays were performed to analyze factor binding to 30S ribosomes. Briefly, 1.2 µM 30S *S. solfataricus* ribosomes, 3 µM ABCE1 and/or 3 µM pre-assembled aIF2 were incubated once for 10 min (binding ability, Figure 14) or two times for 5 min (order of binding events, Figure S7) at 70 °C in the presence of 1 mM GMP-PNP and AMP-PNP in 20 mM HEPES-KOH pH 7.5, 30 mM KCl, 10 mM $MgCl_2$, 2 mM DTT. Higher molecular weight aggregates were removed for 5 min at 16,000 x *g* and 4 °C and the samples were loaded onto 500 µl of 10% (w/v) sucrose in 20 mM TRIS-HCl pH 8.0, 150 mM KCl, 10 mM $MgCl_2$, 1 mM DTT. Unbound proteins were separated for 30 min at 70,000 rpm in a TLA110 rotor (Beckmann Coulter). 30 µl of the top fraction were stored on ice and the ribosomal complexes in the pellet were resuspended in 30 µl of the reaction buffer for analysis by SDS-PAGE.

3.6.3. SDG centrifugation binding assay

To confirm that initiation complexes are intact and sediment comparably to 30S subunits, SDG centrifugation experiments were performed. 1 µM 30S, 2 µM ABCE1, 1 mM AMP-PNP and pre-assembled trimeric complex comprising 4 µM aIF2, 4.8 µM Met-$tRNA^{fMet}$, 1 mM GMP-PNP or 4 µM aIF2 alone with 1 mM GMP-PNP were incubated for 10 min at 65 °C in a total volume of 100 µl in 20 mM HEPES-KOH pH 7.5, 30 mM KCl, 10 mM $MgCl_2$, 1 mM DTT. Samples were chilled on ice and crosslinked with 2% (v/v) formaldehyde for 30 min on ice. Higher molecular weight

aggregates were removed for 5 min at 16,000 x *g* and 4 °C and the samples were loaded onto 5-15% (w/v) sucrose gradients in the reaction buffer. Gradients were centrifuged, fractionated, and samples were prepared as for 70S binding (see section 3.6.3) followed by SDS-PAGE analysis.

3.6.4. Co-immunoprecipitation

Simultaneous binding of archaeal initiation factors and ABCE1 to 30S ribosomes was confirmed by co-immunoprecipitation with ABCE1-FLAG. Briefly, complexes were assembled in a total volume of 100 µl from 2 µM 30S, 4 µM ABCE1-FLAG, pre-assembled trimeric complex (4 µM aIF2, 4.8 µM Met-tRNA^{fMet}, 1 mM GMP-PNP), 4 µM aIF1/1A, 20 µM mRNA and 1 mM AMP-PNP for 10 min at 65 °C in 20 mM HEPES-KOH pH 7.5, 30 mM KCl, 10 mM $MgCl_2$. ABCE1 was omitted for negative control of unspecific binding. Reaction buffer did not contain DTT or other reducing agent since it damages the antibodies. After complex formation, samples were diluted with reaction buffer to a total volume of 500 µl and incubated with 40 µl of Anti-FLAG® 2 Affinity Gel (Sigma Aldrich) while mildly agitating at room temperature for 1 h. Beads were washed twice with 800 µl of reaction buffer and ABCE1-FLAG was specifically eluted by proteolytic cleavage of the 3C recognition sequence between ABCE1 and the C-terminal FLAG tag by 5 µg of 3C protease (kindly provided by Charlott Stock, Hänelt Lab) in 50 µl of reaction buffer for 30 min at 35 °C and 400 rpm in a Thermomixer (Eppendorf). Beads were removed by centrifugation and the load, flow-through, wash and elution fractions were analyzed by SDS-PAGE.

3.7. Cryo- and negative stain electron microscopy

3.7.1. Sample preparation

Samples were prepared as illustrated in Figure S8. To mimic the physiological translation pathway, post-splitting complexes were generated by splitting of 1 nmol purified 70S ribosomes from *T. celer* by ABCE1$^{E238A/E485A}$ (8 µM), aPelota and aRF1 (5 µM each) in the presence of 0.5 mM AMP-PNP in 50 mM HEPES-KOH pH 7.5, 30 mM KCl, 10 mM $MgCl_2$ and 2 mM DTT. After splitting, post-SCs were decorated with aIF1, aIF1A and mRNA (5 µM each) by incubation at 65 °C for 2 min. The trimeric complex aIF2-Met-tRNA^{fMet}-GMP-PNP was preformed separately with freshly charged Met-tRNA^{fMet} to avoid blocking of free aIF2 by the excess mRNA due to its mRNA protection activity. The post-splitting/pre-initiation complexes were diluted to a $MgCl_2$ concentration of 2 mM, the trimeric complex (6.3 µM aIF2, 4.5 µM Met-tRNA^{fMet}, 0.6 mM GMP-PNP) was added and incubated at 65 °C for additional 15 min to allow full binding of all factors. Samples were chilled on ice and separated in two equal parts. One half was crosslinked with 1% formaldehyde for 30 min on ice. Higher molecular weight aggregates were removed for 15 min at 16,000 x *g* and 4 °C. Samples were loaded onto 10-30% (w/v) SDG in 50 mM HEPES-KOH pH 7.5, 30 mM KCl, 0.5 mM $MgCl_2$ and 2 mM DTT and ribosomal particles were separated by centrifugation for 13.5 h at 21,000 rpm and 4 °C in a SW40 rotor (Beckmann Coulter). Gradients were fractionated into 0.3 ml fractions using Piston Gradient Fractionator (Biocomp Instruments) while recording A_{260}. Fractions containing 40S were pooled and sucrose was removed by gravity flow size-exclusion columns (GE Healthcare). Ribosomes were diluted to concentrations of 50-70 nM (based on OD_{260}) for quality control by negative stain EM. Samples were vitrified on the same day.

3.7.2. Negative stain-EM

Freshly prepared samples were applied onto carbon coated Quantifoil 3/3 grids, stained with uranyl-acetate and imaged on a MORGAGNI TEM (FEI Company).

3.7.3. Cryo-EM of the archaeal post-splitting complex

Freshly prepared samples were applied to 2-nm pre-coated Quantifoil R3/3 holey carbon supported grids. For the post-splitting complex, data were collected on a TITAN KRIOS^{TM} cryo-TEM (FEI Company) equipped with a Falcon II direct electron detector at 300 keV under low dose conditions of about 2.4 $e^{-}/Å^2$ per frame for 10 frames (plus 4 $e^{-}/Å^2$ pre-exposure) resulting in a dose of 28 $e^{-}/Å^2$ in total. The software EM-TOOLS (TVIPS) and a defocus range of −0.8 to −2.5 µm (underfocus) was used. Magnification settings resulted in a pixel size of 1.084 Å/pixel. Original image stacks were summed and corrected for drift and beam-induced motion at micrograph level using MotionCor2 (Zheng et al., 2017). The contrast transfer function parameters and resolution range of each micrograph were estimated by GCTF (http://www.mrc-lmb.cam.ac.uk/kzhang/).

All 2D and 3D classifications and refinements were performed with RELION-2 after automated particle picking by Gautomatch (http://www.mrc-lmb.cam.ac.uk/kzhang/). 1.3 million particles from good classes were selected for 3D refinement. Notably, the first 3D reconstructions displayed a distortion in one direction resulting from preferred orientation of 30S particles on the carbon-coated grid and also misalignment.

The best resolved class showed a well resolved 30S body with stoichiometric occupancy of ABCE1. This final volume was refined to 3.8 Å, corrected for the modulation transfer function of the Falcon 2 detector and sharpened by applying a negative B-factor automatically estimated by RELION-2.

3.7.4. Model building of the archaeal post-splitting complex

For molecular interpretation of the 30S subunit, I used the model based on intermediate-resolution cryo-EM of the archaeal initiation complex (PDB 5JBH). A homology model of archaeal ABCE1 was generated based on the structure of yeast ABCE1 engaged in the post-SC (PDB 5LL6). Models were initially fitted into the electron density as rigid bodies using UCSF Chimera (Pettersen et al., 2004) and jiggle-fitted using Coot (Emsley et al., 2010). Finally, the model of the archaeal post-SC was subjected to real-space refinement in PHENIX.

3.7.5. Cryo-EM of the archaeal initiation complexes with ABCE1

Freshly prepared samples were applied to 2-nm pre-coated Quantifoil R3/3 holey carbon supported grids. For the post-splitting complex, data were collected on a

TECNAI^{TM} SPIRIT cryo-TEM (FEI Company) equipped with a TIETZ 8K TecCam 816 camera. Magnification settings resulted in a pixel size of 2.85 Å/pixel. A small dataset (approx. 20,000 particles) was recorded to check sample quality. It was processed with GAUTOMATCH (particle picking) and RELION-2.0 (refinement and classification).

For 3D classification the dataset was split into for classes. All classes showed strong extra density for ABCE1. Additional density was detected for aIF1, aIF1A and tRNA as indicated in Figure 15. Densities were interpreted using molecular models based on the intermediate-resolution cryo-EM of the archaeal initiation complex (PDB 5JBH). For rigid body docking UCSF Chimera (Pettersen et al., 2004) was used.

3.8. Graphics

Structural figures were generated using Pymol (Schrödinger) or UCSF Chimera (Pettersen et al., 2004). Diagrams were generated with Origin (OriginLab). Gels and TLC images were analyzed with ImageJ (NIH, USA). All figures were compiled and reworked with Adobe Illustrator®.

References

Abele, R., and Tampé, R. (2004). The ABCs of immunology: structure and function of TAP, the transporter associated with antigen processing. Physiology (Bethesda) *19*, 216-224.

Afonine, P.V., Grosse-Kunstleve, R.W., Echols, N., Headd, J.J., Moriarty, N.W., Mustyakimov, M., Terwilliger, T.C., Urzhumtsev, A., Zwart, P.H., and Adams, P.D. (2012). Towards automated crystallographic structure refinement with phenix.refine. Acta Crystallogr D Biol Crystallogr *68*, 352-367.

Agrawal, R.K., Penczek, P., Grassucci, R.A., Li, Y., Leith, A., Nierhaus, K.H., and Frank, J. (1996). Direct visualization of A-, P-, and E-site transfer RNAs in the Escherichia coli ribosome. Science *271*, 1000-1002.

Aitken, C.E., Petrov, A., and Puglisi, J.D. (2010). Single ribosome dynamics and the mechanism of translation. Annu Rev Biophys *39*, 491-513.

Alkalaeva, E.Z., Pisarev, A.V., Frolova, L.Y., Kisselev, L.L., and Pestova, T.V. (2006). In vitro reconstitution of eukaryotic translation reveals cooperativity between release factors eRF1 and eRF3. Cell *125*, 1125-1136.

Andersen, D.S., and Leevers, S.J. (2007). The essential Drosophila ATP-binding cassette domain protein, pixie, binds the 40 S ribosome in an ATP-dependent manner and is required for translation initiation. J Biol Chem *282*, 14752-14760.

Barik, S. (1996). Site-directed mutagenesis in vitro by megaprimer PCR. Methods Mol Biol *57*, 203-215.

Barthelme, D., Dinkelaker, S., Albers, S.V., Londei, P., Ermler, U., and Tampé, R. (2011). Ribosome recycling depends on a mechanistic link between the FeS cluster domain and a conformational switch of the twin-ATPase ABCE1. Proc Natl Acad Sci U S A *108*, 3228-3233.

Barthelme, D., Scheele, U., Dinkelaker, S., Janoschka, A., Macmillan, F., Albers, S.V., Driessen, A.J., Stagni, M.S., Bill, E., Meyer-Klaucke, W.*, et al.* (2007). Structural organization of essential iron-sulfur clusters in the evolutionarily highly conserved ATP-binding cassette protein ABCE1. J Biol Chem *282*, 14598-14607.

Bautista-Santos, A., and Zinker, S. (2014). The P1/P2 protein heterodimers assemble to the ribosomal stalk at the moment when the ribosome is committed to translation but not to the native 60S ribosomal subunit in Saccharomyces cerevisiae. Biochemistry *53*, 4105-4112.

Becker, T., Armache, J.P., Jarasch, A., Anger, A.M., Villa, E., Sieber, H., Motaal, B.A., Mielke, T., Berninghausen, O., and Beckmann, R. (2011). Structure of the no-go mRNA decay complex Dom34-Hbs1 bound to a stalled 80S ribosome. Nat Struct Mol Biol *18*, 715-720.

Becker, T., Franckenberg, S., Wickles, S., Shoemaker, C.J., Anger, A.M., Armache, J.P., Sieber, H., Ungewickell, C., Berninghausen, O., Daberkow, I.*, et al.* (2012). Structural basis of highly conserved ribosome recycling in eukaryotes and archaea. Nature *482*, 501-506.

Belardinelli, R., Sharma, H., Peske, F., Wintermeyer, W., and Rodnina, M.V. (2016). Translocation as continuous movement through the ribosome. RNA Biol *13*, 1197-1203.

Benelli, D., Maone, E., and Londei, P. (2003). Two different mechanisms for ribosome/mRNA interaction in archaeal translation initiation. Mol Microbiol *50*, 635-643.

References

Benelli, D., Marzi, S., Mancone, C., Alonzi, T., la Teana, A., and Londei, P. (2009). Function and ribosomal localization of aIF6, a translational regulator shared by archaea and eukarya. Nucleic Acids Res *37*, 256-267.

Bickmore, W.A., and van Steensel, B. (2013). Genome architecture: domain organization of interphase chromosomes. Cell *152*, 1270-1284.

Boel, G., Smith, P.C., Ning, W., Englander, M.T., Chen, B., Hashem, Y., Testa, A.J., Fischer, J.J., Wieden, H.J., Frank, J.*, et al.* (2014). The ABC-F protein EttA gates ribosome entry into the translation elongation cycle. Nat Struct Mol Biol *21*, 143-151.

Brandman, O., and Hegde, R.S. (2016). Ribosome-associated protein quality control. Nat Struct Mol Biol *23*, 7-15.

Brock, T.D., Brock, K.M., Belly, R.T., and Weiss, R.L. (1972). Sulfolobus: a new genus of sulfur-oxidizing bacteria living at low pH and high temperature. Arch Mikrobiol *84*, 54-68.

Brown, A., Shao, S., Murray, J., Hegde, R.S., and Ramakrishnan, V. (2015). Structural basis for stop codon recognition in eukaryotes. Nature *524*, 493-496.

Burnette, W.N. (1981). "Western blotting": electrophoretic transfer of proteins from sodium dodecyl sulfate--polyacrylamide gels to unmodified nitrocellulose and radiographic detection with antibody and radioiodinated protein A. Anal Biochem *112*, 195-203.

Buskirk, A.R., and Green, R. (2017). Ribosome pausing, arrest and rescue in bacteria and eukaryotes. Philos Trans R Soc Lond B Biol Sci *372*, DOI 10.1098/rstb.2016.0183.

Chen, L., Muhlrad, D., Hauryliuk, V., Cheng, Z., Lim, M.K., Shyp, V., Parker, R., and Song, H. (2010). Structure of the Dom34-Hbs1 complex and implications for no-go decay. Nat Struct Mol Biol *17*, 1233-1240.

Chen, Z.Q., Dong, J., Ishimura, A., Daar, I., Hinnebusch, A.G., and Dean, M. (2006). The essential vertebrate ABCE1 protein interacts with eukaryotic initiation factors. J Biol Chem *281*, 7452-7457.

Clemens, M.J., Pain, V.M., Wong, S.T., and Henshaw, E.C. (1982). Phosphorylation inhibits guanine nucleotide exchange on eukaryotic initiation factor 2. Nature *296*, 93-95.

Coelho, C.M., Kolevski, B., Bunn, C., Walker, C., Dahanukar, A., and Leevers, S.J. (2005). Growth and cell survival are unevenly impaired in pixie mutant wing discs. Development *132*, 5411-5424.

Coureux, P.D., Lazennec-Schurdevin, C., Monestier, A., Larquet, E., Cladiere, L., Klaholz, B.P., Schmitt, E., and Mechulam, Y. (2016). Cryo-EM study of start codon selection during archaeal translation initiation. Nat Commun *7*, 13366.

Dever, T.E., and Green, R. (2012). The elongation, termination, and recycling phases of translation in eukaryotes. Cold Spring Harb Perspect Biol *4*, a013706.

Diaconu, M., Kothe, U., Schlunzen, F., Fischer, N., Harms, J.M., Tonevitsky, A.G., Stark, H., Rodnina, M.V., and Wahl, M.C. (2005). Structural basis for the function of the ribosomal L7/12 stalk in factor binding and GTPase activation. Cell *121*, 991-1004.

Dmitriev, S.E., Stolboushkina, E.A., Terenin, I.M., Andreev, D.E., Garber, M.B., and Shatsky, I.N. (2011). Archaeal translation initiation factor aIF2 can substitute for eukaryotic eIF2 in ribosomal scanning during mammalian 48S complex formation. J Mol Biol *413*, 106-114.

Doerfel, L.K., Wohlgemuth, I., Kothe, C., Peske, F., Urlaub, H., and Rodnina, M.V. (2013). EF-P is essential for rapid synthesis of proteins containing consecutive proline residues. Science *339*, 85-88.

Dong, J., Lai, R., Nielsen, K., Fekete, C.A., Qiu, H., and Hinnebusch, A.G. (2004). The essential ATP-binding cassette protein RLI1 functions in translation by promoting preinitiation complex assembly. J Biol Chem *279*, 42157-42168.

References

Duncan, R., and Hershey, J.W. (1983). Identification and quantitation of levels of protein synthesis initiation factors in crude HeLa cell lysates by two-dimensional polyacrylamide gel electrophoresis. J Biol Chem *258*, 7228-7235.

Emsley, P., Lohkamp, B., Scott, W.G., and Cowtan, K. (2010). Features and development of Coot. Acta Crystallogr D Biol Crystallogr *66*, 486-501.

Endoh, T., Kanai, T., Sato, Y.T., Liu, D.V., Yoshikawa, K., Atomi, H., and Imanaka, T. (2006). Cell-free protein synthesis at high temperatures using the lysate of a hyperthermophile. J Biotechnol *126*, 186-195.

Failmezger, J., Nitschel, R., Sanchez-Kopper, A., Kraml, M., and Siemann-Herzberg, M. (2016). Site-Specific Cleavage of Ribosomal RNA in Escherichia coli-Based Cell-Free Protein Synthesis Systems. PLoS One *11*, e0168764.

Fernandez, I.S., Bai, X.C., Hussain, T., Kelley, A.C., Lorsch, J.R., Ramakrishnan, V., and Scheres, S.H.W. (2013). Molecular architecture of a eukaryotic translational initiation complex. Science *342*, 1240585.

French, S.L., Santangelo, T.J., Beyer, A.L., and Reeve, J.N. (2007). Transcription and translation are coupled in Archaea. Mol Biol Evol *24*, 893-895.

Frolova, L.Y., Tsivkovskii, R.Y., Sivolobova, G.F., Oparina, N.Y., Serpinsky, O.I., Blinov, V.M., Tatkov, S.I., and Kisselev, L.L. (1999). Mutations in the highly conserved GGQ motif of class 1 polypeptide release factors abolish ability of human eRF1 to trigger peptidyl-tRNA hydrolysis. RNA *5*, 1014-1020.

Gabel, K., Schmitt, J., Schulz, S., Nather, D.J., and Soppa, J. (2013). A comprehensive analysis of the importance of translation initiation factors for Haloferax volcanii applying deletion and conditional depletion mutants. PLoS One *8*, e77188.

Garcia-Ortega, L., Alvarez-Garcia, E., Gavilanes, J.G., Martinez-del-Pozo, A., and Joseph, S. (2010). Cleavage of the sarcin-ricin loop of 23S rRNA differentially affects EF-G and EF-Tu binding. Nucleic Acids Res *38*, 4108-4119.

Gerovac M., and Tampé R. (2018) Control of mRNA Translation by Versatile ATP-driven Machines. Trends Biochem Sci, in press

Glick, B.R., and Ganoza, M.C. (1975). Identification of a soluble protein that stimulates peptide bond synthesis. Proc Natl Acad Sci U S A *72*, 4257-4260.

Graille, M., and Seraphin, B. (2012). Surveillance pathways rescuing eukaryotic ribosomes lost in translation. Nat Rev Mol Cell Biol *13*, 727-735.

Greber, B.J., and Ban, N. (2016). Structure and Function of the Mitochondrial Ribosome. Annu Rev Biochem *85*, 103-132.

Gromadski, K.B., Schummer, T., Stromgaard, A., Knudsen, C.R., Kinzy, T.G., and Rodnina, M.V. (2007). Kinetics of the interactions between yeast elongation factors 1A and 1Balpha, guanine nucleotides, and aminoacyl-tRNA. J Biol Chem *282*, 35629-35637.

Grossmann, N., Vakkasoglu, A.S., Hulpke, S., Abele, R., Gaudet, R., and Tampé, R. (2014). Mechanistic determinants of the directionality and energetics of active export by a heterodimeric ABC transporter. Nat Commun *5*, 5419.

Hasenohrl, D., Fabbretti, A., Londei, P., Gualerzi, C.O., and Blasi, U. (2009). Translation initiation complex formation in the crenarchaeon Sulfolobus solfataricus. RNA *15*, 2288-2298.

Hashem, Y., and Frank, J. (2018). The Jigsaw Puzzle of mRNA Translation Initiation in Eukaryotes: A Decade of Structures Unraveling the Mechanics of the Process. Annu Rev Biophys. DOI 10.1146/annurev-biophys-070816-034034

References

Hayes, C.S., and Keiler, K.C. (2010). Beyond ribosome rescue: tmRNA and co-translational processes. FEBS Lett *584*, 413-419.

He, F., Li, X., Spatrick, P., Casillo, R., Dong, S., and Jacobson, A. (2003). Genome-wide analysis of mRNAs regulated by the nonsense-mediated and 5' to 3' mRNA decay pathways in yeast. Mol Cell *12*, 1439-1452.

Hellen, C.U.T. (2018). Translation Termination and Ribosome Recycling in Eukaryotes. Cold Spring Harb Perspect Biol *10*, DOI 10.1101/cshperspect.a032656.

Heuer, A., Gerovac, M., Schmidt, C., Trowitzsch, S., Preis, A., Kotter, P., Berninghausen, O., Becker, T., Beckmann, R., and Tampé, R. (2017). Structure of the 40S-ABCE1 post-splitting complex in ribosome recycling and translation initiation. Nat Struct Mol Biol *24*, 453-460.

Hinnebusch, A.G., and Lorsch, J.R. (2012). The mechanism of eukaryotic translation initiation: new insights and challenges. Cold Spring Harb Perspect Biol *4*, DOI 10.1101/cshperspect.a011544.

Hirano, T. (2002). The ABCs of SMC proteins: two-armed ATPases for chromosome condensation, cohesion, and repair. Genes Dev *16*, 399-414.

Hohl, M., Hurlimann, L.M., Bohm, S., Schoppe, J., Grutter, M.G., Bordignon, E., and Seeger, M.A. (2014). Structural basis for allosteric cross-talk between the asymmetric nucleotide binding sites of a heterodimeric ABC exporter. Proc Natl Acad Sci U S A *111*, 11025-11030.

Hopfner, K.P. (2009). DNA double-strand breaks come into focus. Cell *139*, 25-27.

Hopfner, K.P., and Tainer, J.A. (2003). Rad50/SMC proteins and ABC transporters: unifying concepts from high-resolution structures. Curr Opin Struct Biol *13*, 249-255.

Hung, L.W., Wang, I.X., Nikaido, K., Liu, P.Q., Ames, G.F., and Kim, S.H. (1998). Crystal structure of the ATP-binding subunit of an ABC transporter. Nature *396*, 703-707.

Huter, P., Muller, C., Arenz, S., Beckert, B., and Wilson, D.N. (2017). Structural Basis for Ribosome Rescue in Bacteria. Trends Biochem Sci *42*, 669-680.

Imai, H., Abe, T., Miyoshi, T., Nishikawa, S.I., Ito, K., and Uchiumi, T. (2018). The ribosomal stalk protein is crucial for the action of the conserved ATPase ABCE1. Nucleic Acids Res *46*, 7820-7830

Jackson, R.J., Hellen, C.U., and Pestova, T.V. (2010). The mechanism of eukaryotic translation initiation and principles of its regulation. Nat Rev Mol Cell Biol *11*, 113-127.

Janas, E., Hofacker, M., Chen, M., Gompf, S., van der Does, C., and Tampé, R. (2003). The ATP hydrolysis cycle of the nucleotide-binding domain of the mitochondrial ATP-binding cassette transporter Mdl1p. J Biol Chem *278*, 26862-26869.

Jenner, L., Demeshkina, N., Yusupova, G., and Yusupov, M. (2010). Structural rearrangements of the ribosome at the tRNA proofreading step. Nat Struct Mol Biol *17*, 1072-1078.

Jenner, L., Melnikov, S., Garreau de Loubresse, N., Ben-Shem, A., Iskakova, M., Urzhumtsev, A., Meskauskas, A., Dinman, J., Yusupova, G., and Yusupov, M. (2012). Crystal structure of the 80S yeast ribosome. Curr Opin Struct Biol *22*, 759-767.

Karcher, A., Buttner, K., Martens, B., Jansen, R.P., and Hopfner, K.P. (2005). X-ray structure of RLI, an essential twin cassette ABC ATPase involved in ribosome biogenesis and HIV capsid assembly. Structure *13*, 649-659.

Karcher, A., Schele, A., and Hopfner, K.P. (2008). X-ray structure of the complete ABC enzyme ABCE1 from Pyrococcus abyssi. J Biol Chem *283*, 7962-7971.

Karimi, R., Pavlov, M.Y., Buckingham, R.H., and Ehrenberg, M. (1999). Novel roles for classical factors at the interface between translation termination and initiation. Mol Cell *3*, 601-609.

References

Karpowich, N., Martsinkevich, O., Millen, L., Yuan, Y.R., Dai, P.L., MacVey, K., Thomas, P.J., and Hunt, J.F. (2001). Crystal structures of the MJ1267 ATP binding cassette reveal an induced-fit effect at the ATPase active site of an ABC transporter. Structure *9*, 571-586.

Keiler, K.C. (2008). Biology of trans-translation. Annu Rev Microbiol *62*, 133-151.

Keiler, K.C., Waller, P.R., and Sauer, R.T. (1996). Role of a peptide tagging system in degradation of proteins synthesized from damaged messenger RNA. Science *271*, 990-993.

Khan, Z., Ford, M.J., Cusanovich, D.A., Mitrano, A., Pritchard, J.K., and Gilad, Y. (2013). Primate transcript and protein expression levels evolve under compensatory selection pressures. Science *342*, 1100-1104.

Kiosze-Becker, K., Ori, A., Gerovac, M., Heuer, A., Nürenberg-Goloub, E., Rashid, U.J., Becker, T., Beckmann, R., Beck, M., and Tampé, R. (2016). Structure of the ribosome post-recycling complex probed by chemical cross-linking and mass spectrometry. Nat Commun *7*, 13248.

Klinge, S., Voigts-Hoffmann, F., Leibundgut, M., and Ban, N. (2012). Atomic structures of the eukaryotic ribosome. Trends Biochem Sci *37*, 189-198.

Kobayashi, K., Kikuno, I., Kuroha, K., Saito, K., Ito, K., Ishitani, R., Inada, T., and Nureki, O. (2010). Structural basis for mRNA surveillance by archaeal Pelota and GTP-bound EF1alpha complex. Proc Natl Acad Sci U S A *107*, 17575-17579.

Kobayashi, K., Saito, K., Ishitani, R., Ito, K., and Nureki, O. (2012). Structural basis for translation termination by archaeal RF1 and GTP-bound EF1alpha complex. Nucleic Acids Res *40*, 9319-9328.

Korostelev, A.A. (2011). Structural aspects of translation termination on the ribosome. RNA *17*, 1409-1421.

Kozak, L., Gopal, G., Yoon, J.H., Sauna, Z.E., Ambudkar, S.V., Thakurta, A.G., and Dhar, R. (2002). Elf1p, a member of the ABC class of ATPases, functions as a mRNA export factor in Schizosacchromyces pombe. J Biol Chem *277*, 33580-33589.

Kozak, M. (1999). Initiation of translation in prokaryotes and eukaryotes. Gene *234*, 187-208.

Kramer, G., Boehringer, D., Ban, N., and Bukau, B. (2009). The ribosome as a platform for co-translational processing, folding and targeting of newly synthesized proteins. Nat Struct Mol Biol *16*, 589-597.

Kressler, D., Hurt, E., and Bassler, J. (2017). A Puzzle of Life: Crafting Ribosomal Subunits. Trends Biochem Sci *42*, 640-654.

Kurosaki, T., and Maquat, L.E. (2016). Nonsense-mediated mRNA decay in humans at a glance. J Cell Sci *129*, 461-467.

La Teana, A., Benelli, D., Londei, P., and Blasi, U. (2013). Translation initiation in the crenarchaeon Sulfolobus solfataricus: eukaryotic features but bacterial route. Biochem Soc Trans *41*, 350-355.

Laemmli, U.K. (1970). Cleavage of structural proteins during the assembly of the head of bacteriophage T4. Nature *227*, 680-685.

Lake, J.A. (1976). Ribosome structure determined by electron microscopy of Escherichia coli small subunits, large subunits and monomeric ribosomes. J Mol Biol *105*, 131-139.

Lammens, K., Bemeleit, D.J., Mockel, C., Clausing, E., Schele, A., Hartung, S., Schiller, C.B., Lucas, M., Angermuller, C., Soding, J.*, et al.* (2011). The Mre11:Rad50 structure shows an ATP-dependent molecular clamp in DNA double-strand break repair. Cell *145*, 54-66.

References

Leroux, A., and London, I.M. (1982). Regulation of protein synthesis by phosphorylation of eukaryotic initiation factor 2 alpha in intact reticulocytes and reticulocyte lysates. Proc Natl Acad Sci U S A *79*, 2147-2151.

Linder, B., Fischer, U., and Gehring, N.H. (2015). mRNA metabolism and neuronal disease. FEBS Lett *589*, 1598-1606.

Linton, K.J. (2007). Structure and function of ABC transporters. Physiology (Bethesda) *22*, 122-130.

Liu, Q., and Fredrick, K. (2016). Intersubunit Bridges of the Bacterial Ribosome. J Mol Biol *428*, 2146-2164.

Locher, K.P. (2016). Mechanistic diversity in ATP-binding cassette (ABC) transporters. Nat Struct Mol Biol *23*, 487-493.

Lomakin, I.B., Stolboushkina, E.A., Vaidya, A.T., Zhao, C., Garber, M.B., Dmitriev, S.E., and Steitz, T.A. (2017). Crystal Structure of the Human Ribosome in Complex with DENR-MCT-1. Cell Rep *20*, 521-528.

Londei, P., Altamura, S., Cammarano, P., and Petrucci, L. (1986). Differential features of ribosomes and of poly(U)-programmed cell-free systems derived from sulphur-dependent archaebacterial species. Eur J Biochem *157*, 455-462.

Maag, D., Algire, M.A., and Lorsch, J.R. (2006). Communication between eukaryotic translation initiation factors 5 and 1A within the ribosomal pre-initiation complex plays a role in start site selection. J Mol Biol *356*, 724-737.

Maag, D., and Lorsch, J.R. (2003). Communication between eukaryotic translation initiation factors 1 and 1A on the yeast small ribosomal subunit. J Mol Biol *330*, 917-924.

Maone, E., Di Stefano, M., Berardi, A., Benelli, D., Marzi, S., La Teana, A., and Londei, P. (2007). Functional analysis of the translation factor aIF2/5B in the thermophilic archaeon Sulfolobus solfataricus. Mol Microbiol *65*, 700-713.

Martens, B., Manoharadas, S., Hasenohrl, D., Zeichen, L., and Blasi, U. (2014). Back to translation: removal of aIF2 from the 5'-end of mRNAs by translation recovery factor in the crenarchaeon Sulfolobus solfataricus. Nucleic Acids Res *42*, 2505-2511.

Mills, E.W., and Green, R. (2017). Ribosomopathies: There's strength in numbers. Science *358*, DOI 10.1126/science.aan2755.

Milon, P., Carotti, M., Konevega, A.L., Wintermeyer, W., Rodnina, M.V., and Gualerzi, C.O. (2010). The ribosome-bound initiation factor 2 recruits initiator tRNA to the 30S initiation complex. EMBO Rep *11*, 312-316.

Milon, P., and Rodnina, M.V. (2012). Kinetic control of translation initiation in bacteria. Crit Rev Biochem Mol Biol *47*, 334-348.

Mitchell, S.F., and Lorsch, J.R. (2008). Should I stay or should I go? Eukaryotic translation initiation factors 1 and 1A control start codon recognition. J Biol Chem *283*, 27345-27349.

Moll, I., Hirokawa, G., Kiel, M.C., Kaji, A., and Blasi, U. (2004). Translation initiation with 70S ribosomes: an alternative pathway for leaderless mRNAs. Nucleic Acids Res *32*, 3354-3363.

Murakami, R., Singh, C.R., Morris, J., Tang, L., Harmon, I., Takasu, A., Miyoshi, T., Ito, K., Asano, K., and Uchiumi, T. (2018). The Interaction between the Ribosomal Stalk Proteins and Translation Initiation Factor 5B Promotes Translation Initiation. Mol Cellular Biol *38*, DOI 10.1128/MCB.00067-18

Murina, V., Kasari, M., Hauryliuk, V., and Atkinson, G.C. (2018). Antibiotic resistance ABCF proteins reset the peptidyl transferase centre of the ribosome to counter translational arrest. Nucleic Acids Res *46*, 3753-3763.

References

Naganuma, T., Nomura, N., Yao, M., Mochizuki, M., Uchiumi, T., and Tanaka, I. (2010). Structural basis for translation factor recruitment to the eukaryotic/archaeal ribosomes. J Biol Chem *285*, 4747-4756.

Narla, A., and Ebert, B.L. (2010). Ribosomopathies: human disorders of ribosome dysfunction. Blood *115*, 3196-3205.

Newman, J.R., Ghaemmaghami, S., Ihmels, J., Breslow, D.K., Noble, M., DeRisi, J.L., and Weissman, J.S. (2006). Single-cell proteomic analysis of S. cerevisiae reveals the architecture of biological noise. Nature *441*, 840-846.

Nürenberg-Goloub, E., Heinemann, H., Gerovac, M., and Tampé, R. (2018). Ribosome recycling is coordinated by processive events in two asymmetric ATP sites of ABCE1. Life Sci Alliance *1*, e201800095

Nürenberg, E., and Tampé, R. (2013). Tying up loose ends: ribosome recycling in eukaryotes and archaea. Trends Biochem Sci *38*, 64-74.

Ogle, J.M., Murphy, F.V., Tarry, M.J., and Ramakrishnan, V. (2002). Selection of tRNA by the ribosome requires a transition from an open to a closed form. Cell *111*, 721-732.

Oswald, C., Holland, I.B., and Schmitt, L. (2006). The motor domains of ABC-transporters. What can structures tell us? Naunyn Schmiedebergs Arch Pharmacol *372*, 385-399.

Passmore, L.A., Schmeing, T.M., Maag, D., Applefield, D.J., Acker, M.G., Algire, M.A., Lorsch, J.R., and Ramakrishnan, V. (2007). The eukaryotic translation initiation factors eIF1 and eIF1A induce an open conformation of the 40S ribosome. Mol Cell *26*, 41-50.

Peske, F., Rodnina, M.V., and Wintermeyer, W. (2005). Sequence of steps in ribosome recycling as defined by kinetic analysis. Mol Cell *18*, 403-412.

Pestova, T.V., Borukhov, S.I., and Hellen, C.U. (1998). Eukaryotic ribosomes require initiation factors 1 and 1A to locate initiation codons. Nature *394*, 854-859.

Pettersen, E.F., Goddard, T.D., Huang, C.C., Couch, G.S., Greenblatt, D.M., Meng, E.C., and Ferrin, T.E. (2004). UCSF Chimera--a visualization system for exploratory research and analysis. J Comput Chem *25*, 1605-1612.

Piir, K., Paier, A., Liiv, A., Tenson, T., and Maivali, U. (2011). Ribosome degradation in growing bacteria. EMBO Rep *12*, 458-462.

Pisarev, A.V., Skabkin, M.A., Pisareva, V.P., Skabkina, O.V., Rakotondrafara, A.M., Hentze, M.W., Hellen, C.U., and Pestova, T.V. (2010). The role of ABCE1 in eukaryotic posttermination ribosomal recycling. Mol Cell *37*, 196-210.

Prunetti, L., Graf, M., Blaby, I.K., Peil, L., Makkay, A.M., Starosta, A.L., Papke, R.T., Oshima, T., Wilson, D.N., and de Crecy-Lagard, V. (2016). Deciphering the Translation Initiation Factor 5A Modification Pathway in Halophilic Archaea. Archaea *2016*, 7316725.

Puglisi, J.D., Blanchard, S.C., and Green, R. (2000). Approaching translation at atomic resolution. Nat Struct Biol *7*, 855-861.

Qin, D., Liu, Q., Devaraj, A., and Fredrick, K. (2012). Role of helix 44 of 16S rRNA in the fidelity of translation initiation. RNA *18*, 485-495.

Ramakrishnan, V. (2014). The ribosome emerges from a black box. Cell *159*, 979-984.

Renart, J., Reiser, J., and Stark, G.R. (1979). Transfer of proteins from gels to diazobenzyloxymethyl-paper and detection with antisera: a method for studying antibody specificity and antigen structure. Proc Natl Acad Sci U S A *76*, 3116-3120.

References

Rheinberger, H.J., Sternbach, H., and Nierhaus, K.H. (1981). Three tRNA binding sites on Escherichia coli ribosomes. Proc Natl Acad Sci U S A *78*, 5310-5314.

Richter, D., and Lipmann, F. (1970). Formation of a ternary complex between formylatable yeast Met-tRNA, GTP and binding factor T of yeast and of E. coli. Nature *227*, 1212-1214.

Rodnina, M.V. (2016). The ribosome in action: Tuning of translational efficiency and protein folding. Protein Sci *25*, 1390-1406.

Rodnina, M.V., and Wintermeyer, W. (2009). Recent mechanistic insights into eukaryotic ribosomes. Curr Opin Cell Biol *21*, 435-443.

Saito, S., Hosoda, N., and Hoshino, S. (2013). The Hbs1-Dom34 protein complex functions in non-stop mRNA decay in mammalian cells. J Biol Chem *288*, 17832-17843.

Schmidt, C., Becker, T., Heuer, A., Braunger, K., Shanmuganathan, V., Pech, M., Berninghausen, O., Wilson, D.N., and Beckmann, R. (2016). Structure of the hypusinylated eukaryotic translation factor eIF-5A bound to the ribosome. Nucleic Acids Res *44*, 1944-1951.

Schmitt, L., and Tampé, R. (2002). Structure and mechanism of ABC transporters. Curr Opin Struct Biol *12*, 754-760.

Schuller, A.P., Wu, C.C., Dever, T.E., Buskirk, A.R., and Green, R. (2017). eIF5A Functions Globally in Translation Elongation and Termination. Mol Cell *66*, 194-205.e5.

Schultz, K.M., Merten, J.A., and Klug, C.S. (2011). Characterization of the E506Q and H537A dysfunctional mutants in the E. coli ABC transporter MsbA. Biochemistry *50*, 3599-3608.

Senior, A.E., al-Shawi, M.K., and Urbatsch, I.L. (1995). The catalytic cycle of P-glycoprotein. FEBS Lett *377*, 285-289.

Shao, S., Murray, J., Brown, A., Taunton, J., Ramakrishnan, V., and Hegde, R.S. (2016). Decoding Mammalian Ribosome-mRNA States by Translational GTPase Complexes. Cell *167*, 1229-1240.

She, Q., Singh, R.K., Confalonieri, F., Zivanovic, Y., Allard, G., Awayez, M.J., Chan-Weiher, C.C., Clausen, I.G., Curtis, B.A., De Moors, A*., et al.* (2001). The complete genome of the crenarchaeon Sulfolobus solfataricus P2. Proc Natl Acad Sci U S A *98*, 7835-7840.

Shoemaker, C.J., Eyler, D.E., and Green, R. (2010). Dom34:Hbs1 promotes subunit dissociation and peptidyl-tRNA drop-off to initiate no-go decay. Science *330*, 369-372.

Shoemaker, C.J., and Green, R. (2011). Kinetic analysis reveals the ordered coupling of translation termination and ribosome recycling in yeast. Proc Natl Acad Sci U S A *108*, E1392-1398.

Sievers, A., Beringer, M., Rodnina, M.V., and Wolfenden, R. (2004). The ribosome as an entropy trap. Proc Natl Acad Sci U S A *101*, 7897-7901.

Skabkin, M.A., Skabkina, O.V., Hellen, C.U., and Pestova, T.V. (2013). Reinitiation and other unconventional posttermination events during eukaryotic translation. Mol Cell *51*, 249-264.

Smith, P.C., Karpowich, N., Millen, L., Moody, J.E., Rosen, J., Thomas, P.J., and Hunt, J.F. (2002). ATP binding to the motor domain from an ABC transporter drives formation of a nucleotide sandwich dimer. Mol Cell *10*, 139-149.

Song, H., Mugnier, P., Das, A.K., Webb, H.M., Evans, D.R., Tuite, M.F., Hemmings, B.A., and Barford, D. (2000). The crystal structure of human eukaryotic release factor eRF1--mechanism of stop codon recognition and peptidyl-tRNA hydrolysis. Cell *100*, 311-321.

Sorum, B., Torocsik, B., and Csanady, L. (2017). Asymmetry of movements in CFTR's two ATP sites during pore opening serves their distinct functions. eLife *6* e29013.

References

Stark, H., Rodnina, M.V., Rinke-Appel, J., Brimacombe, R., Wintermeyer, W., and van Heel, M. (1997). Visualization of elongation factor Tu on the Escherichia coli ribosome. Nature *389*, 403-406.

Steitz, T.A. (2008). A structural understanding of the dynamic ribosome machine. Nat Rev Mol Cell Biol *9*, 242-253.

Stolboushkina, E., Nikonov, S., Zelinskaya, N., Arkhipova, V., Nikulin, A., Garber, M., and Nikonov, O. (2013). Crystal structure of the archaeal translation initiation factor 2 in complex with a GTP analogue and Met-tRNAf(Met.). J Mol Biol *425*, 989-998.

Strunk, B.S., Novak, M.N., Young, C.L., and Karbstein, K. (2012). A translation-like cycle is a quality control checkpoint for maturing 40S ribosome subunits. Cell *150*, 111-121.

Szentpetery, Z., Kern, A., Liliom, K., Sarkadi, B., Varadi, A., and Bakos, E. (2004). The role of the conserved glycines of ATP-binding cassette signature motifs of MRP1 in the communication between the substrate-binding site and the catalytic centers. J Biol Chem *279*, 41670-41678.

Tanzawa, T., Kato, K., Girodat, D., Ose, T., Kumakura, Y., Wieden, H.J., Uchiumi, T., Tanaka, I., and Yao, M. (2018). The C-terminal helix of ribosomal P stalk recognizes a hydrophobic groove of elongation factor 2 in a novel fashion. Nucleic Acids Res *46*, 3232-3244.

Terenin, I.M., Dmitriev, S.E., Andreev, D.E., and Shatsky, I.N. (2008). Eukaryotic translation initiation machinery can operate in a bacterial-like mode without eIF2. Nat Struct Mol Biol *15*, 836-841.

Theodoulou, F.L., and Kerr, I.D. (2015). ABC transporter research: going strong 40 years on. Biochem Soc Trans *43*, 1033-1040.

Thomas, C., and Tampé, R. (2018). Multifaceted structures and mechanisms of ABC transport systems in health and disease. Curr Opin Struct Biol *51*, 116-128.

Timachi, M.H., Hutter, C.A., Hohl, M., Assafa, T., Bohm, S., Mittal, A., Seeger, M.A., and Bordignon, E. (2017). Exploring conformational equilibria of a heterodimeric ABC transporter. eLife *6* e20236.

Urbatsch, I.L., Julien, M., Carrier, I., Rousseau, M.E., Cayrol, R., and Gros, P. (2000). Mutational analysis of conserved carboxylate residues in the nucleotide binding sites of P-glycoprotein. Biochemistry *39*, 14138-14149.

van den Elzen, A.M., Schuller, A., Green, R., and Seraphin, B. (2014). Dom34-Hbs1 mediated dissociation of inactive 80S ribosomes promotes restart of translation after stress. EMBO J *33*, 265-276.

van der Does, C., and Tampé, R. (2004). How do ABC transporters drive transport? Biol Chem *385*, 927-933.

Vedovato, N., Ashcroft, F.M., and Puljung, M.C. (2015). The Nucleotide-Binding Sites of SUR1: A Mechanistic Model. Biophys J *109*, 2452-2460.

Voorhees, R.M., and Ramakrishnan, V. (2013). Structural basis of the translational elongation cycle. Annu Rev Biochem *82*, 203-236.

Voorhees, R.M., Schmeing, T.M., Kelley, A.C., and Ramakrishnan, V. (2010). The mechanism for activation of GTP hydrolysis on the ribosome. Science *330*, 835-838.

Warner, J.R. (1999). The economics of ribosome biosynthesis in yeast. Trends Biochem Sci *24*, 437-440.

Weinger, J.S., Parnell, K.M., Dorner, S., Green, R., and Strobel, S.A. (2004). Substrate-assisted catalysis of peptide bond formation by the ribosome. Nat Struct Mol Biol *11*, 1101-1106.

Wilson, D.N. (2014). Ribosome-targeting antibiotics and mechanisms of bacterial resistance. Nat Rev Microbiol *12*, 35-48.

References

Woese, C.R. (1968). The fundamental nature of the genetic code: prebiotic interactions between polynucleotides and polyamino acids or their derivatives. Proc Natl Acad Sci U S A *59*, 110-117.

Woese, C.R. (2001). Translation: in retrospect and prospect. RNA *7*, 1055-1067.

Xue, S., and Barna, M. (2012). Specialized ribosomes: a new frontier in gene regulation and organismal biology. Nat Rev Mol Cell Biol *13*, 355-369.

Yap, K., and Makeyev, E.V. (2013). Regulation of gene expression in mammalian nervous system through alternative pre-mRNA splicing coupled with RNA quality control mechanisms. Mol Cell Neurosci *56*, 420-428.

Young, D.J., Guydosh, N.R., Zhang, F., Hinnebusch, A.G., and Green, R. (2015). Rli1/ABCE1 Recycles Terminating Ribosomes and Controls Translation Reinitiation in 3'UTRs In Vivo. Cell *162*, 872-884.

Zhao, Z., Fang, L.L., Johnsen, R., and Baillie, D.L. (2004). ATP-binding cassette protein E is involved in gene transcription and translation in Caenorhabditis elegans. Biochem Biophys Res Commun *323*, 104-111.

Zheng, S.Q., Palovcak, E., Armache, J.P., Verba, K.A., Cheng, Y., and Agard, D.A. (2017). MotionCor2: anisotropic correction of beam-induced motion for improved cryo-electron microscopy. Nat Methods *14*, 331-332.

Zhouravleva, G., Frolova, L., Le Goff, X., Le Guellec, R., Inge-Vechtomov, S., Kisselev, L., and Philippe, M. (1995). Termination of translation in eukaryotes is governed by two interacting polypeptide chain release factors, eRF1 and eRF3. EMBO J *14*, 4065-4072.

Supplementary Information

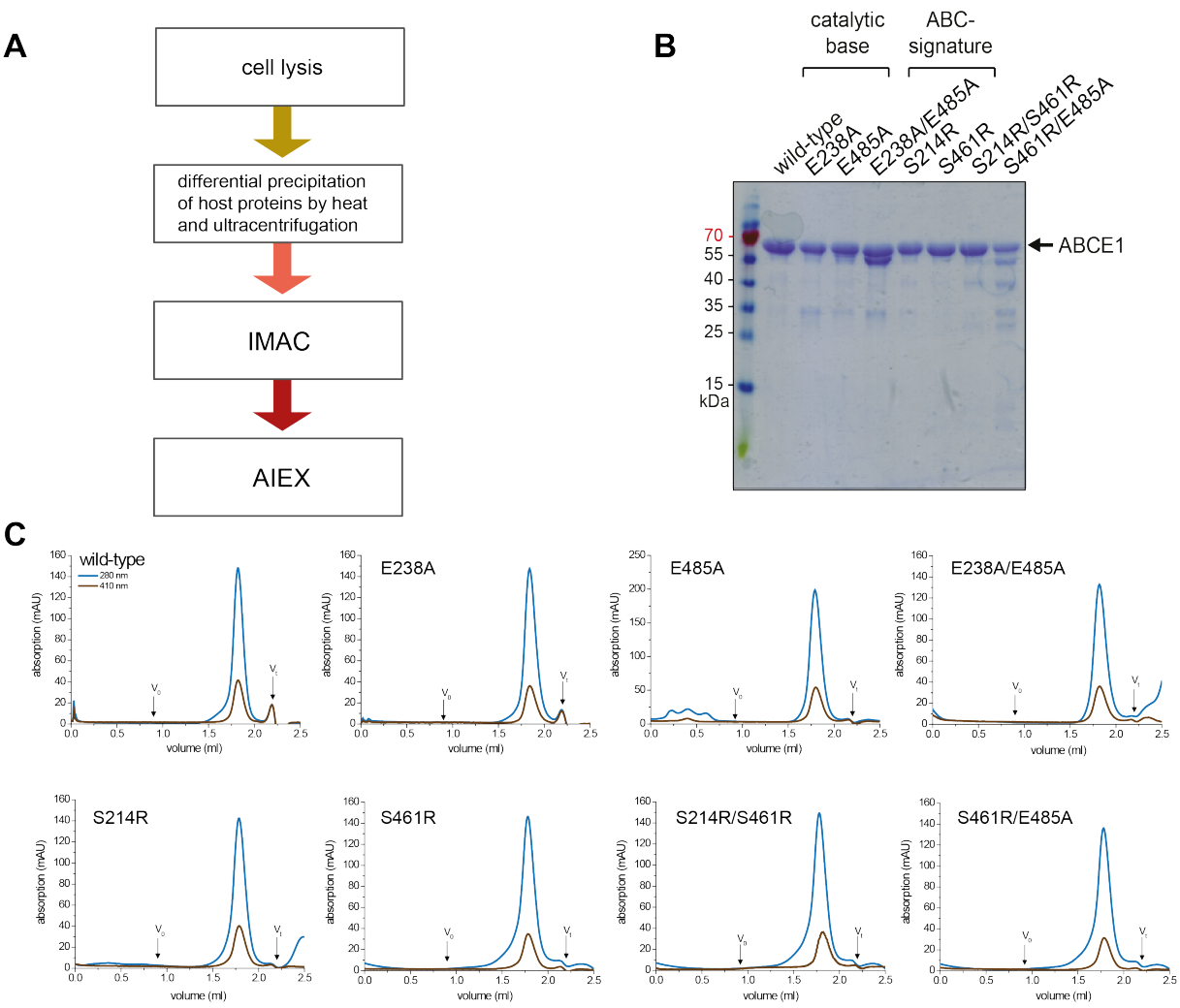

Figure S1: Protein purification and quality control. A) All splitting factors were purified from *E. coli* in a three-step process after lysis; differential precipitation at 65 °C removed the majority of host proteins. In a second purification step, ABCE1 was isolated *via* a C-terminal His_6 affinity tag by immobilized metal-chelate chromatography (IMAC). ABCE1 with disassembled iron-sulfur clusters and most degradation products were removed by subsequent anion exchange chromatography (AIEX). **B)** Purified ABCE1 was analyzed by SDS-PAGE (12.5%, Coomassie staining). Some of the mutants show degradation products. **C)** In SEC, all ABCE1 variants eluted in a single peak as seen by absorption at 280 nm (blue). Additional absorption at 410 nm (brown) demonstrates an assembled iron-sulfur cluster. SEC was performed in 20 mM Tris pH 7.5, 150 mM NaCl, 5 mM $MgCl_2$ and 1 mM DTT on a Superose™ 6 2.4 ml analytical grade column (GE Healthcare) applying 20-30 µg of protein (Nürenberg-Goloub et al., 2018).

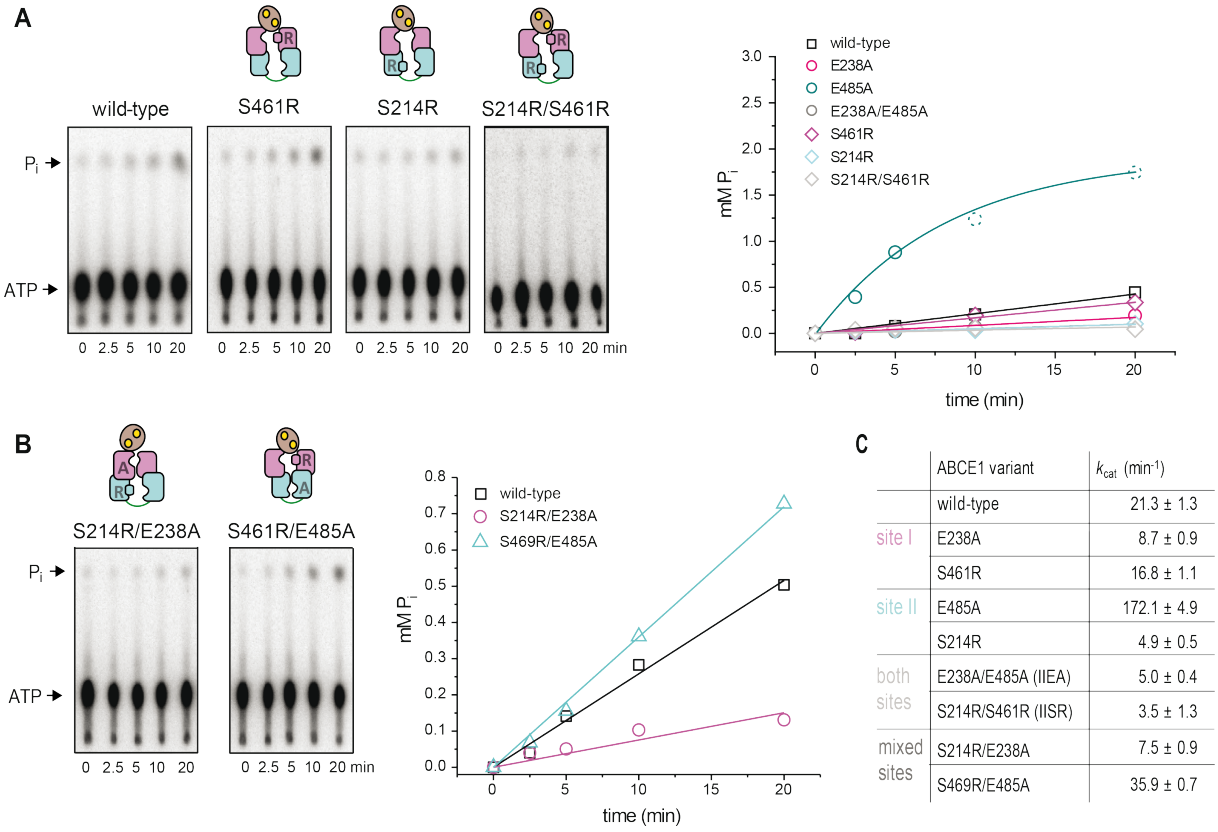

	ABCE1 variant	k_{cat} (min^{-1})
	wild-type	21.3 ± 1.3
site I	E238A	8.7 ± 0.9
	S461R	16.8 ± 1.1
site II	E485A	172.1 ± 4.9
	S214R	4.9 ± 0.5
both sites	E238A/E485A (IIEA)	5.0 ± 0.4
	S214R/S461R (IISR)	3.5 ± 1.3
mixed sites	S214R/E238A	7.5 ± 0.9
	S469R/E485A	35.9 ± 0.7

Figure S2: ATPase activity of the ABCE1 mutants. A) TLC radiograms of ^{32}P-γ-ATP (5 mM) and analysis of the ATPase assay for the SR variants of ABCE1 (1 µM). ATP turnover of all ABCE1 variants was determined as the initial rate constants of the exponential increase of inorganic phosphate in a time window of 20 min. For the hyperactive ABCE1^{E485A}, ATP turnover was determined within the first 5 min. **B)** Radiograms and analysis of the ATPase assay for mutants with mixed mutations; disengagement in site I and catalytic base exchange in site II or *vice versa*. **C)** Overview of the ATPase activity for all mutants in this study at optimal conditions (70 °C, 2.5 mM Mg^{2+}) (Nürenberg-Goloub et al., 2018).

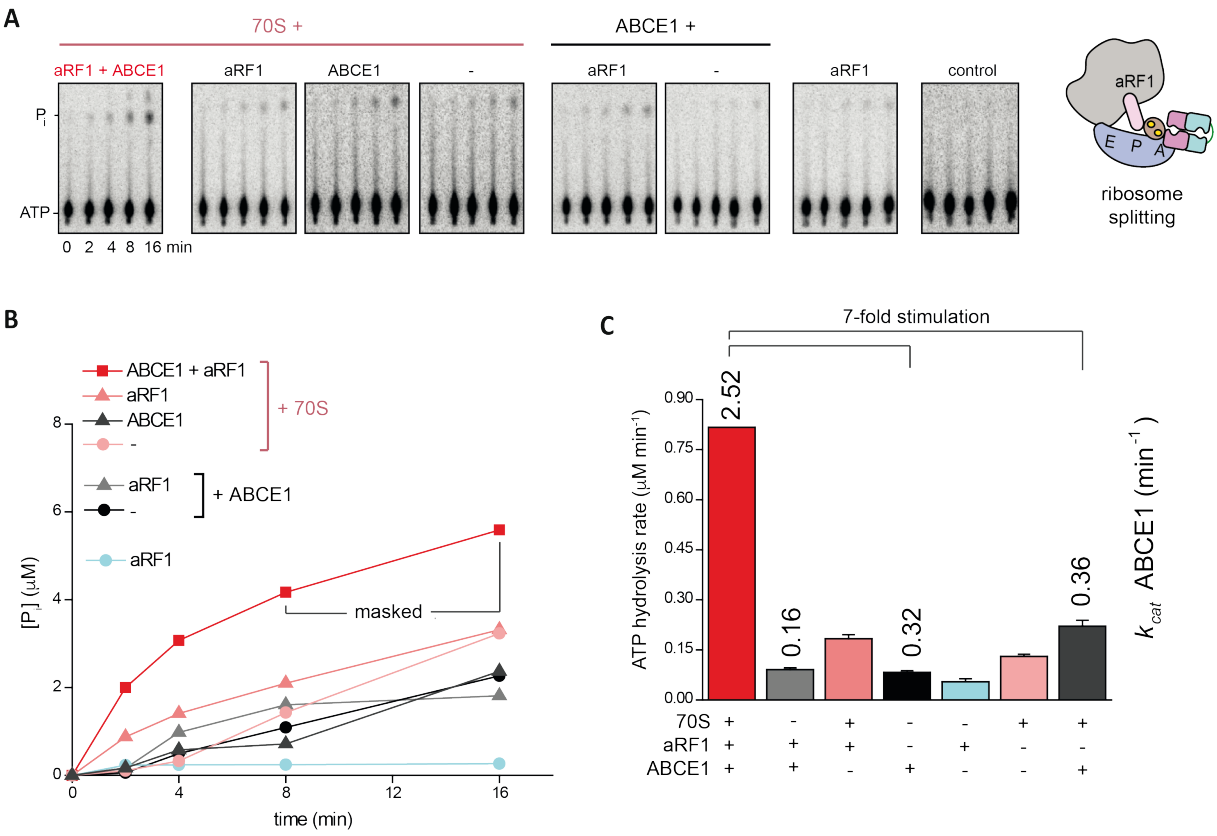

Figure S3: ATPase activity of ABCE1 is stimulated by 70S and aRF1 during ribosome splitting. **A)** TLC radiograms of ^{32}P-γ-ATP (37.5 µM) showing the stimulation of wild-type ABCE1 (1 µM) by 70S in concert with aRF1. **B)** ATPase activity measured by phosphate release during ribosome splitting. The marked values at 8 and 16 min were excluded from the analysis as they obviously are outside the linear range for this reaction. **C)** Total ATP hydrolysis rate in each sample (bars) and the turnover number for ABCE1 after subtraction of control experiments. Interestingly, while 70S alone does not influence ATPase activity of ABCE1, the presence of aRF1 leads to a reproducibly slight inhibiting effect. Notably, the overall drop in ATPase activity results from the lowered temperature (45 °C) and high Mg^{2+} concentration (25 mM) at 70S splitting conditions (Nürenberg-Goloub et al., 2018).

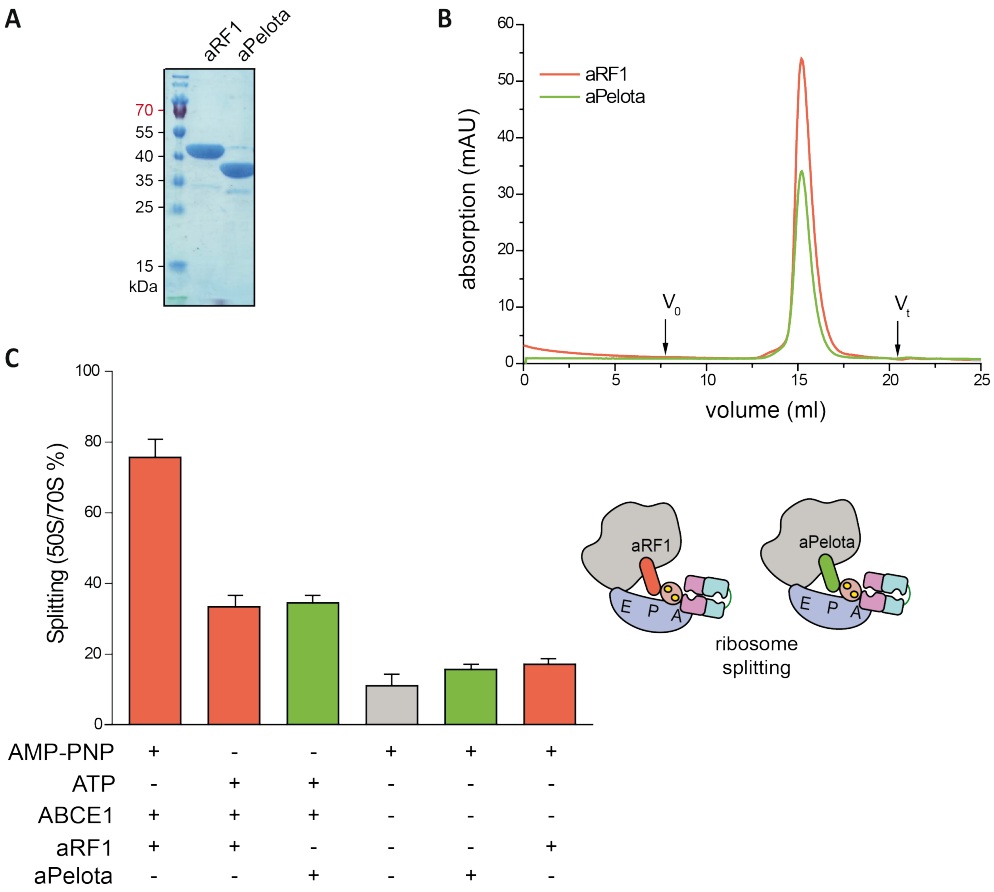

Figure S4: ABCE1 splits 70S with the canonical aRF1 and the ribosome rescue factor aPelota. A) The canonical release factor aRF1 acting on mRNA stop codon and the codon-independent release factor aPelota were purified by C-terminal and N-terminal His_6 affinity tag, respectively. Purification steps were the same as for ABCE1 (see Fig S1). **B)** Both factors eluted in a single peak in SEC (20 mM Tris pH 8.5, 250 mM NaCl, 5 mM $MgCl_2$, Superdex® 200 24 ml analytical grade, GE Healthcare). **C)** The ribosome splitting efficiency (n=2) by wild-type ABCE1 does not depend on the supplemented release factor (33% with aRF1 and 34% with aPelota). In the absence of ABCE1 or release factors the splitting rates remained > 20% (Nürenberg-Goloub et al., 2018).

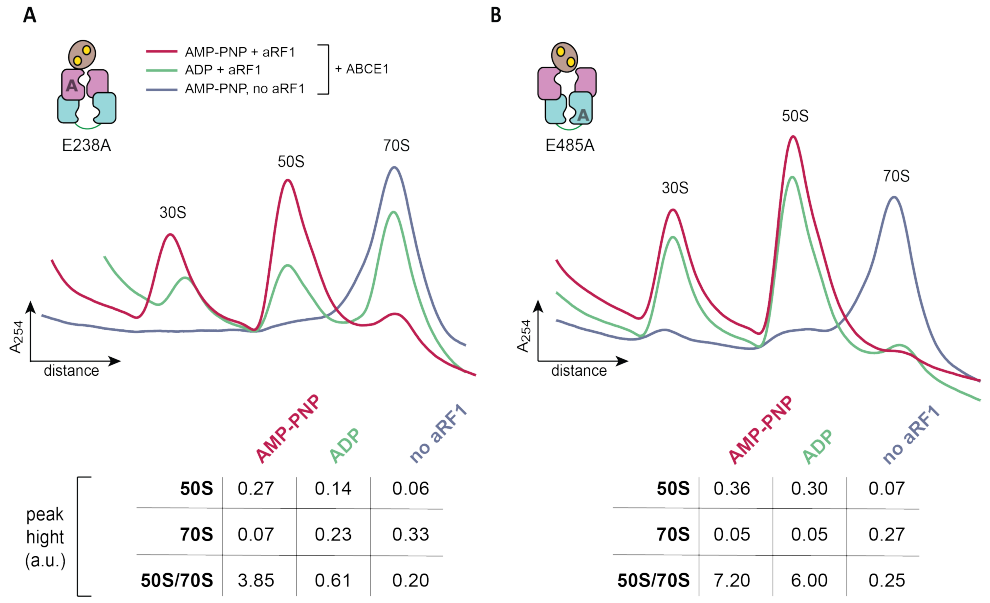

Figure S5: Functional mutants of ABCE1 are potent ribosome splitting factors. 70S splitting efficiency of ABCE1 with functional mutations of the catalytic base was assayed by SDG and quantified by the peak height ratios. In the presence of AMP-PNP (pink trace), both variants **A)** ABCE1^{E238A} and **B)** ABCE1^{E485A} are significantly more potent ribosome splitting factors than wild-type ABCE1 (compare Fig 9C). Major difference between site I and site II is revealed in samples with ADP (green trace). Here, only ABCE1^{E485A} with site II in an occluded state is able to split 70S, while ABCE1^{E238A} has a significantly lower activity. Both factors require the presence of excess release factor showing that splitting is an active and specific process (> 4% splitting in the absence of aRF1, blue trace) (Nürenberg-Goloub et al., 2018).

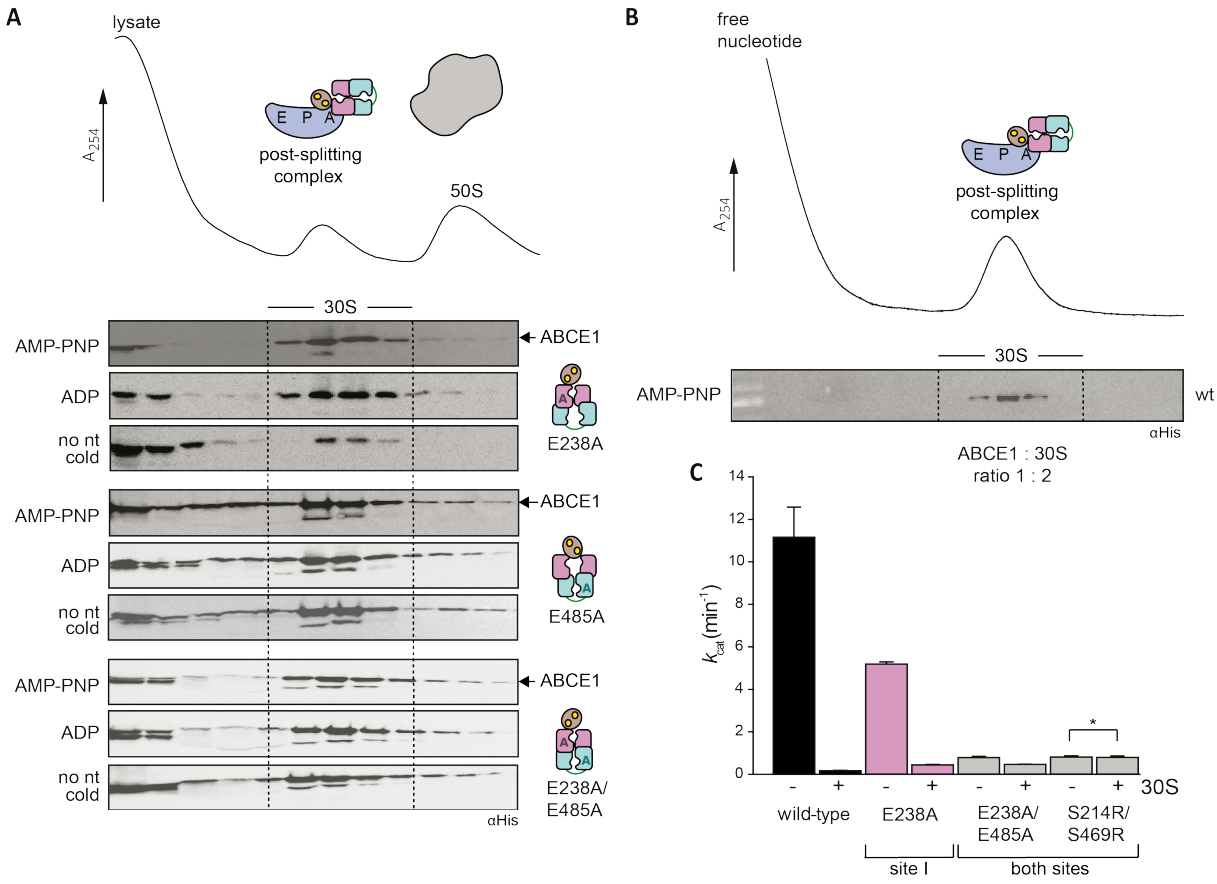

Figure S6: Formation of the post-splitting complex and ATPase activity of 30S bound ABCE1. A) If site II of ABCE1 is degenerated by E485A substitution, a stable post-SC is formed with AMP-PNP, ADP, and in the absence of a nucleotide at 4 °C. In contrast, ABCE1^{E238A} binds 30S with AMP-PNP and ADP however only moderately without the addition of nucleotides. **B)** ABCE1 is quantitatively engaged in the post-SC when purified ribosomes are added in a ratio of 1:2 (ABCE1:30S). **C)** ATPase activity of all ABCE1 mutants competent in post-SC formation is inhibited upon addition of 30S. No change occurs for the S214R/S469R variant (*), which does not bind to 30S. Notably, the overall drop in ATPase activity results from the high Mg^{2+} concentration (20 mM) at 30S binding conditions (65 °C) (Nürenberg-Goloub et al., 2018).

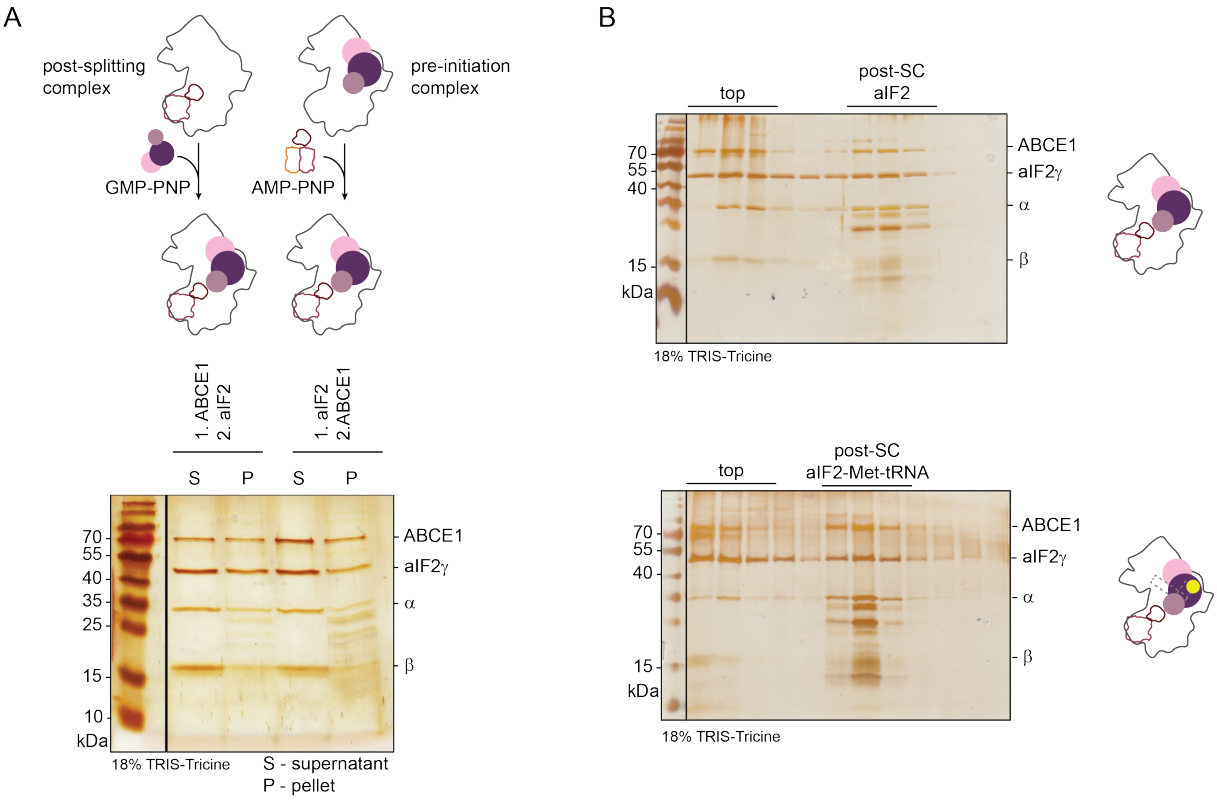

Figure S7: aIF2 binds 30S ribosomes independently of ABCE1 and Met-tRNA^{fMet} in the absence of aIF1/1A and mRNA. A) Pelleting assays with post-splitting/pre-initiation complexes assembled in different order shows no dependency of aIF2 or ABCE1 (3 µM each) recruitment to 30S ribosomes (1.2 µM) on each other at steady state conditions in the presence of non-hydrolysable nucleotide analoga (1 mM). **B)** Consistent with *in vitro* studies (Hasenohrl et al., 2009), aIF2 binds post-SCs similar as 30S-aIF1-aIF1A pre-initiation complexes and apo 30S subunits in the absence of Met-tRNA^{fMet} but can also as trimeric complex similar to the function of its eukaryotic homolog eIF2 (Richter and Lipmann, 1970).

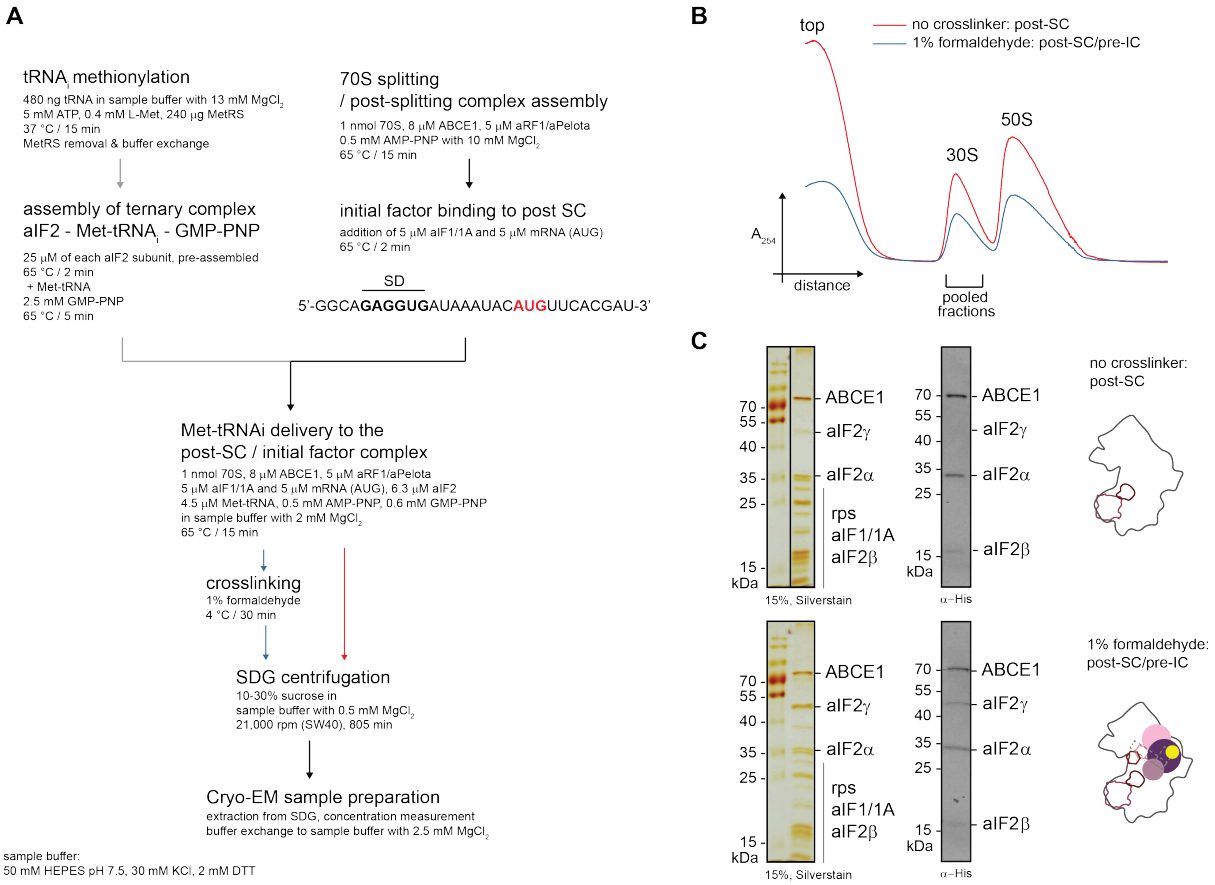

Figure S8: Reconstitution of the archaeal post-splitting and initiation complexes for cryo-EM. A) Exact assembly line beginning with 70S splitting and decoration of the post-SC with aIF1/1A and Shine-Dalgarno (SD) -leadered mRNA with an AUG start codon (black arrows), parallel $tRNA^{fMet}$ methionylation and assembly of the trimeric complex (grey arrows), and final formation of the complete initiation complex with subsequent crosslinking and purification. **B)** SDG profile of the samples, which contained **C)** only residual amounts of initiation factors in the non-crosslinked sample or stoichiometric amounts in the crosslinked sample as confirmed by SDS-PAGE stained with silver or analyzed by immunoblotting.

Abbreviations

a	archaeal
A	absorption, adenine, alanine, aromatic
Å	Ångström
aa	aminoacylated
α-His	anti-hexahistidine (antibody)
ABC	ATP-binding cassette
ABCE1	ATP-binding cassette subfamily E protein 1
ADP	adenosinediphosphate
AIEX	anion-exchange chromatography
AMP-PNP	adenylylimidodiphosphate
APS	ammoniumpersulfate
Arg	arginine
Asn	asparagine
ATP	adenosinetriphosphate
BME	beta-mercapthoethanol
C	cysteine, cytosine
CIEX	cation-exchange chromatography
Cys	cysteine
D	aspartate
DNA	deoxyribonucleic acid
DTT	dithiothreitol
e	eukaryotic
E	glutamate
EDTA	ethylenediaminetetraacetic acid
EF	elongation factor
EM	electron microscopy
F	phenylalanie
FeS	iron-sulfur
fMet	*N*-formylmethionine
G	glycine, guanine
GDP	guanosinediphosphate

Gln	glutamine
Glu	glutamate
GMP-PNP	guanylylimidodiphosphate
GTP	guanosinetriphosphate
h	helix
H	histidine
HEPES	hydroxyethylpiperazineethanesulfonic acid
IC	initiation complex
IF	initiation factor
IMAC	immobilized metal-chelate chromatography
K	lysine
L	leucine
Lys	lysine
Met	methionine
mRNA	messenger ribonucleic acid
NBD	nucleotide binding domain
NBS	nucleotide binding site
NGD	no-go decay
NMD	nonsense-mediated decay
NSD	no-stopp decay
nt	nucleotide
NTA	nitriloacetic acid
ORF	open reading frame
PAGE	polyacrylamidegel electrophoresis
PIC	pre-initiation complex
PTC	peptidyl-transferase center
Q	glutamine
R	arginine
RF	release factor
RMSD	root mean square deviation
RNA	ribonucleic acid
rRNA	ribosomal ribonucleic acid
rp(s)	ribosomal protein(s)
RQC	ribosome-associated quality control

S	serine, Svedberg
SC	splitting complex
SD	Shine-Dalgarno
SDG	sucrose density gradient
SDS	sodium dodecyl sulfate
SEC	size exclusion chromatography
SRL	sarcin-ricin loop
T	threonine
TAE	TRIS acetate EDTA
TBE	TRIS borate EDTA
TC	termination complex
TEM	transmission electron microscope
TEMED	tetramethylenediamine
TLC	thin layer chromatography
TRIS	trishydroxymethylaminomethane
tRNA	transfer ribonucleic acid
Tyr	tyrosine
U	uracile
UTR	untranslated region
Y	tyrosine